UNIVERSITÀ
DEGLI STUDI
DI PADOVA

UNIVERSITÀ DEGLI STUDI DI PADOVA

DIPARTIMENTO DI INGEGNERIA INDUSTRIALE DII

CORSO DI LAUREA MAGISTRALE IN INGEGNERIA AEROSPAZIALE

Dynamic Reference Model (DRM) for Hypersonic Rocket Performance Evaluation Assessment

Relatore:

Prof. Carlo BETTANINI FECIA DI COSSATO

Tutor Aziendale:

Ing. Federico FUNE

Laureanda:

Alessia TOMMASI

MATRICOLA N. 1242029

Anno accademico 2021/2022

UNIVERSITÀ
DEGLI STUDI
DI PADOVA

UNIVERSITÀ DEGLI STUDI DI PADOVA

DIPARTIMENTO DI INGEGNERIA INDUSTRIALE DII

CORSO DI LAUREA MAGISTRALE IN INGEGNERIA AEROSPAZIALE

Dynamic Reference Model (DRM) for Hypersonic Rocket Performance Evaluation Assessment

Relatore:

Prof. Carlo BETTANINI FECIA DI COSSATO

Tutor Aziendale:

Ing. Federico FUNE

Laureanda:

Alessia TOMMASI

MATRICOLA N. 1242029

Anno accademico 2021/2022

"Why, sometimes I've believed as many as six impossible things before breakfast."

L. Carroll - Alice in Wonderland

Abstract [ENG]

The purpose of this thesis is to build a dynamic model capable of providing an estimate, as well as an evaluation, of a generic aircraft that could be a rocket, rather than a small plane or any object capable of reaching hypersonic speeds. To do this, it was decided to use Matlab as software for the creation of the initialization scripts and Simulink for the construction of the model itself. It was chosen to follow a top-down approach, so that, starting with the implementation of simple but functional things, it could always be possible to complicate the model with any detail, while obtaining reliable dynamics of the aircraft. The model consists of an initialization block that calls the Matlab scripts on Simulink to provide the zero state of motion of the aircraft. This connects to the guidance system, together with an initialization block of the point to be intercepted. The guide is based on the Proportional Navigation law, the oldest and also one of the most used even today, which is based on the simple principle that, by maintaining constant the orientation of the displacement vector that connects the aircraft to the point to be intercepted, the latter will be reached. From the guidance, an acceleration command is given which is passed to the autopilot and saturated with aerodynamic accelerations to provide the aircraft with active accelerations which are then translated into angular deflection commands through the hypothesis of trimmed motion. However, the trimmed motion would not be ideal for the analysis of the motion of the aircraft in question, as it is desired to be able to reach the possibility of also carrying out a pull-up maneuver, for this reason, these hypotheses were revisited and made less binding to also allow a component of pitch moment in addition to those of drag and lift. The angular deflection command is then transmitted to the environment of the aircraft, to be able to calculate its subsequent state by evaluating the forces acting on it and implementing the equations of motion. Finally, position, speed, acceleration, and attitude will arise to be given in feedback to the guide for the calculation of the next command in the order of intercepting the desired point. Once the construction of the model was completed, it was tested to evaluate its functioning. First, the result produced by the software developed in this thesis was compared with the one already implemented on Simulink, thus testing the reliability of the equations of motion that produced the same results. After that, the flight performance was evaluated, by building a grid of positions of points to be intercepted to observe how many of these points would have been practiced, at what speed,

and with how much time. This has produced results that have demonstrated the sensitivity of the vehicle to its initial and final state, due to the extremely high speed and to the conditions of trimmed motion imposed. By imposing a disturbance of 2 degrees on the deflection of surfaces after 10 seconds of flight, its stability was tested and the ease with which the aircraft was able to recover its attitude. Thus, it was shown that the disturbance has never influenced the ability to reach the point concerned, producing appreciable effects only at very high Mach when the flight time is shorter and the deflection angles of the surfaces are close normally to zero. Finally, the ability to perform a pull-up maneuver at various altitudes was tested, which led to highlighting that not all of them can produce a hypersonic flight: the smaller ones produce a drag too high to be able to exceed Mach 3, and the higher ones have an atmosphere that is too thin for the airbreathing system, so it takes more time to sufficiently increase the speed. The last thing studied in the arc of this thesis was a thermoelastic effect on the deflection surfaces of the aircraft which influences the flight mechanics at high speeds: when the temperature becomes higher, these surfaces, are likely to be subject to bending. Thus, a wider opening angle is required for carrying out a maneuver, which leads to an increase in drag and, consequently, a drastic decrease in speed. All this means that the aircraft is not always able to reach hypersonic speeds but is much more maneuverable through the control logic implemented in the model due to lower velocity and has been verified by repeating the same tests used for the verification of the model.

Abstract [ITA]

Lo scopo di questa tesi è quello di costruire un modello dinamico in grado di fornire una stima, oltre che una valutazione, di un velivolo generico, il quale potrebbe essere tanto un razzo quanto un piccolo aereo o un qualsiasi oggetto in grado di raggiungere velocità ipersoniche. Per fare ciò è stato scelto di impiegare Matlab come software per la realizzazione degli script di inizializzazione e l'ambiente Simulink per la costruzione del modello in sé. È stato scelto di seguire un approccio top-down, così che, iniziando dall'implementazione di cose semplici ma funzionanti, potesse sempre essere possibile complicare il modello con qualsivoglia dettaglio, pur ottenendo una dinamica affidabile del velivolo. Il modello si compone di un blocco di inizializzazione che richiama gli script di Matlab su Simulink in modo da fornire lo stato di moto zero del velivolo. Questo si collega al sistema di guida, assieme ad un blocco di inizializzazione del punto da intercettare. La guida sfrutta la legge di navigazione proporzionale, la più antica ed anche una delle più usate ancor oggi, che si basa sul semplice principio che, mantenendo costante l'orientazione del vettore spostamento che collega il velivolo al punto da intercettare, quest'ultimo verrà raggiunto. Dal blocco di guida si ottiene un'accelerazione comandata che viene passata all'autopilota e saturata con le accelerazioni aerodinamiche per fornire al velivolo le accelerazioni attive che vengono poi tradotte in comandi di deflessione angolare tramite l'ipotesi di moto trimmato. Tuttavia, il moto trimmato non sarebbe ideale per l'analisi di moto del velivolo in oggetto, in quanto si desidera poter effettuare anche una manovra di pull-up. Per questo motivo, sono state sfruttate ipotesi rivisitate e rese meno vincolanti così da concedere anche una componente di momento di pitch oltre a quelle di drag e portanza. Il comando di deflessione angolare viene poi trasmesso all'ambiente del velivolo, in modo da poter calcolarne lo stato successivo tramite la valutazione di forze agenti su di esso e l'implementazione delle equazioni del moto, da cui, infine, scaturiranno posizione, velocità, accelerazione e assetto da dare in feedback alla guida per il calcolo del comando successivo nell'ordine di intercettare il punto desiderato. Una volta completata la costruzione del modello, questo è stato testato per valutarne il funzionamento. Come prima cosa, sono stati messi a confronto i risultati prodotti dal software sviluppato in questa tesi con quello già implementato su Simulink, testando così l'affidabilità delle equazioni del moto che hanno prodotto gli stessi risultati. Dopo di che sono state valutate le performance di volo, tramite la costruzione di una griglia di posizioni da

intercettare per poter osservare quanti punti sarebbero stati presi, a che velocità e in quanto tempo. Questo ha prodotto dei risultati che hanno dimostrato la grande sensibilità del velivolo nei confronti di posizione iniziale e punto di arrivo a causa dall'alta velocità oltre che dei limiti delle condizioni di volo imposte. Imponendo un disturbo di 2 gradi sulla deflessione delle superfici dopo 10 secondi di volo è stata testata la sua stabilità e la facilità con cui il velivolo riuscisse a recuperare l'assetto. Così si è provato che il disturbo non ha mai influenzato la capacità di raggiungimento del punto interessato, producendo effetti apprezzabili solamente a Mach molto elevati quando il tempo di volo è più breve e gli angoli di deflessione delle superfici sono vicini allo zero. Infine, è stata testata la capacità di realizzare una manovra pull-up a varie altitudini, che ha portato ad evidenziare che non tutte sono in grado di produrre un volo ipersonico: quelle minori producono un drag troppo alto per poter superare Mach 3 e quelle maggiori possiedono un'atmosfera troppo rarefatta per il sistema di airbreathing, per cui occorre più tempo per incrementare a sufficienza la velocità. L'ultima cosa studiata nell'arco di questa tesi è stato un effetto termoelastico sulle superfici di deflessione del velivolo che influenza la meccanica di volo ad alte velocità, quando la temperatura si fa più alta e, queste superfici, rischiano di essere soggette a flessione. Così, è necessario un angolo più ampio di apertura per la realizzazione di una manovra, il che porta ad un incremento del drag e, conseguentemente, a una drastica diminuzione della velocità. Tutto ciò fa si che il velivolo non sempre riesca a raggiungere velocità ipersoniche, ma sia molto più manovrabile tramite la logica di controllo implementata ed è stato verificato riproponendo gli stessi test usati per la verifica del modello.

Contents

List of Figures

List of Tables

Nomenclature

$[T]^{XY}$	Rotational Matrix from X to Y reference system
α	angle of attack, rad
α	angular acceleration, rad/s^2
$\bar{C}_{2,0}$	Second-Degree Zonal Gravitational Coefficient
β	angle of drift, rad
δ_E	Elevon deflections, deg
$\dot{\gamma}$	Flight-Path time rate of change, deg/s
$\dot{\lambda}$	LOS time rate of change, deg/s
$\dot{m}$	Mass flow, kg/s
$\dot{m}_p$	Propellant consumption per second, kg/s
γ	Flight-Path angle, deg
γ	Specific Heat Ratio
λ	LOS angle, deg
λ	Latitude, deg
μ	Longitude, deg
	Navigation ratio
Ω	Earth angular velocity,15°/h
ϕ	roll angle, rad
ψ	yaw angle, rad
ρ	Air Density, kg/m^3
τ	Tangential Stresses, Pa
θ	pitch angle, rad
A	Aerodynamic Force, N
a	Acceleration, m/s^2

a	Speed of Sound, m/s
c	exhaust stream velocity, m/s
C_D	Drag Aerodynamic Coefficient
C_F	Aerodynamic Coefficients
C_L	Lift Aerodynamic Coefficient
C_l	Rolling Moment Coefficient
C_m	Pitching Moment Coefficient
C_n	Yawing Moment Coefficient
C_Y	Deviant Aerodynamic Coefficient
D	Drag Force, N
E	Young Modulus, N/m^2
F	Force acting on a body, N
F_A	Aerodynamic Force,N
GM	Earth Gravitational Constant, kgm^3/s^2
I	Moment of inertia acting on a body, $kg * m^2$
I_{sp}	Specific Impulse, 1/s
L	Lift Force,N
M	Moment acting on a body, $N * m$
m	Mass, kg
Ma	Mach Number
n	Normal Versor
p	Normal Pressure, Pa
p, q, r	body rates, rad/s
Q	Dynamic Pressure, Pa
q_n	Rotation Quaternions
R	Specific Constant of the Gas
Re	Reynolds Number
S	Surface, m^2
s_E	position in ECEF, m
T	Thrust Force, N

t	Tangential Versor
T_t	Total Temperature, K
u, v, w	velocity, m/s
v_E	velocity in ECEF, m
W	Weight, N
Y	Deviant Force, N
g_0	Earth's gravity= $9.80665 m/s^2$

Acronyms

I_{sp} Specific Impulse

2-D Two Dimensional

3-D Three Dimensional

6DOF Six Degrees of Freedom

CFD Computational Fluid Dynamics

ECEF Earth Centered Earth Fixed frame

ISA International Standard Atmosphere

LOS Line-of-Sight Vector

NED North East Down Coordinate System

PN Proportional Navigation

TBCC Turbine-Based Combined Cycle

WGS U.S. World Geodetic System 1984

Chapter 1

Introduction

Nowadays hypersonic research is still a hot topic, due to its military, scientific and tourist applications which can bring a massive change in today's life. The interest in this topic was increased by the scramjet-powered X-43, which brought to life an airbreathing hypersonic engine [2]. Using this propulsive technology, leads the hypersonic flight to a new life, forgetting, at least in part, the rocket-based propulsion, which is much more expensive and less stable, risking affecting the safety of the aircraft [24]. The possibility of making hypersonic flight feasible has taken a lot of important research centers to develop engines always better, as well as more suitable aerodynamic geometries and materials, making it necessary to build more and more accurate models to be able to test them in suitable flight conditions [25]. The purpose of this thesis is therefore to build six degrees of freedom model where it is possible to test any aircraft with minor modifications, including its aerodynamics and propulsion to gain an idea of its functionality. Of course, it is an ambitious work and, to gain reliable software before all, it was chosen to follow a top-down approach, starting with the implementation of simple things, to complicating them step by step. The aim is to gain a reliable tool today that hypersonic weapons are a serious threat [33] and space tourism is an increasingly less abstract reality. The first thing to do was searching some previous experience in this theme that could help this work to reach its purpose. The University of Kansas has come up with interesting studies [19],[20],[18],[21],[22],[23], which provide research on a ramjet and scramjet engine for a generic hypersonic vehicle, the development of an aerodynamic database, and, lastly, the modeling and simulation of a generic hypersonic vehicle, for control and navigation purpose. This research

gave an important first view on the functioning of a hypersonic engine as well as a solid idea of the trend of aerodynamic coefficients, to reach a critical view on how results could be to be acceptable or not.

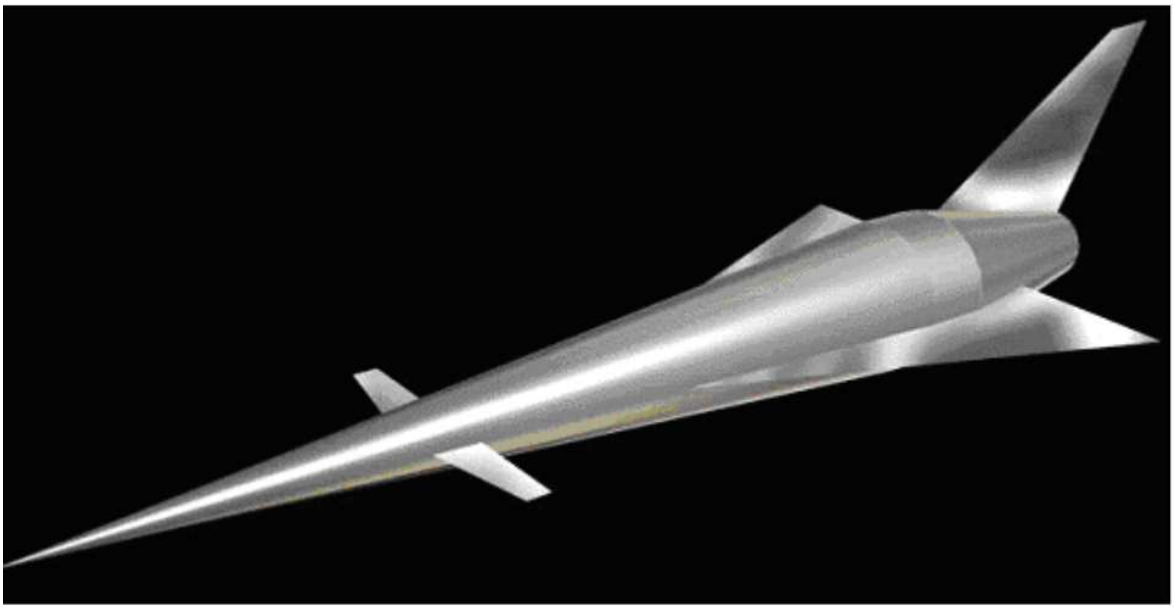

Figure 1.1: Generic Hypersonic Vehicle of the Kansas and NASA study [19] [32].

This study was assumed to be reliable because it was based on a NASA study [32] which had the main objective to develop a horizontal takeoff and land landing, single-stage airbreathing vehicle. With this paper, the National Aero-Space Plane (NASP) Program presented the aerodynamic, propulsion, and mass results, as well as model for a generic hypersonic vehicle in winged-cone configuration. These results have been taken by Kansas University to produce fitting equations that could be used to describe aircraft flight mechanics. Following this example but working with other scope and hypotheses, this thesis has been done, with the main topics organized as follows:

- **Vehicle Flight Simulation**. This chapter gives an overview of all the theoretical notions needed for the 6DOF model building, stepping from the main reason to build a simulation model, to the anatomy of a generic vehicle, talking about the importance of reference frames and coordinate systems, and concepts that lead to the most important equations of the model such as the one of motion, thrust and aerodynamic;
- **Geometry of the Vehicle**. Here it's presented the actual vehicle chosen from literature

as a reference for the model, giving an overview of its materials, its geometry, and its mass;

- **Building of the Model** is the chapter where there is the explained the architecture of the 6DOF model built in this thesis, analyzing every single subsystem and all the hypotheses beyond every decision that has to be made;
- **Model Tests and Performance**. After the building of the model, came the necessity to test its results. First of all, in this chapter, it's presented the validation of the motion equations, step then to the actual results data analysis for flight performances, disturbance effects, and a pull-up maneuver;
- **Hypersonic Effect in the 6DOF Model** presents a thermoelastic effect acting on the elevons deflection which was implemented in the model. After its implementation, follows a comparison between the result obtained with this effect and the one of the previous sections.

Chapter 2

Vehicle Flight Simulation

A vehicle flight simulation is a computational tool, involving mathematical models of the vehicle itself, target and environment, based on equations to describe physical laws and logical consequences. Executing a model is important to visualize the dynamic behavior of an object without building the object itself. The vehicle model is the richest in terms of details: it has to fully describe the carrier in all its aspects such as mass, geometry, thrust, aerodynamics and many more. The target one, instead, can be less accurate, providing, at least, its position and velocity in order to be intercepted. Last but not least, the environment model is implemented to gain details about atmospheric characteristics and gravity (fig.2.1). It has to be noticed that even the smallest variation in any of the subsystems written above can lead to a drastically changed type of motion.

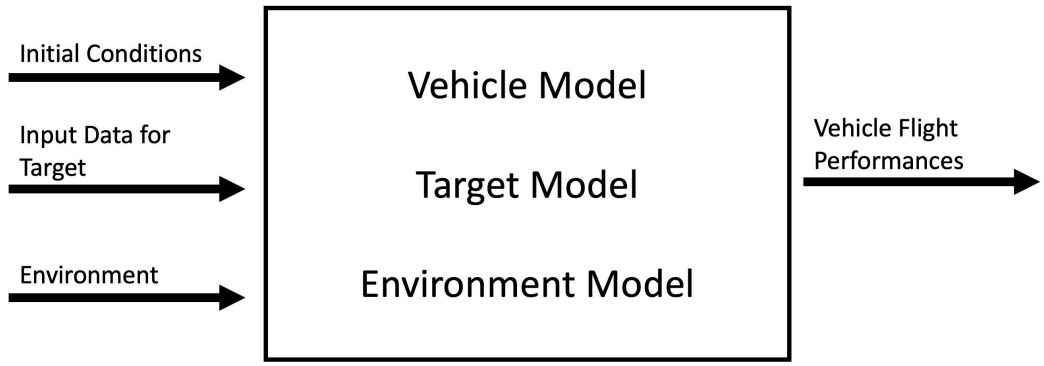

Figure 2.1: Vehicle Flight Simulation

The model of the aerospace vehicle is based on classical mechanics. The most important

physical laws for the simulation are the motion ones due to gravity, aerodynamics or thrust. In fact, an aerospace vehicle is characterized by six degrees of freedom, three translational and three of attitude, which provided, in order, the center of mass motion (eq.2.1) and the vehicle orientation (eq.2.2).

$$F = ma; \tag{2.1}$$

$$M = I\alpha; \tag{2.2}$$

A lot of soft-wares can be used to model flight dynamics. Specifically, for the development of this thesis, MATLAB® has been selected, with large use of Simulink® , which is helpful to design a really difficult model in a simple way, as it can be shown in chapter 4.

2.1 Aerospace Vehicle Anatomy

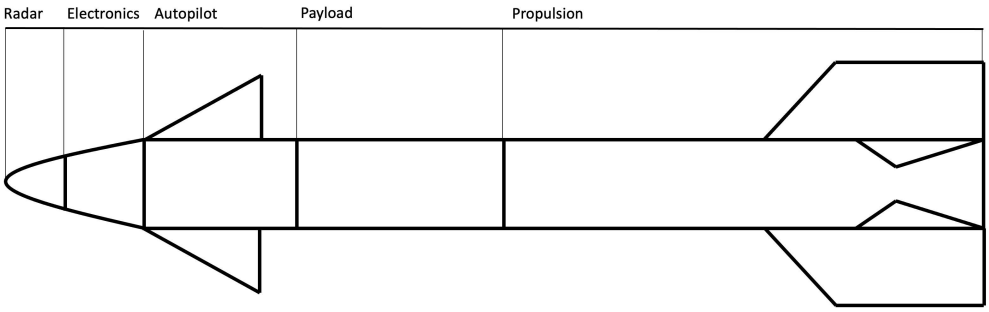

Figure 2.2: Aerospace Vehicle Anatomy

As it's shown in Fig. 2.2 an aerospace vehicle is composed of various parts. The radar is needed to reach information about the desired point to intercept, using a tracking function to keep the vehicle pointed toward the objective and for this reason, is usually located on the nose cone. The field of view is around ±40 to ±60 deg using a gimbaled system. The electronics part is necessary to elaborate on data gained from the radar and transmit the information to the autopilot in form of an electrical signal. With a fin deflection command, the aerospace

vehicle can correct its motion in order to reach the desired point. The design of the autopilot depends on the aerodynamics and on the type of control used, to compensate possible peculiar characteristics of the vehicle itself. Then there's the part where is located the payload and the last one is the leave to the motor or propulsion system, which provides the thrust force to the aerospace vehicle. The propulsion design is usually a trade-off between the characteristics needed and can involve all the motors type, from the solid ones to the liquids, and so on. Anyway, generally, a solid propellant rocket motor is employed for the long-term reliability.

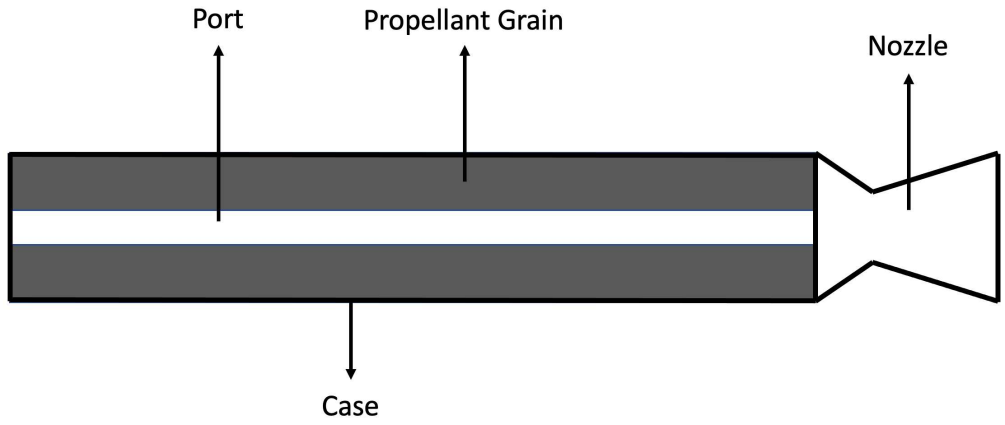

Figure 2.3: Solid Propellant Rocket Motor

This type of motor is usually composed by:

- a case, it contains the motor and it has to be built in a high resistance material, to survive to temperature and kinetic stresses;
- the propellant grain which contains the fuel and oxidizer to generate a thermal reaction;
- the port area that increases along the consumption of propellant and its variable with the shape of propellant grain;
- the nozzle which converts the thermal energy of the chemical reaction in kinetic energy.

2.2 Frames and Coordinate Systems

A frame is an unbounded continuous set of points over the Euclidean three-space with invariant distances and which possesses, as a subset, at least three non-collinear points [34]. Those three

points are necessary to obtain a three-dimensional space.

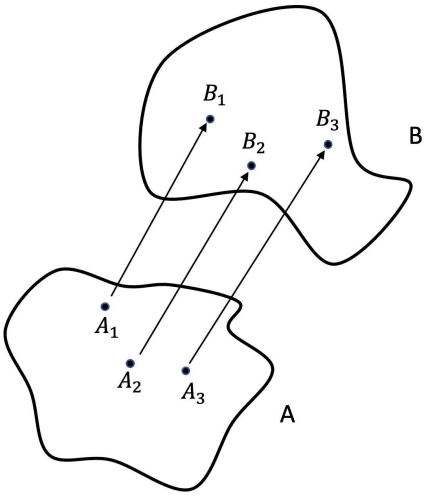

Figure 2.4: Frame position

Let's consider two different frames A and B containing three non-collinear points such as in Fig. 2.4. The coordinates of B with respect to A are determined from the displacement vectors $s_{B_iA_i}$, with $i = 1, 2, 3$. In this way, it is shown that a frame has six degrees of freedom three of displacement and three of rotation because six of the nine vectors are independent.

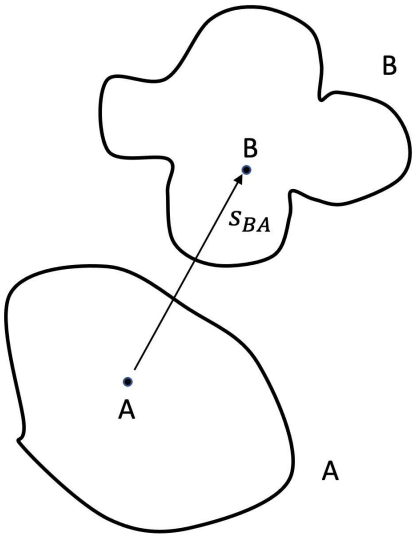

Figure 2.5: Frame location

If there's only one point per frame (Fig. 2.5), the displacement vector $s_{B_iA_i}$ gives the

location of the second frame with respect to the first one, leaving the frames freedom of orientation. The two points are named base points.

Then, choose a set of three orthonormal base vectors:

$$a_1, a_2, a_3 \text{ where } \bar{a}_i a_j = \begin{cases} 0 & for \quad i \neq j \\ 1 & for \quad i = j \end{cases} \quad ; \quad \text{i = 1,2,3; j = 1,2,3.}$$

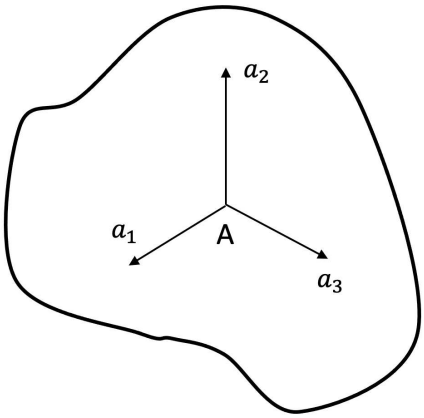

Figure 2.6: Frame orientation

The orientation of the frame is given (Fig.2.6). Location and orientation are both required to know the exact position of a frame. The most important coordinate system of a frame is called preferred coordinate system and is the one in which the base vectors are simply defined as follows: $[a_1]^A = [1 \quad 0 \quad 0]$, $[a_2]^A = [0 \quad 1 \quad 0]$, $[a_3]^A = [0 \quad 0 \quad 1]$. This is the base of coordinate systems, which are a cornerstone for flight dynamics. In Tab. 2.1 is presented an overview of the most important reference frames.

Frame	Base point	Base vectors	First direction	Third direction
Heliocentric	H center of sun	$\boldsymbol{h}_1, \boldsymbol{h}_2, \boldsymbol{h}_3$	$\boldsymbol{h}_1$ Aries	$\boldsymbol{h}_3$ normal of ecliptic
Inertial	I center of Earth	$\boldsymbol{i}_1, \boldsymbol{i}_2, \boldsymbol{i}_3$	$\boldsymbol{i}_1$ vernal equinox	$\boldsymbol{i}_3$ Earth's spin axis
Earth	E center of Earth	$\boldsymbol{e}_1, \boldsymbol{e}_2, \boldsymbol{e}_3$	$\boldsymbol{e}_1$ Greenwich	$\boldsymbol{e}_3$ Earth's spin axis
Body	B center of mass	$\boldsymbol{b}_1, \boldsymbol{b}_2, \boldsymbol{b}_3$	$\boldsymbol{b}_1$ nose	$\boldsymbol{b}_3$ down

Table 2.1: Reference frames [34]

Generally, working with aerospace vehicles, some assumptions are made:

- The Earth can be considered flat, nonrotating and approximately an inertial reference frame, which is true for short distance flights. Gravity is barely constant and perpendic-

ular to the Earth's surface, building, in this way, the flat Earth model.

- Atmospheric properties are a function of altitude only. [16]

For these reasons, one of the most used coordinate systems in flight dynamics, even in this thesis, is *North East Down Coordinate System (NED).*

NED coordinates are related to body coordinates by Euler angles ψ, θ, ϕ, even known as, in order, yaw angle, pitch angle and roll angle [35].

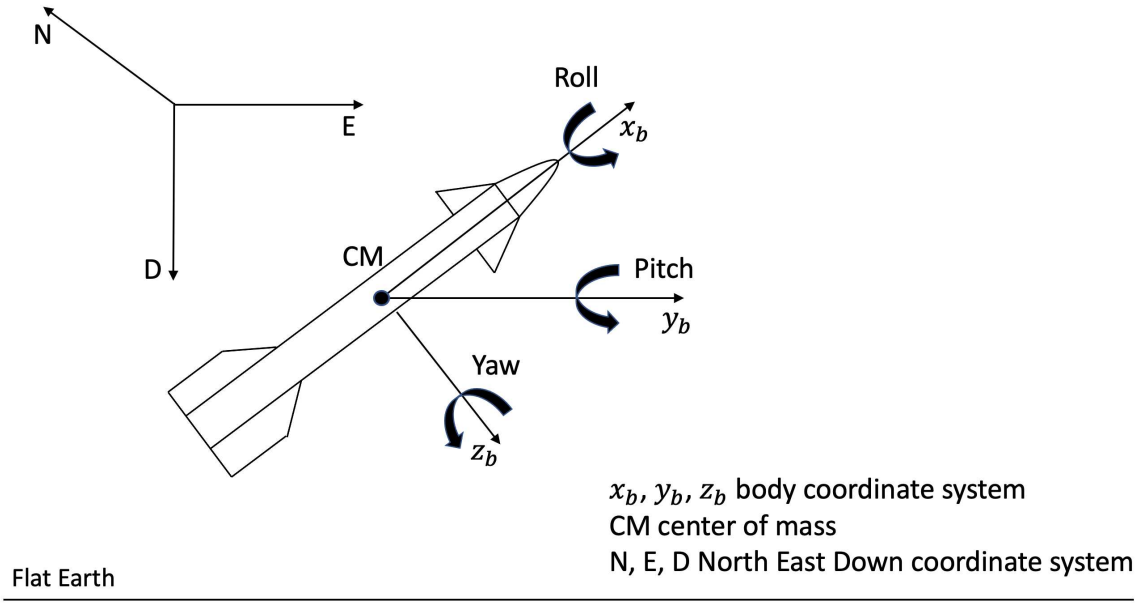

Figure 2.7: Local Level and body coordinates systems

It is possible to move from one coordinate system to another using a transformation matrix. Specifically, to move from body to NED, it's used the Euler transformation matrix, sometimes known as direction cosine matrix, which is the product of three sequential coordinate transformations: the first around ϕ, the second around θ and the third around ψ. Giving eq.2.3:

$$[T]^{BL} = \begin{bmatrix} \cos\psi\cos\theta & \sin\psi\cos\theta & -\sin\theta \\ \cos\psi\sin\theta\sin\phi - \sin\psi\cos\phi & \sin\psi\sin\theta\sin\phi + \cos\psi\cos\phi & \cos\theta\sin\phi \\ \cos\psi\sin\theta\cos\phi + \sin\psi\sin\phi & \sin\psi\sin\theta\cos\phi - \cos\psi\sin\phi & \cos\theta\cos\phi \end{bmatrix} \tag{2.3}$$

However, working with a hypersonic vehicle, these approximations, especially the flat Earth one, are becoming less accurate.

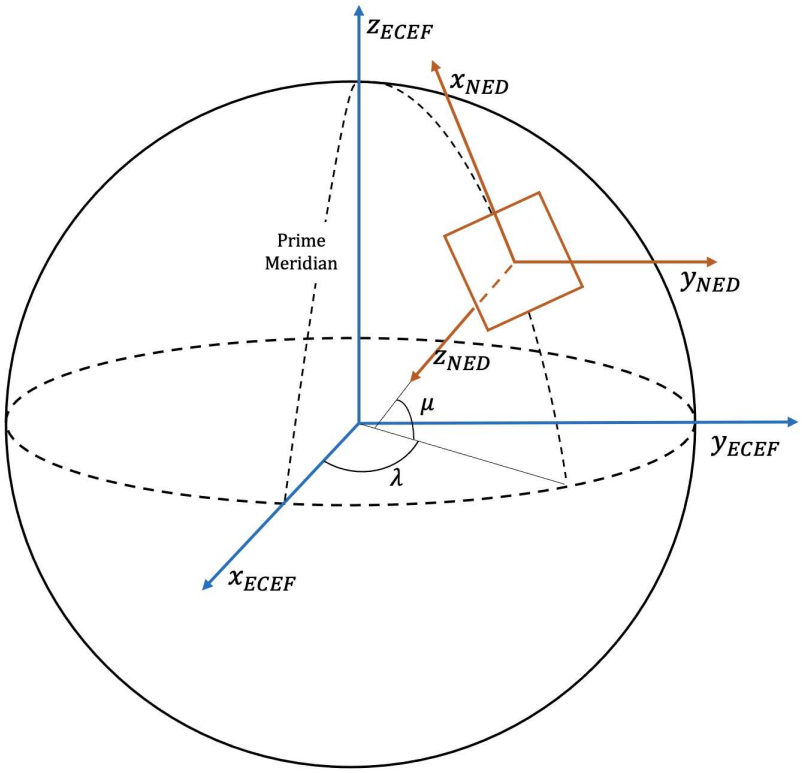

Figure 2.8: NED (orange) and ECEF (blue) coordinates system. [10]

In order to gain a better data approximation, the *Earth Centered Earth Fixed frame (ECEF)* frame can be used. ECEF is a cartesian coordinate system with its origin fixed at the Earth's center of mass. The intersection between Earth's equatorial plane and the Greenwich Meridian gives the x-axis direction, the z-axis points towards the North Pole and the y-one complete the triad, lying on the equatorial plane, as it's shown in Fig. 2.8. Here, the ECEF frame is pictured with respect to the NED coordinate system. In order to step from NED to ECEF the rotational matrix 2.4 is required:

$$[T]^{EL} = \begin{bmatrix} -\sin\mu\cos\lambda & \sin\lambda & -\cos\mu\cos\lambda \\ -\sin\mu\sin\lambda & \cos\lambda & -\cos\mu\sin\lambda \\ \cos\mu & 0 & -\sin\mu \end{bmatrix} \tag{2.4}$$

Last but not least, there's another reference frame that is involved in a Six Degrees of Freedom (6DOF) Model, especially to write down Aerodynamic equations in a simple way,

that is the wind coordinates system (Fig. 2.9).

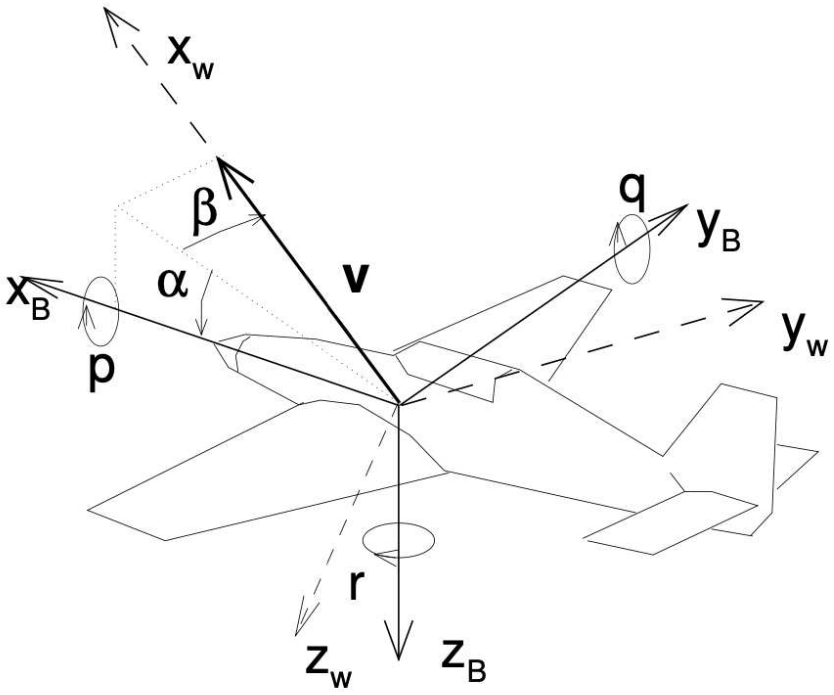

Figure 2.9: Wind Coordinates System [11]

The x_w axis of the wind coordinates system is aligned with the relative velocity, z_w is perpendicular to x_w and on the symmetry plane of the vehicle, y_b completes the triad. This coordinates system is bounded to the body frame with two angles: α angle of attack and β angle of drift.

In the body axis, the velocity is:

$$[v]^B = \begin{bmatrix} u \\ v \\ w \end{bmatrix} = V \begin{bmatrix} \cos\alpha\cos\beta \\ \sin\beta \\ \sin\alpha\cos\beta \end{bmatrix} \tag{2.5}$$

From which the relation between body velocity and aerodynamic angles are obtained:

$$\alpha = atan\frac{w}{u}; \qquad \beta = asin\frac{v}{V}. \tag{2.6}$$

2.3 Rotation Quaternions

While working with goniometric functions such as sine and cosine, it is advisable to run into singularities. To get around this problem, it is possible to take advantage of quaternions algebra. Quaternions are four parameters that identifies the direction of the axis of instant rotation and the entity of this rotation. The fourth parameter imposes a unitary norm. It is possible to calculate the value of quaternions from Euler angles as in eq.2.7:

$$\begin{aligned} q0 &= \cos\frac{\psi}{2}\cos\frac{\theta}{2}\cos\frac{\phi}{2} + \sin\frac{\psi}{2}\sin\frac{\theta}{2}\sin\frac{\phi}{2}; \\ q1 &= \cos\frac{\psi}{2}\cos\frac{\theta}{2}\sin\frac{\phi}{2} - \sin\frac{\psi}{2}\sin\frac{\theta}{2}\cos\frac{\phi}{2}; \\ q2 &= \cos\frac{\psi}{2}\sin\frac{\theta}{2}\cos\frac{\phi}{2} + \sin\frac{\psi}{2}\cos\frac{\theta}{2}\sin\frac{\phi}{2}; \\ q3 &= \sin\frac{\psi}{2}\cos\frac{\theta}{2}\cos\frac{\phi}{2} - \cos\frac{\psi}{2}\sin\frac{\theta}{2}\sin\frac{\phi}{2}. \end{aligned} \tag{2.7}$$

Similarly, even the Euler Angles can be derived from quaternions and it's useful in order to obtain an easier view of the results:

$$\begin{aligned} \tan\psi &= \frac{2(q_1q_2 + q_0q_3)}{q_0^2 + q_1^2 - q_2^2 - q_3^2}; \\ \sin\theta &= -2(q_1q_3 - q_0q_2); \\ \tan\phi &= \frac{2(q_2q_3 + q_0q_1)}{q_0^2 - q_1^2 - q_2^2 + q_3^2}. \end{aligned} \tag{2.8}$$

2.4 Equations of Motion

As previously said, the vehicle motion is governed by the two equations 2.1 and 2.2 which provide the relation between force and acceleration, as well as momentum and angular acceleration, where the first is proportional to mass and the second to the inertial moment. Forces acting on a flight vehicle are [16]:

$$F = T + A + W; \tag{2.9}$$

where T is Thrust, A is the aerodynamic force and W is weight. Obviously, if these force

are not centered on the center of gravity of the vehicle, they produce a moment. So, the dynamic of a 6DOF system can be summarized as in Fig. 2.10, where the kinematic part is the one that provides the calculation of quaternions and Euler angles. The time derivative of the rotation quaternion is closely related to the body rates [p,q,r] shown in fig.2.9 thanks to the differential equation 2.10, which allows the attitude determination.

$$\begin{bmatrix} \dot{q_0} \\ \dot{q_1} \\ \dot{q_2} \\ \dot{q_3} \end{bmatrix} = \frac{1}{2} \begin{bmatrix} 0 & -p & -q & -r \\ p & 0 & r & -q \\ q & -r & 0 & p \\ r & q & -p & 0 \end{bmatrix} \begin{bmatrix} q_0 \\ q_1 \\ q_2 \\ q_3 \end{bmatrix} \tag{2.10}$$

Attitude is one of the main topics of a 6DOF model, and it can be expressed in Euler angles with the eq.2.8 to gain a better view of the vehicle attitude motion.

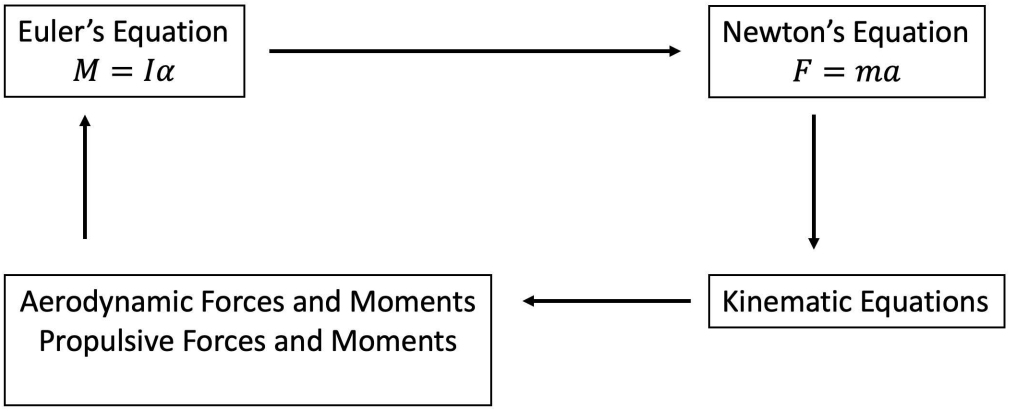

Figure 2.10: Summary of equations of motion of a vehicle [34].

Moving a step back to Newton's Law 2.1, it is important to say that it must be referred to an inertial frame of reference, however, it is possible to switch from a frame to another with a rotational matrix, even to noninertial reference frame, using additional terms as corrections, obtaining a result such as eq.2.11.

$$ma = F + correction \;\; terms \tag{2.11}$$

Referring these correction terms to the particular case taken into account in this thesis, and

so shifting from NED to ECEF and vice versa, it is necessary to include the Earth's angular velocity. In order to do this, two accelerations terms are introduced with eq.2.12:

$$Coriolis\ \ acceleration = 2\Omega \times v_E; \quad Centrifugal\ acceleration = \Omega \times (\Omega \times s_E); \tag{2.12}$$

Where Ω is the Earth velocity, which corresponds to 15°/h, v_E is the vehicle velocity in ECEF and s_E is the position of the vehicle in ECEF.

2.5 Propulsion

A thrust force is needed to overcome drag, gravity and generate the speed necessary to keep flying. Usually, it is directed parallel to the vehicle symmetry axis. Again, the basic principle of rocket thrust is Newton's second law, applied to exhaust stream with velocity c and mass flow $\dot{m}$ (eq.2.13):

$$F = \dot{m}c \tag{2.13}$$

However, the parameter c is barely used, instead, the specific impulse I_{sp} is considered:

$$I_{sp} = \frac{F\delta t}{\dot{m}g_0\delta t} = \frac{F}{\dot{m}g_0} \tag{2.14}$$

where $g_0 = 9.80665\ m/s^2$ and it's Earth's gravity. Solving for F it is obtained:

$$F = I_{sp}\dot{m}g_0 \tag{2.15}$$

And combining the eq.2.13 with the eq.2.15, it's shown the connection between c and I_{sp}: $c = I_{sp}g_0$. This parameter gives an explicit description of the vehicle engine and its propellant. Generally, the thrust is given at sea level and so a correction has to be employed in function of the altitude.

A propulsion technology that is more and more used nowadays is the airbreathing system. It is an engine that absorbs atmospheric air, then compress it, heats and finally expands it again at atmospheric pressure with a nozzle, obtaining a thrust force. Another step, between

the heating and the expansion, can even be included to cool down the air with another nozzle. This one is the turbine gas engine, and the one that doesn't use this additional step can be a ramjet engine or a pulsejet, which is much lighter in terms of weight for this reason. As it can be seen in sec. 4.5.1, the ramjet engine has been selected for the hypersonic vehicle in analysis in this thesis. This type of motor has better performances around Mach 3 and can work even until Mach 6, sometimes exceeding this value. It is composed of three parts:

- an entrance to compress the atmosphere air absorbed;
- a combustion chamber to heat and combust the fuel;
- a nozzle to convert thermic energy in thrust.

A limitation of ramjet engines is that are noncapable to produce thrust if they're not moving and have better performances at high speed, especially in supersonic regimes. However, the air combustion is made at subsonic speeds once the flow has entranced the motor, it drastically slows down to be burnt. The first ramjet motor was designed by I.A. Merkulov and was first tested in 1933. It was the GIRD-04, it was fueled with hydrogen and fed with compressed air up to 200 atm to simulate the supersonic flight [17].

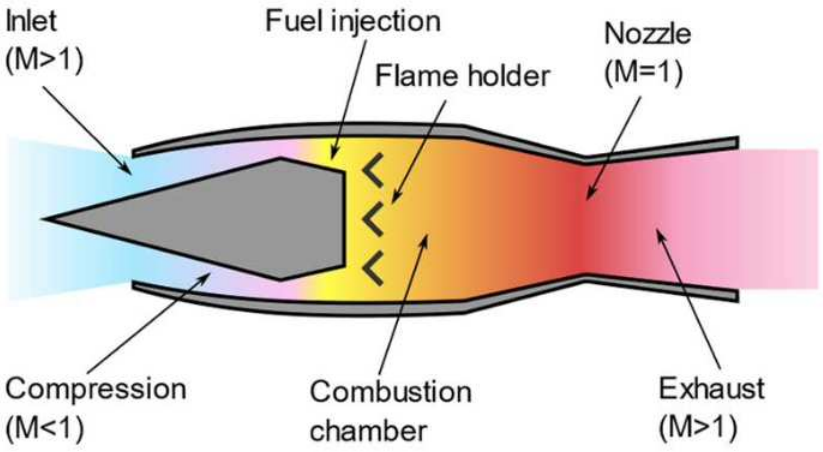

Figure 2.11: Scheme of a ramjet engine [17]

2.6 Aerodynamics

The aerodynamic forces and moments depend on a lot of aspects such as air conditions, attitude and speed. The resultant aerodynamic force F_A can be calculated in any coordinate system, giving three orthogonal components. If it's used the wind coordinate system (fig.2.12), F_A lies in the $x_w z_w$ plane, and there is no side force. The projection of F_A on the x_w axis is called drag force D and the one on the z_w axis is the lift force L.

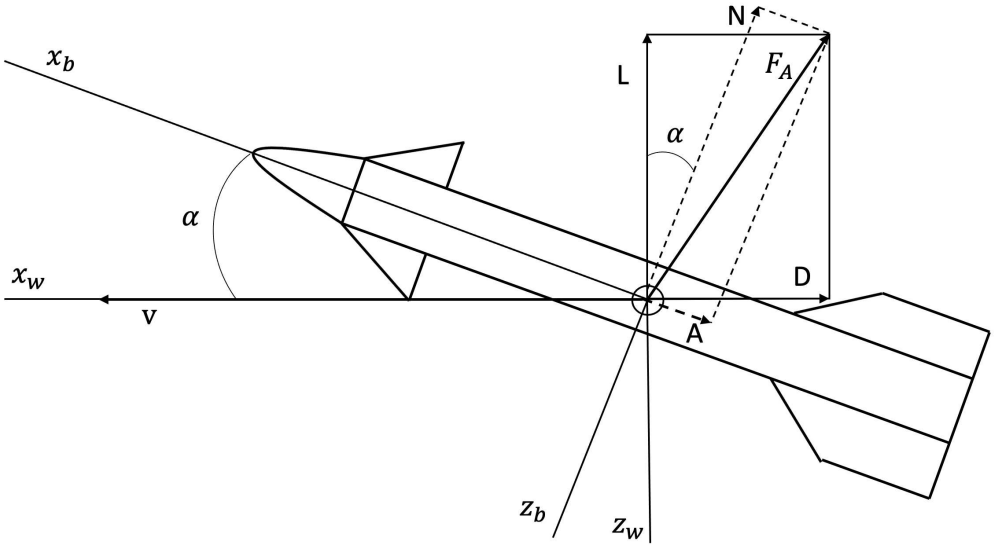

Figure 2.12: Aerodynamics forces in the wind and body coordinate systems.

Of course, if the forces are expressed in the wind coordinate system, they have to be transformed into another body frame to be used in the motion equation (eq.2.16):

$$A = D\cos\alpha - L\sin\alpha; \quad N = D\sin\alpha + L\cos\alpha. \tag{2.16}$$

And once the forces are written down in body coordinates, they can be rotated in NED or ECEF or whatever reference system with the opportune rotating matrix. Whatever the coordinate system is, the fluid in which the vehicle exercises a force due to normal pressures and tangential stresses caused by the relative motion between air and surface S of the vehicle [11]:

$$\mathbf{F} = -\iint_S p\mathbf{n}dS + \iint_S \tau\mathbf{t}dS \tag{2.17}$$

where **n** and **t** are, respectively, normal and tangent versors to the flight object surface. Generally, the force F can be expressed as well as:

$$\mathbf{F} = \frac{1}{2}\rho V^2 S \ \mathrm{C}_{\mathbf{F}} \tag{2.18}$$

Considering the wind axis, C_F is a vector parallel to **F**, where its components are the aerodynamic coefficients that depend on aerodynamic angles, angular velocity of the vehicle, Reynolds number *Re* and Mach number *Ma*.

So, the aerodynamic force can be expressed as in relation 2.19:

$$\mathbf{F} \equiv -\begin{bmatrix} D \\ Y \\ L \end{bmatrix} = -\frac{1}{2}\rho V^2 \ \mathrm{S} \begin{bmatrix} C_D \\ C_Y \\ C_L \end{bmatrix} \tag{2.19}$$

The equation 2.19 gives the definitions of Drag, Deviant and Lift forces. Lift and Drag are extremely important for the evaluation of vehicle performances because of their dependency on the vehicle's aerodynamic characteristics. Deviant force, instead, is a non-zero value only in a drift maneuver and for $\beta \neq 0$ it produces a reduction of the flight performances. Drag force is parallel and opposite of the rocket velocity, gaining the aspect of a dissipative force. The lift and the drag forces are perpendicular to the velocity, with a null work.

2.7 Gravity Model

According to Newton's theory, the force of attraction F between two bodies M and m with a respective distance r is 2.20:

$$F = G\frac{Mm}{r^2} \tag{2.20}$$

With G as the universal gravitational constant. Considering m as the rocket mass and M as the Earth one, the gravity acceleration on the flight vehicle is 2.21:

$$g = \frac{F}{m} = \frac{GM}{r^2} \tag{2.21}$$

Equation 2.21 could be a great approximation if Earth had a spherical shape. But, being Earth a geoid, the expression needs a little complication to gain major accuracy. It is necessary to involve spherical harmonics to improve the representation of the gravitational field.

This work came from the Defense Mapping Agency's "U.S. World Geodetic System 1984 (WGS84)" study [9].

The *U.S. World Geodetic System 1984 (WGS)* Committee determined that the value of GM is 3.986005×10^{14} m^3/s^2 and that the second-degree zonal gravitational coefficient is $\bar{C}_{2,0} = -4.841668 \times 10^{-4}$. So, considering the Earth as an ellipsoid, the gravitational acceleration acting on the flight vehicle is 2.22 [34]:

$$[g]^G = \frac{GM}{|s_{BI}|^2} \begin{bmatrix} -3\sqrt{5}\bar{C}_{2,0} \left(\frac{a}{|s_{BI}|}\right)^2 \sin\lambda_c \cos\lambda_c \\ 0 \\ 1 + \frac{3}{2}\sqrt{5}\bar{C}_{2,0} \left(\frac{a}{|s_{BI}|}\right)^2 \left(3\sin^2\lambda_c - 1\right) \end{bmatrix} \tag{2.22}$$

It is well to notice that imposing $\bar{C}_{2,0} = 0$ the expression 2.22 leads to 2.21.

Chapter 3

Geometry of the Vehicle

Searching the literature about vehicle geometries and relative datasets was necessary to gain a flight simulation with reliable results. It was not that easy to find clear documentation with all the data needed for a generic hypersonic vehicle, but after a while, an interesting research jumped to the eye. It was not properly the vehicle waited for, but it was a nice compromise to test the model. It is a preliminary study of a small hypersonic airplane named HyPlane. [31] With the privatization of the space market, the authors of this work have caught the urge to a different approach even to the tourism market, in which private companies are investing. In a few words, it is an experience where a human can test microgravity (thank's to the sub-orbital trajectory) and a really fast point-to-point transportation. The most important specifications of the aircraft are:

- high aerodynamic efficiency and low wing loading;
- thrust coming from two Turbine Based Combined Cycle (TBCC) engines, plus a Rocket motor;
- materials can withstand the aero-thermoelastic stress due to hypersonic flight.

These features guarantee the capability of the HyPlane to stand subsonic, transonic, supersonic and even hypersonic flight, with the last one being the most challenging to study for the authors, due to the aero-thermoelastic effects that this type of motion implies.

3.1 HyPlane Aircraft

This vehicle is a concept of the University of Naples "Federico II" with the support of other academic institutions. This small airplane is designed to have six seats and to guarantee a sub-orbital trajectory of long duration flying up to hypersonic speed.

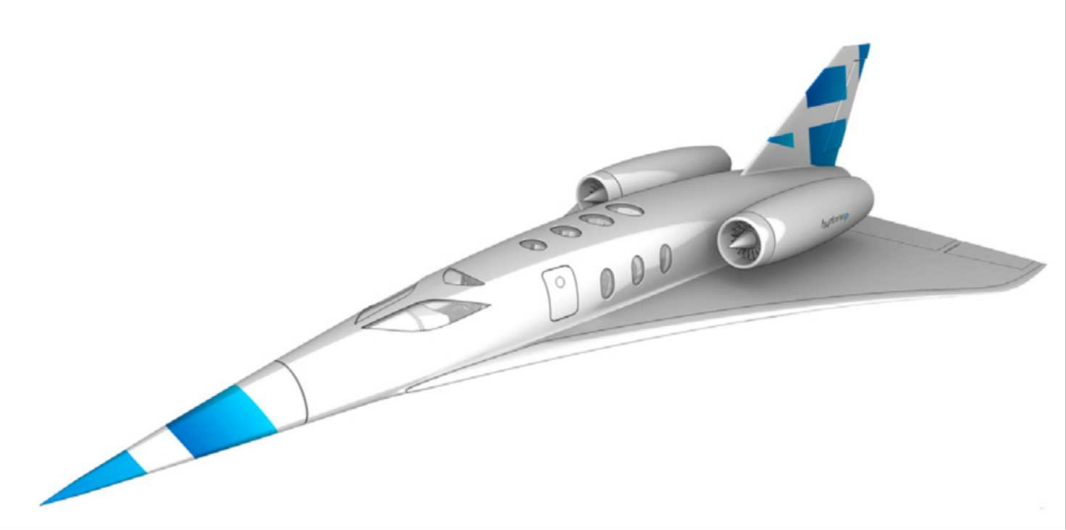

Figure 3.1: HyPlane concept design.[13]

This concept came from other available technologies already flying and other studies in this compound. It is composed of a fuselage, a variable delta wing with four elevons (two internal providing pitch control and two external named ailerons, providing roll control), and a vertical tail with a rudder. The wing area is big enough to guarantee the vehicle takeoff with low velocity and to reduce as much as possible the sonic boom and the heating problems due to high speed.

Vehicle geometry can be summarized in table 3.1.

3.2 Possible Materials for the HyPlane

Working with a hypersonic vehicle, the material choices are even more important than the ones made for other aircrafts. All the HyPlane parts have to resist extremely high stresses due to the aero-thermoelastic effects of this high velocity. After a preliminary CFD analysis, it was possible to gain a possible material scenario for some critical parts of the vehicle. So, as it might be noticed in Figure 3.2, the nose, wing and vertical tail leading edge, and control

Geometric Parameters	
Fuselage length [m]	23.6
Nose radius of curvature [m]	0.03
Wing area [m ^{2}]	140
Wing span [m]	13.5
Vertical tail span [m]	3.6
Vertical tail area [m ^{2}]	14
Wing mean aerodynamic chord [m]	12
Airfoil leading edge radius of curvature [% chord]	0.07
Airfoil maximum thickness]	3
Airfoil thickness location [% chord]	30
Center of gravity longitudinal position at takeoff condition [m]	16
Center of gravity longitudinal position at zero-fuel condition [m]	14
Pole longitudinal position for pitching moment calculation [m]	15

Table 3.1: Geometry configuration of the vehicle. [13]

surfaces reach the highest temperatures of the vehicle, exceeding 400°C. For these surfaces, materials such as Carbon fiber reinforced ceramics or actively cooled solutions, seem to be a proper choice. Going a bit down with the temperature, there are wing and fuselage surfaces, stepping from 300 to 400°C. For these areas, a Titanium alloy could be a good solution. For the other parts, where the temperature is always under 300°C, the material choices are less restricted. Wanting to make a clever trade-off between resistance to stress and weight, a light-temperature carbon fiber composite material could be selected Fig. 3.3.

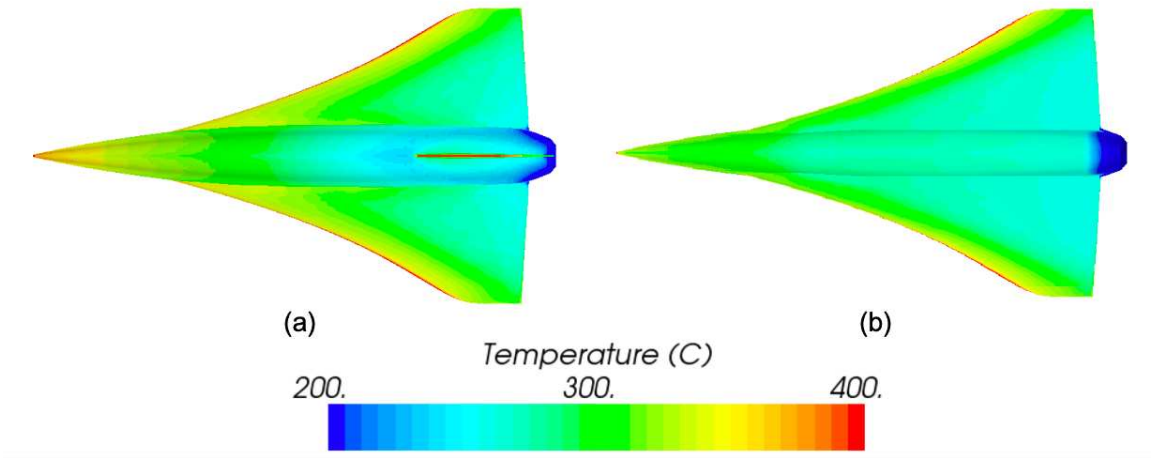

Figure 3.2: Temperature Distribution with CFD simulations, M=4, H=30km.[31]

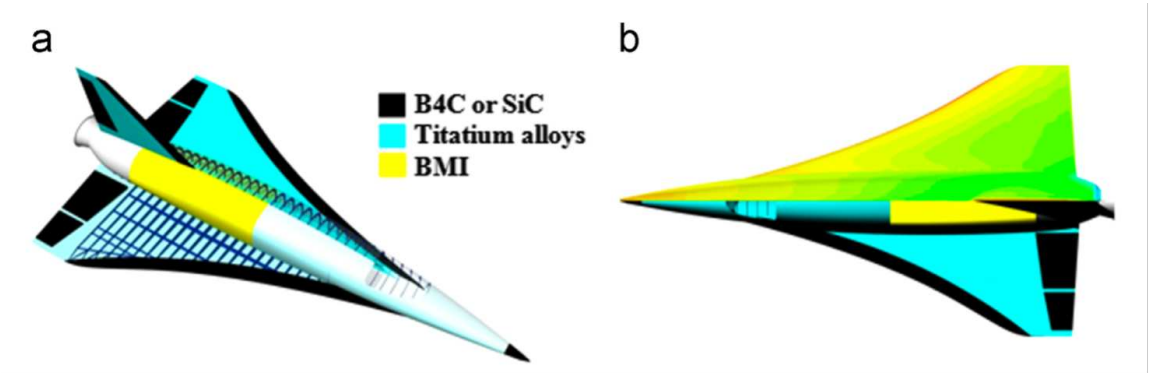

Figure 3.3: Possible choice of materials for the HyPlane. [31]

3.3 Mass Distribution

Now, having an idea of the material densities, the total mass of the HyPlane can be found easily with a preliminary mass budget studying the internal configuration of the vehicle.

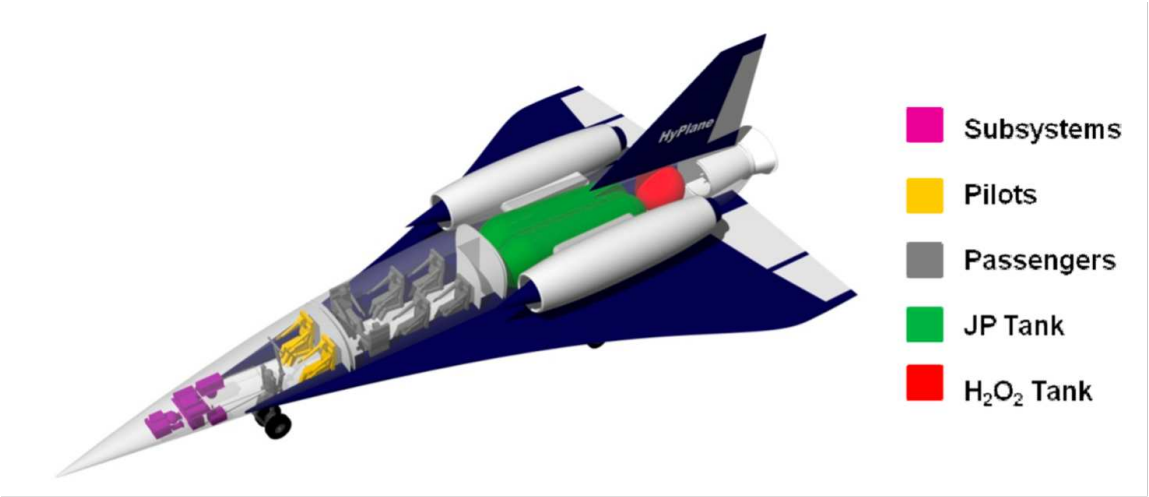

Figure 3.4: Mass distribution throw the vehicle. [31]

Analyzing other vehicles and following the engineering design of the subsystem in Figure 3.4, some assumptions were made:

- Following either the worst case possible and the Federal Aviation Administration, passengers, and crew weight has been estimated as 100 kg per person, considering all the people as male passengers traveling in winter;
- The propellant mass at the beginning of the mission depends on the mission itself;
- The empty HyPlane mass has been estimated from the HASA model. [14]

For this study, it has been considered a crew composed of two members, six passengers traveling, and a fuel mass of 60% of the vehicle. With an accuracy of 20%, it has been calculated that the total mass of the HyPlane is around 26 tons and its distribution is similar to Figure 3.4. The percentage of the mass of the parts of the aircraft is presented in Table 3.2 and Table 3.3. It is easy to determine that the structural mass is nearly 5.5 tons with its most percentage in the HyPlane body, followed by the wing, and the vehicle weight without fuel is around 10 tons.

Vehicle main components	Percentage of the total mass [%]
Fuel	61
Structure	21
Propulsion	9
Subsystem and crew	6
Payload	3

Table 3.2: Mass distribution throw the vehicle in percentage. [31]

Structural components	Percentage of the total structural mass [%]
Body	60
Wing	17
Landing gear	12
Vertical tail	7
Thermal protection system	4

Table 3.3: Mass distribution throw the HyPlane structure. [31]

Considering the total length of the aircraft, which is 23.6m, the center of gravity is located at 16m at takeoff and it moves two meters with the consumption of fuel, arriving at 14m when all the propellant has been used.

3.4 Vehicle Mission Scenarios

As previously said at the beginning of this chapter, HyPlane has to be able to fly both in sub-orbital parabolic trajectory and in point-to-point transportation, thank's to the TBCC engines and the rocket motor. It is planned for a horizontal takeoff with turbojet engines, a phase of uphill to reach 30km of altitude where it is possible to reach hypersonic speed. Here the vehicle can perform its nominal mission which is named "the hypersonic cruise over transcontinental distances" for 6000 km with the ramjet engine or a sequence of three suborbital parabolas using

a rocket motor, the second experience can make the condition where all the passengers can try an increase of acceleration finishing with the weight lessness at nearly 65km of altitude. Then, after a maneuver in hypergravity conditions, the vehicle flies in steady conditions following a horizontal path. Last, HyPlane does a gliding landing, ending horizontally. [30]

Engine Type	Ascent RBCC Ejector-rocket Ramjet	 TBCC Turbo-Ramjet// Ramjet	Cruise RBCC	Descent TBCC	Gliding
Average Specific impulse [s]	1200	1715	1700	1700	–
Average Thrust [kN]	140	98	31	37	–
Duration [min]	5.8	8.7	51	57	18.8
Range [km]	305	375	3660	4110	415
Average TSA [g]	1.05	1.05	1.00	1.00	0.630
Maximum L/D [-]	6.0	6.0	3.8	3.9	5.3

Table 3.4: Flight performances during HyPlane flight. [30]

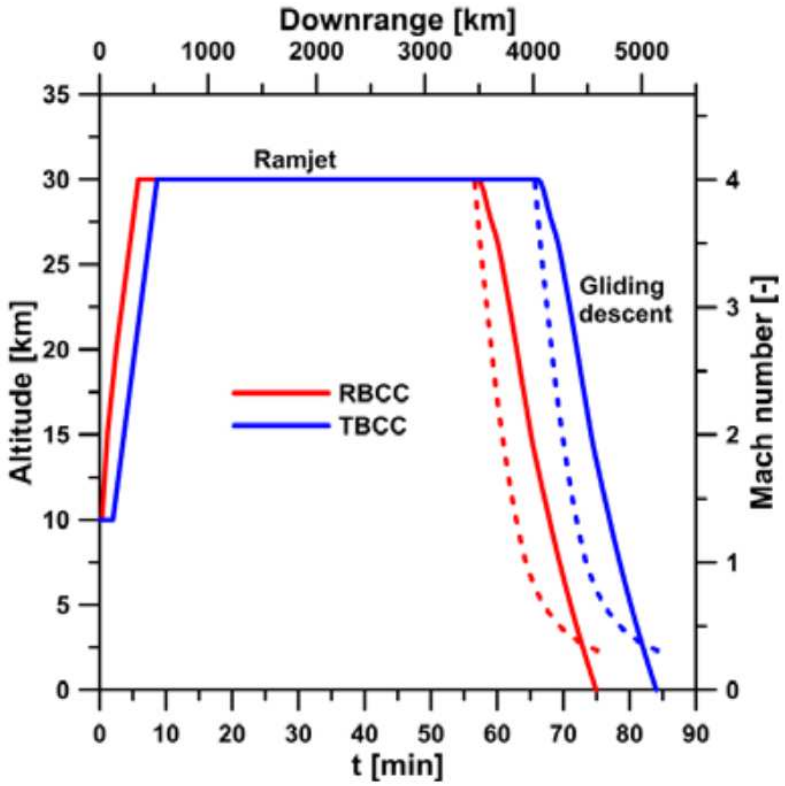

Figure 3.5: Design of a possible trajectory for HyPlane vehicle. [30]

This project taken into analysis, even if it is only a preliminary study, was important for the development of the 6DOF model of this thesis because it was full of all the data needed (that will be discussed in Ch. 3) to gain reliable results.

Chapter 4

Building of the 6DOF Model

Now, having all the theoretical and practical elements needed, the 6DOF can be built. As previously said in Chapter 2, for the development of this thesis, it was used MATLAB® software. Specifically, MATLAB® was used to define all the constants, initial states, and for the look-up tables, and its extension, Simulink® , was employed to build the 6DOF itself. Figure 4.1 presents an overview of the model in macro-blocks to have an idea of how it works.

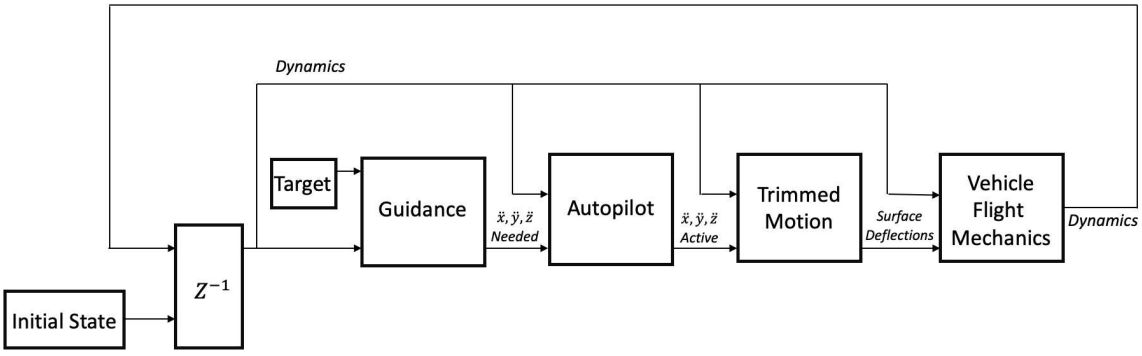

Figure 4.1: Overview of the 6DOF model

The initial state block provides the initial dynamic state of the HyPlane in terms of attitude, position, velocity, acceleration, mass, and inertia. This information is given to the guidance subsystem as well as the initial state of the Target to find the correct acceleration input to give to the aircraft to intercept a desired point. Then, this acceleration is processed in an active acceleration by the autopilot system. Now, the active acceleration can be converted into a

deflection command of the aerodynamic surfaces to reach the correct maneuver. Finally, this control is managed in the flight mechanics subsystem where all the vehicle dynamics details are elaborated to have the next state of the object taken into study.

4.1 Initial State of the Vehicle

In the initial state subsystem, it is defined the initial state of the vehicle, especially through a MATLAB® script providing initial position, velocity, acceleration, attitude, mass, inertia as well as all the geometry data Fig.4.2.

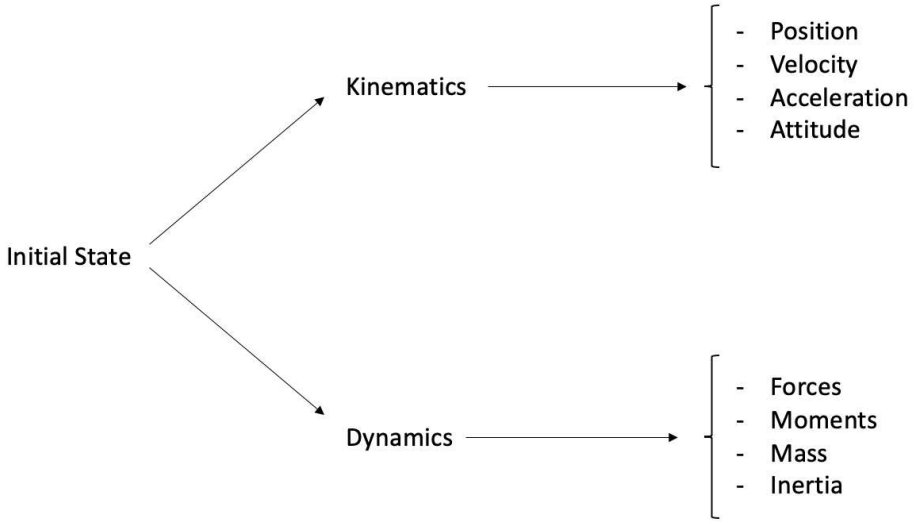

Figure 4.2: Scheme of the initial vehicle data as they are in the Initial State block.

Working with a hypersonic vehicle means, first of all, high speed, high altitude, and long distances. With these hypotheses, the approximation of a flat Earth is less accurate, so it was decided to proceed using ECEF coordinate system. However, to gain a better interpretation of the results, it was chosen to convert the position even in NED. The MATLAB® script with all the information starts giving geometry and mass data. Then, it provides the initial latitude, longitude, and altitude of the vehicle, as well as azimuth and elevation, velocity, and acceleration magnitude, to be converted into all the coordinate systems needed from the model. Proceeding further,it is defined the initial attitude of the HyPlane in Euler angles, converted in quaternions immediately after, initial body rates, and angular acceleration. For

the dynamic part, forces and moments were imposed as zero, except for gravity, which is given in the NED system, in form of acceleration, as a vector with a component only on the z-axis which is the standard $9.81 m/s^2$ value. Lastly, mass and inertia come from the MATLAB® script as previously said.

4.2 Guidance System

The Guidance block in the 6DOF model is needed to give appropriate flight commands to the vehicle to gain certain specific points. Given the state of the vehicle and of the objective, such as position, velocity, and attitude, the guidance block should be able to transmit to the autopilot all the commands to lead the vehicle to the desired point. For flight vehicle simulation models are available a lot of types of guidance systems. In this study, the proportional navigation law was chosen as the foundation for the guidance subsystem. *Proportional Navigation (PN)* is the oldest guidance system. It was a principle used even by pirates to attack other ships and steal all their belongings. It is a very simple and reliable system, and, for these reasons, is still used nowadays as an algorithm to intercept objectives. The *Line-of-Sight Vector (LOS)* vector is the displacement vector between the vehicle and the desired point. To gain the interception of the objective, the LOS vector orientation has to be fixed in inertial space.

Until the relative velocity vector v_{BT}^{E} is pointing to the desired point, the vehicle is going to intercept this one, assuming constant velocities. This triangle, which has taken the name "Engagement triangle" (Fig. 4.3) can be considered in two dimensions as well as in three. For a simpler argumentation let's consider the *Two Dimensional (2-D)* case. To obtain an approach between the target and the vehicle, the flight path angle and the LOS angle have to remain constant during all the trajectories. If the target is moving through an escaping maneuver, the interceptor has to change his velocity vector by consequence, following the angle LOS variation. In other words:

$$\dot{\gamma} = N\dot{\lambda} \tag{4.1}$$

Where N is the navigation ratio, that is a proportionality constant. The eq.4.1 is known as the PN relationship. Generally for N is chosen a value between two and four, for modern

guidance systems it's three in most cases.

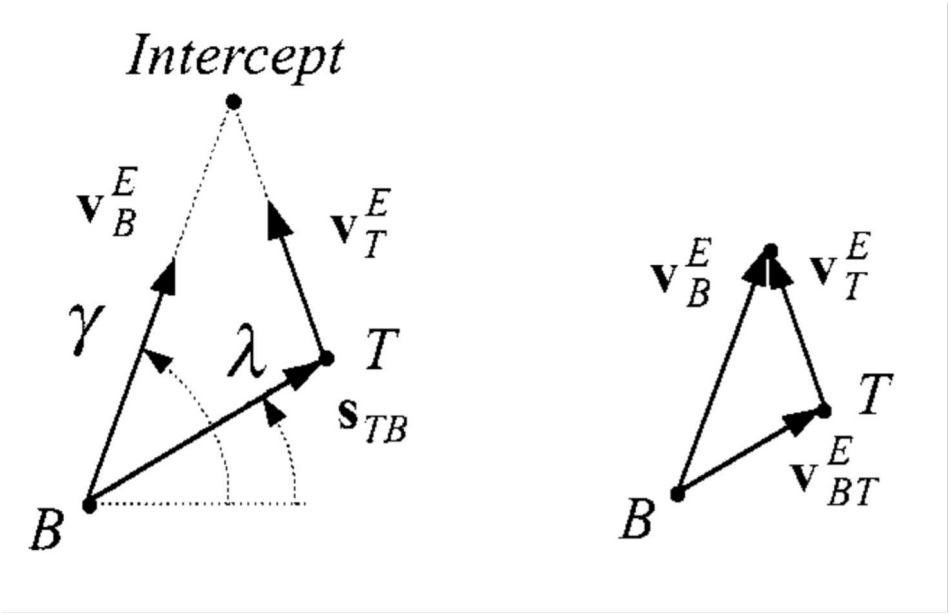

Figure 4.3: Engagement triangle. λ is the LOS angle, γ is flight path angle. T stands for Target and B for the interceptor vehicle. v_{BT}^E is the differential velocity of the vehicle with respect to the target which is obtained as: $\boldsymbol{v}_{BT}^E = \boldsymbol{v}_B^E - \boldsymbol{v}_T^E$. [34]

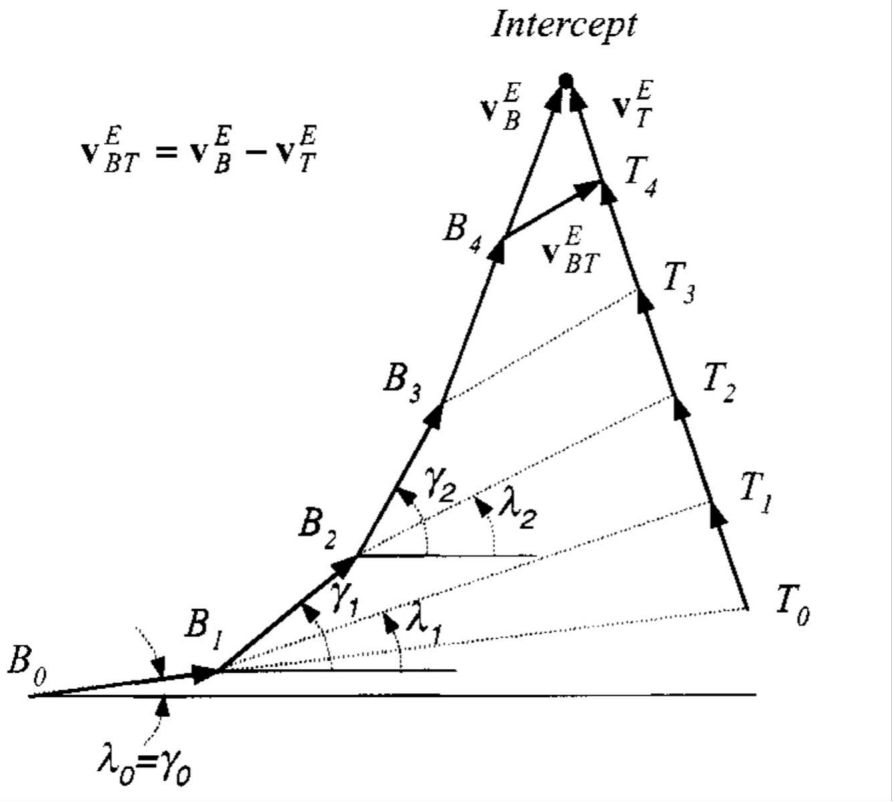

Figure 4.4: Engagement triangle with a moving Target starting from arbitrary conditions. [34]

Taken a look at Fig.4.4 and assuming constant velocities for the vehicle as well as for the desired point, it is noticeable that the advancing of the target leads the LOS angle to a variation $\dot{\lambda}$ that turns the aircraft by $\dot{\gamma}$, magnified by N as seen in the relation 4.1. The LOS variation is converted by the guidance system in an acceleration command to the autopilot as in eq.4.2:

$$a = NV\dot{\lambda} \tag{4.2}$$

Considering the relation 4.1, eq. 4.2 can be written as:

$$a = V\dot{\gamma} \tag{4.3}$$

The relations 4.1 and 4.2 are only for the 2-D case, but considering the *Three Dimensional (3-D)* case, the equations follow by similitude. Considering ω^{UE} as the LOS angular velocity concerning the inertial Earth frame E and $\boldsymbol{\omega}^{VE}$ the angular velocity vector of the v_B^E vector concerning Earth, the eq.4.1 in 3-D is:

$$\boldsymbol{\omega}^{VE} = N\boldsymbol{\omega}^{OE} \tag{4.4}$$

And so, the equivalent in 3-D of the relation 4.3 is:

$$\boldsymbol{a} = V\boldsymbol{\Omega}^{VE}\boldsymbol{u}_v \tag{4.5}$$

Putting together eq.4.4 and 4.5, the guidance acceleration command can be found:

$$\boldsymbol{a} = NV\boldsymbol{\Omega}^{OE}\boldsymbol{u}_v - \boldsymbol{g} \tag{4.6}$$

With, in addition, the gravity term which is fundamental, otherwise zero acceleration would be commanded, founding a simple ballistic trajectory. In Fig.4.5 can be seen a simple scheme of the implementation of the Proportional Navigation Law.

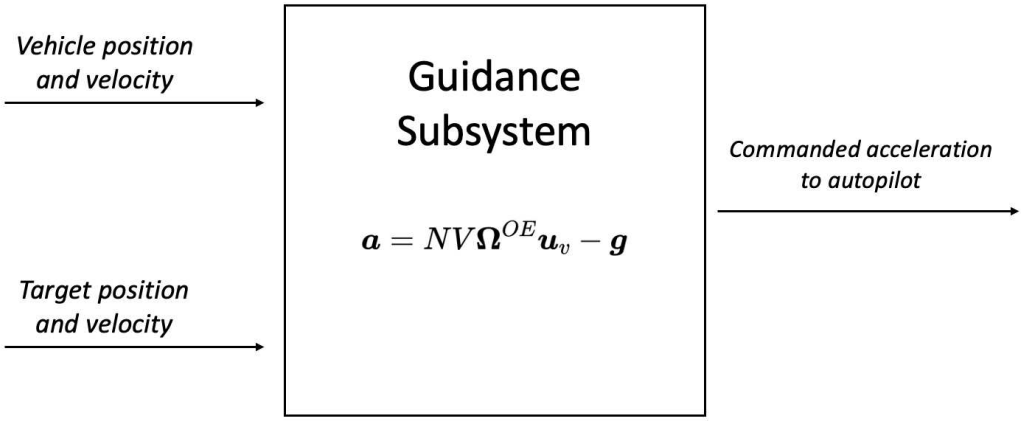

Figure 4.5: Simple scheme of the implementation of the Proportional Navigation Law in a guidance system.

4.3 Autopilot

The autopilot acting on the vehicle presented in this thesis is pretty simple. However, before starting with the explanation of how it works, it is important to recap which are the major forces acting on the aircraft in the body system.

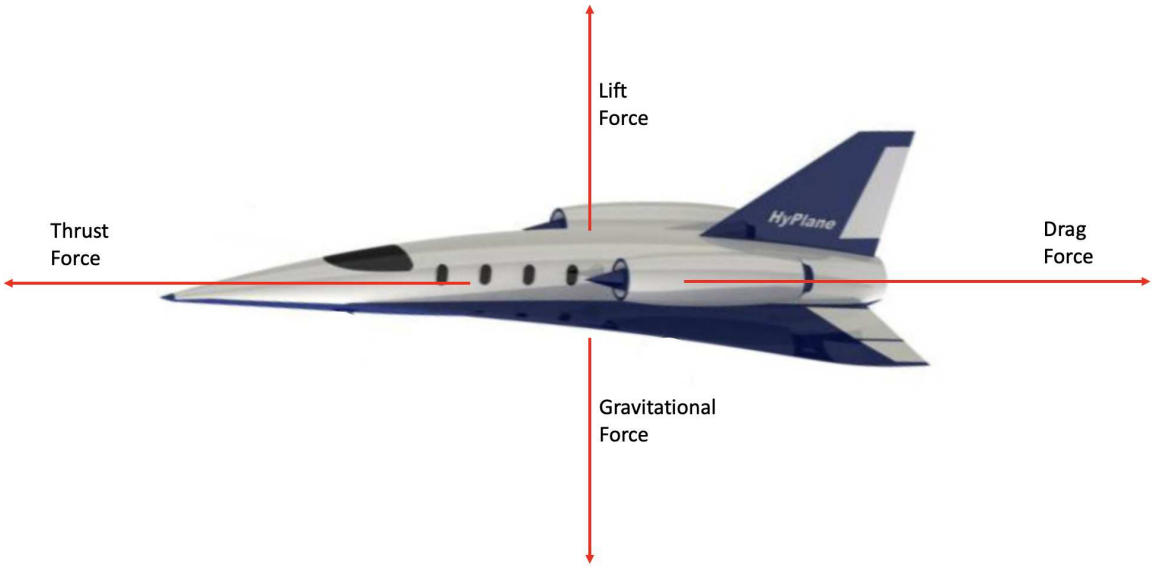

Figure 4.6: Simple scheme of the major forces acting on the vehicle in body system, posing aerodynamic angles α and β equal to zero.

Let's suppose, for now, that the aerodynamic angles α and β are equal to zero, and so that

the wind axis coincides with the body axis. With this hypothesis, the major forces acting on the flight body are those presented in fig.4.6. It is clear to see that Drag Force needs to be balanced by the Thrust one, which is commanded by the motor and is easily maneuverable with a lever. Instead, the gravitational force has to be balanced by the lift one which is way more complicated to manage. One way to increase or decrease efficiently the lift force is the deflection with the moving surfaces of the vehicle, like ailerons, elevons, rudders, etc. Now, let's get back to the autopilot system. As said in section 4.2, the Guidance subsystem gives the autopilot a command in terms of acceleration, in the case of the model implemented for this thesis, in the NED coordinate system. This command is translated into the body system. Only the y and z axis are taken into account, because, as already explained, the drag force is compensated by the thrust force and not really controllable. The accelerations demanded from the guidance subsystem are confronted with the ones coming from aerodynamic to set if the command is actionable. If the aerodynamic accelerations are greater than the ones coming from the guidance, the command is doable and the output of the autopilot is the active acceleration needed to intercept the target. If not, the output of the autopilot is the accelerations that are possible to gain by the vehicle, even if those are not enough to reach the objective (fig.4.7). These active accelerations are given to the next subsystem to be transformed into angular deflection commands.

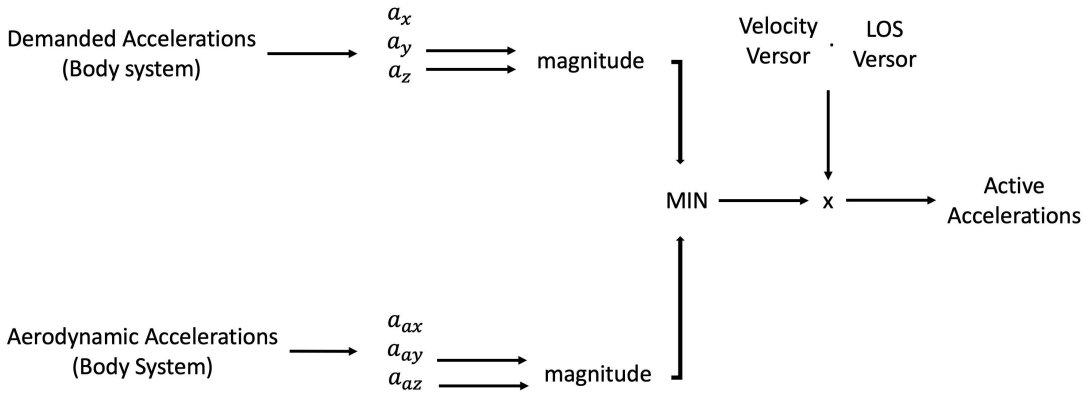

Figure 4.7: Simple scheme of the autopilot subsystem.

4.4 Trimmed Motion

To step from the saturated accelerations of the autopilot system to an angular command of the moving surfaces of the vehicle, it is necessary to introduce another subsystem between the autopilot itself and the vehicle environment. For this thesis, instead of building a complicated control system, a trimmed flight for the aircraft with the addition of a pitching moment to reach the capability of doing a pull-up maneuver, has been supposed. With "Trim" it is intended as a condition for a steady-state flight which provides a lot of simplifications for the flight aerodynamics of the vehicle. The following hypotheses are assumed:

- $\dot{V}, \dot{\gamma}, \dot{Q}, \dot{\alpha}$ and β are zero, with $\dot{Q} = M/I_{yy}$ being the variation of the Pitch rate and M being the Pitching moment;
- γ and α are small;
- $T - D - W\gamma = 0$;
- $L - W = 0$;
- M = 0 [16].

Wanting to write down those conditions in a non-dimensional way, the aerodynamic coefficient can be used (eq. 4.7):

$$\begin{aligned} C_T - C_D - C_W\gamma &= 0 \\ C_L - C_W &= 0 \\ C_m &= 0 \end{aligned} \tag{4.7}$$

All the aerodynamic coefficients are a function of several terms such as M, α, $\dot{\alpha}$, surfaces deflections δ_E, p, q, r, etc. a way to write down their complete expressions could be, for C_L and C_m:

$$\begin{aligned} C_L &= C_{L_0}(M) + C_{L_\alpha}(M)\alpha + C_{L_{\delta_E}}(M)\delta_E \\ C_m &= C_{m_0} + C_{m_\alpha}\alpha + C_{m_{\delta_E}}\delta_E \end{aligned} \tag{4.8}$$

Combining eq. 4.7 with eq. 4.8, eq. 4.9 can be obtained:

$$\begin{aligned} C_T - C_{D_0} - KC_L^2 - C_W\gamma &= 0 \\ C_{L_0} + C_{L_\alpha}\alpha + C_{L_{\delta_E}}\delta_E - C_W &= 0 \\ C_{m_0} + C_{m_\alpha}\alpha + C_{m_{\delta_E}}\delta_E &= 0 \end{aligned} \tag{4.9}$$

Considering that h, M, W, and T are usually given and that the flight path inclination can be calculated, the eq. 4.9 can be solved for α and δ_E:

$$\begin{aligned} \alpha &= \frac{(C_L - C_{L_0})\, C_{m_{\delta_E}} + C_{m_0} C_{L_{\delta_E}}}{C_{L_\alpha} C_{m_{\delta_E}} - C_{m_\alpha} C_{L_{\delta_E}}} \\ \delta_E &= -\frac{C_{L_\alpha} C_{m_0} + C_{m_\alpha}\,(C_L - C_{L_0})}{C_{L_\alpha} C_{m_{\delta_E}} - C_{m_\alpha} C_{L_{\delta_E}}} \end{aligned} \tag{4.10}$$

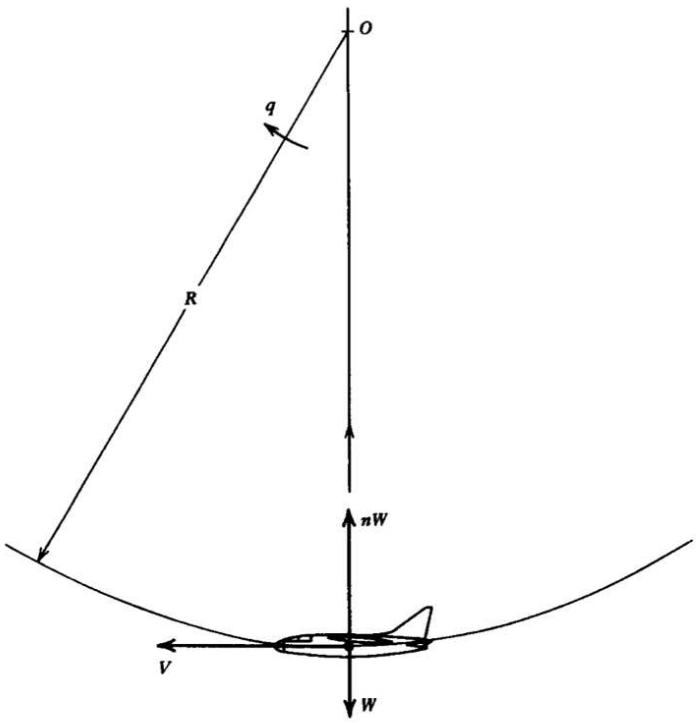

Figure 4.8: Pull up maneuver scheme.[3]

Wanting to reach the capability of doing a pull-up maneuver, it is not possible to consider the C_m moment equal to zero as it is shown in Fig. 4.8, so the hypothesis made for this thesis in this subsystem are a little different than those that were made for a proper trimmed motion. It has been supposed, for a previous preliminary test of the model, that:

- β is equal to zero

- q and $\dot{\alpha}$ are neglectable;
- L is nearly W and D is nearly Thrust (α is little);
- $L - W = 0$;
- p, r, rudder and ailerons deflections are zero;
- the elevons move symmetrically, so the right and left elevon deflections are the same.

So, to transform the autopilot acceleration into an angular command it has been chosen to use the aerodynamic tables, which will be discussed in section 4.5.5, but in reverse.

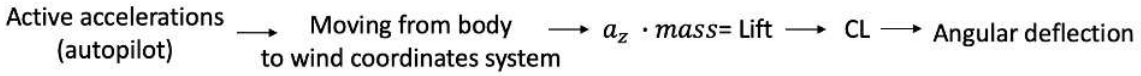

Figure 4.9: Elevon angular deflections calculation method

As it is shown in Fig. 4.9, the active autopilot accelerations are taken and transposed from the body to the wind coordinate system. This way, the acceleration acting on the z-axis has become the lift acceleration as is shown in Fig. 2.9. With the multiplication of the acceleration with the aircraft mass, the acceleration can be transformed into the lift force. Knowing that C_L expression is eq. 2.19, this coefficient can be calculated because ρ, velocity, and the reference surface, which is the wing area, are known. The Look-Up Tables built[12] provides C_L as in eq. 4.11:

$$c_{\mathrm{L}} = c_{\mathrm{L\ basic}} + \Delta c_{\mathrm{L\ elevons}} + \Delta c_{\mathrm{L\ airelons}} + c_{\mathrm{L}\dot{\alpha}} \frac{\dot{\alpha}\bar{c}}{2V} + c_{\mathrm{L}\hat{q}} \frac{q\bar{c}}{2V} \tag{4.11}$$

Posing previous conditions the last three terms are neglectable and from a simple subtraction, $\Delta c_{\mathrm{L\ elevons}}$ can be obtained. Now, reversing the Look-Up Table and knowing Mach number as well as $\Delta c_{\mathrm{L\ elevons}}$, the elevons deflection to reach the target position can be esteemed.

4.5 Vehicle Flight Mechanics

Vehicle flight mechanics is the fulcrum of the model, providing the states of the aircraft by studying forces and moments acting on the flying body and their reactions.

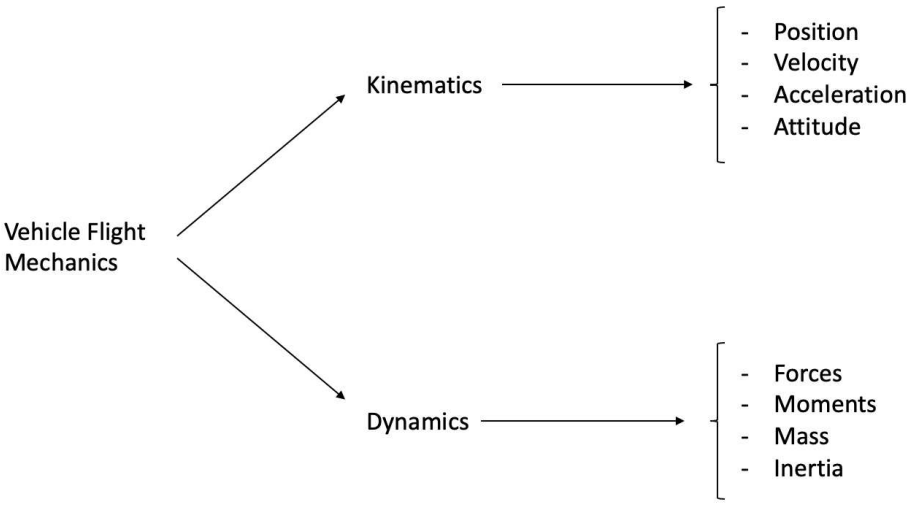

Figure 4.10: Scheme of the vehicle dynamics block.

As it might be seen from fig.4.10 the skeleton of this subsystem is the same as the one of the initial states, but this section provides the vehicle states instant by instant using the Simulink® tool of the Discrete-Time integrator. In particular, Euler backward has been used, with Runge-Kutta as the method of integration, with a fixed step of 0.05 seconds. Proceeding following the exact 6DOF model order, in the dynamic subsystem can be found:

- Thrust subsystem;
- Gravity subsystem;
- Apparent accelerations subsystem;
- Atmosphere model subsystem;
- Aerodynamic subsystem.

Following the kinematics block, there are two main systems:

- Translational motion;
- Angular motion

Each one of these blocks is fully described in the next sections, providing their output and their main scope in this 6DOF model.

4.5.1 Thrust Subsystem

The Thrust subsystem came directly from Fig.4.11, carried to the model as a Look Up Table in the function of altitude and Mach number. But let's take a look at what is presented in the plot.

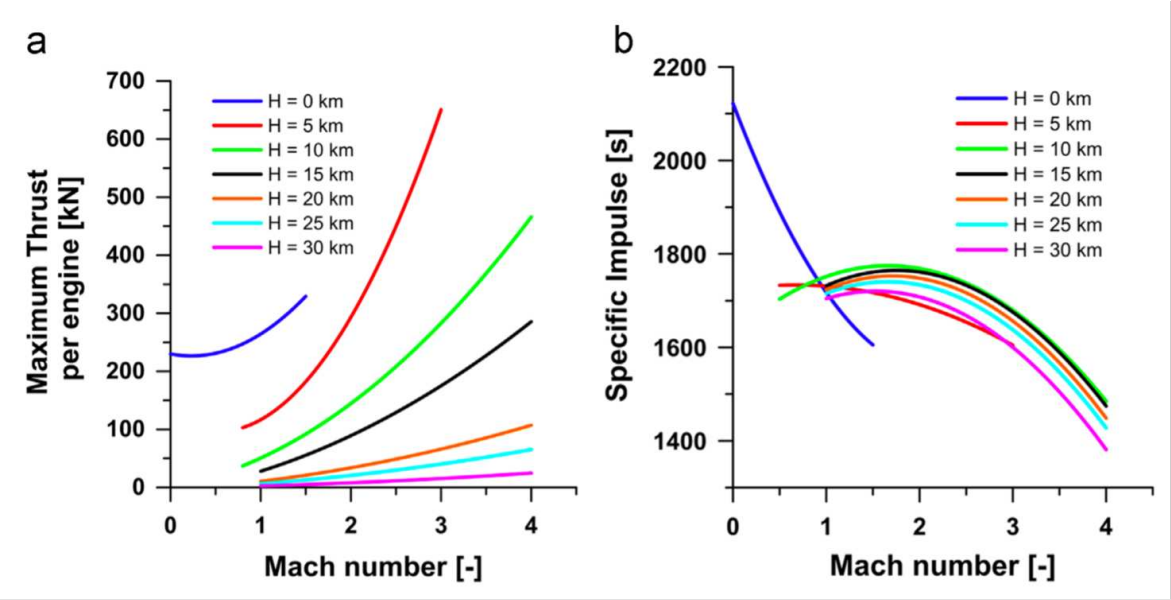

Figure 4.11: a. Maximum Thrust per engine as a function of Mach and altitude. b. I_{sp}. [31]

The HyPlane presented in chapter 3 has been studied to work with the engines whose performances are presented in Fig.4.11. It has been studied that the aircraft taken into exam uses airbreathing hypersonic propulsion, working in multi-modes, and is extremely versatile in a lot of different flight conditions. Wanting to be more specific, the vehicle is thrust by two *Turbine-Based Combined Cycle (TBCC)* engines. This type of engine combines a gas turbine propulsion cycle with a ramjet cycle with a transition that steps over the turbomachinery when the vehicle reaches high Mach numbers, to avoid high temperature, pressure, and flow velocity, because, most of the time, this condition might be impractical or needs engine's redundant parts to guarantee long term work [8]. An example of this technology is the one used in the J-58 engine for the SR71 (Fig. 4.12), which was very innovative for its time (between 1950 and 1960). Putting together the study behind this engine and the state of art innovation technologies, a lot of its downsides can be relieved, using lighter electronic components.

For the HyPlane, has been used a conceptual Mach 4 TBCC developed by the Air Force Research Laboratory, it has been possible to extrapolate the data presented in Fig. 4.11 for

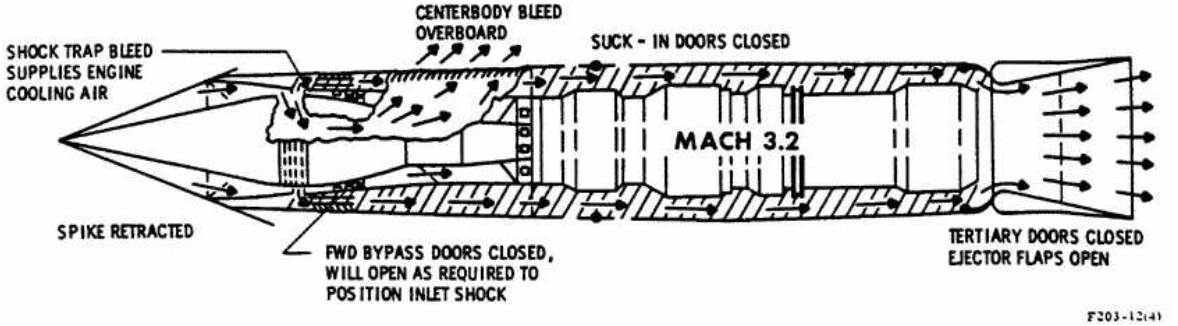

Figure 4.12: TBCC used in J-58 engine. Operation scheme.

Engine	Average thrust [kN]	Average specific impulse [s]
Rocket	200	310

Table 4.1: Rocket engine main parameters.[31]

maximum thrust per engine and specific impulse as a function of Mach and altitude [4]. However, it is not possible to use the TBCC engines for sub-orbital trajectories and so, the HyPlane has been equipped even with a rocket engine, to provide an adequate propulsive force Tab.4.1. It uses H_2O_2 (hydrogen peroxide) as an oxidizer. It can be employed in monopropellant or bipropellant mode, using kerosene as fuel. The second operation mode can guarantee the high thrust needed for suborbital jumps. Moreover, H_2O_2 can guarantee a more than acceptable stability even without a separate ignition system and it is considered a green propellant due to its low emission and toxicity while ensuring high performance.

Another important focus has to be posed in the consumption of propellant: in fact, as the HyPlane flies, the mass changes. The changing of mass changes as well as the inertia moments and the center of gravity (Fig.4.14).

So, the propulsive force has been calculated using Fig.4.11, considering that on the HyPlane there are two engines and that the thrust is applied only on the x-axis in body coordinates producing a null moment. The consumption of fuel has been evaluated with eq.4.12:

$$\dot{m}_p = -\frac{T}{I_{sp} \cdot g_{SL}} \tag{4.12}$$

Where T came from the Thrust of TBCC engines and the I_{sp} is evaluated considering, at the first step, a medium value from Figure 4.12, which is nearly 1700s, g_{SL} is gravity acceleration at sea level.

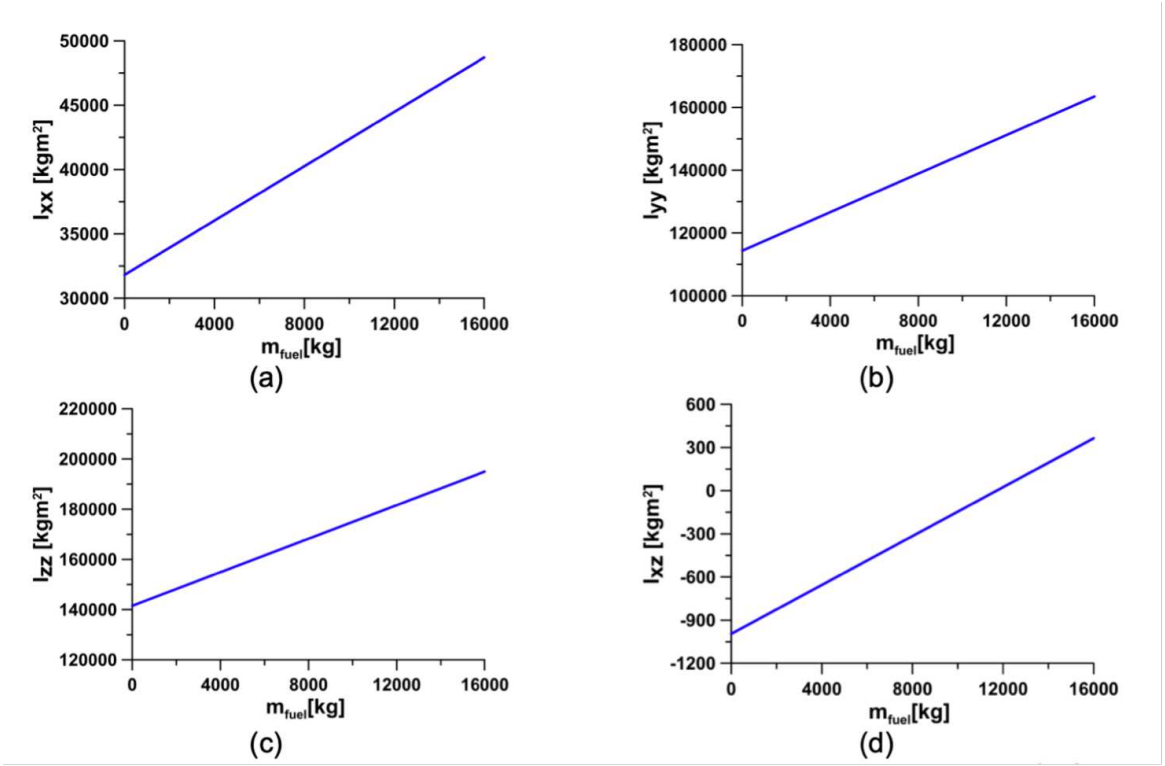

Figure 4.13: Inertia moments decreasing with the consumption of propellant.[12]

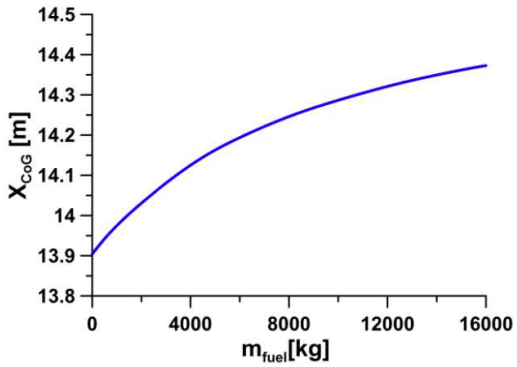

Figure 4.14: Center of Gravity changing its position with the consumption of propellant.[12]

4.5.2 Gravity Subsystem

The model in section 2.7 has been initially considered to work with a major accuracy during the simulation. However, for this initial study of the hypersonic motion of the vehicle, it has been decided to use a simpler formulation of the gravitation effects on the HyPlane, to detect easily eventual errors in the model, with the possibility to complicate the scenario in the future. So, working in NED coordinate system, the gravitational acceleration on the vehicle has been considered as a vector of three components, with the first two equal to zero and the last one positive (because the z-axis is positive downwards in NED) with the value of $9.81 m/s^2$ that is the classical value of gravity on the sea level (eq. 4.13). Due even to the coordinate system, the Earth has been supposed flat (Fig. 4.15).

$$[g]^G = \begin{bmatrix} 0 \\ 0 \\ 9.81 \end{bmatrix} [m/s^2] \tag{4.13}$$

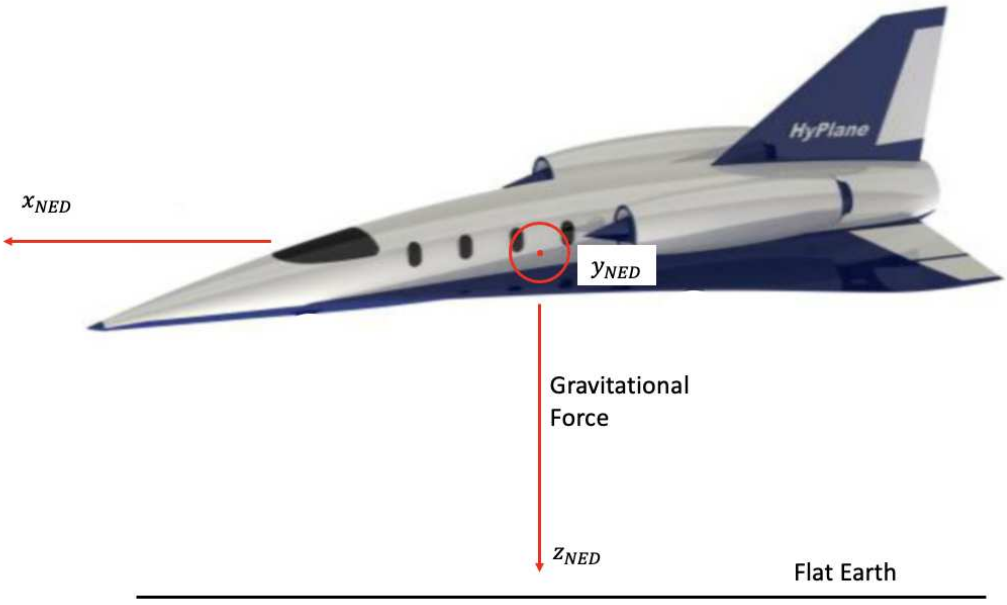

Figure 4.15: Gravitational force acting on the HyPlane vehicle.[31]

It is only an approximation, but for this initial step of the work is enough to gain reliable results and to establish in a more certain way if the model is correctly working.

4.5.3 Apparent Accelerations Subsystem

For this section of the model, apparent accelerations were taken into account. These terms were already presented in section 2.4 with eq. 2.12. Coriolis acceleration is a motion to which a body is subjected when its shift is observed from a reference system that has an angular motion concerning an inertial reference frame (Fig. 4.16). It can be neglected if the vehicle distance is short, but, moving with a hypersonic vehicle, becomes an effect with not so negligible consequences.

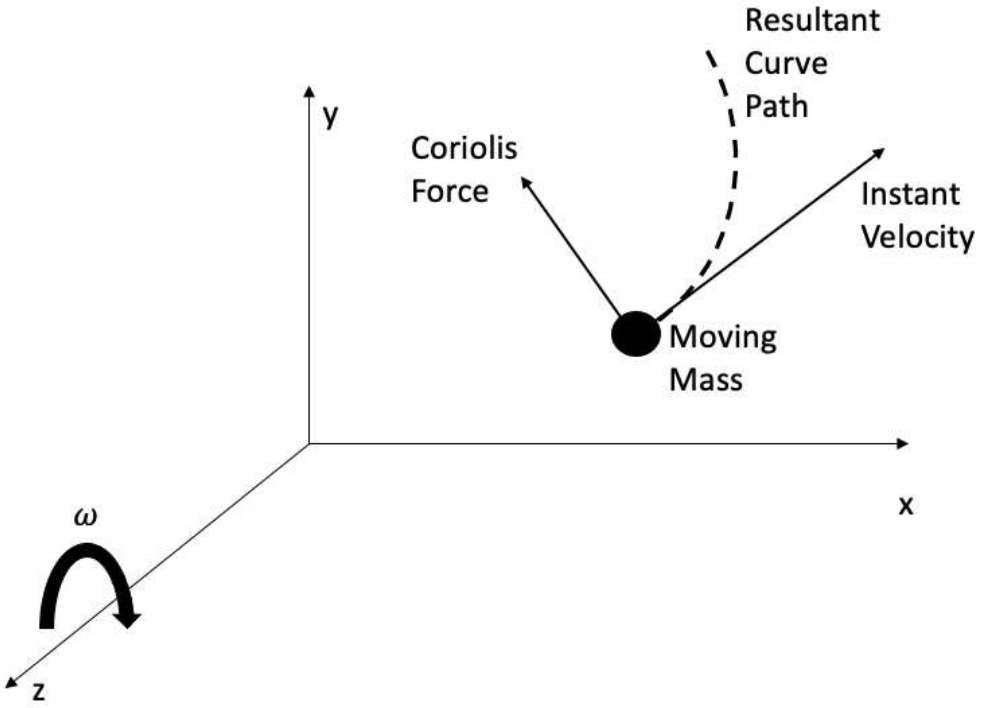

Figure 4.16: Coriolis acceleration. [27]

The other one is the centrifugal acceleration. This one is an acceleration of inertia which appears when a body moves with an angular motion if the motion is analyzed in a noninertial reference system that moves with the body in object. However, it is not really applied to the body, because only the centripetal one exists.

Pressure	$p_0 = 101325\ \mathrm{N/m^2} = 1013.25\mathrm{hPa}$
Density	$\rho_0 = 1.225\ \mathrm{kg/m^3}$
Temperature	$T_0 = 288.15°\mathrm{K}\,(15°\mathrm{C})$
Speed of sound	$a_0 = 340.294\ \mathrm{m/sec}$
Acceleration of gravity	$g_0 = 9.80665\ \mathrm{m/sec^2}$

Table 4.2: Atmosphere parameters at mean sea level. [6]

4.5.4 Atmosphere Subsystem

The atmosphere model used for this thesis is the one already implemented in Simulink® , more precisely the *International Standard Atmosphere (ISA)* model. It implements the atmosphere model presented in U.S. Standard Atmosphere [28]. It is important to use an actual reliable model because the atmosphere influences the missile dynamics in a lot of ways, so putting a simple constant value would not give a reliable missile behavior. However, as it is only a model, some assumptions were meant to be made: the air has no dust, moisture, and water vapor inside. The mean sea level conditions of the atmosphere are presented in 4.2

The model is reliable from 0 up to 20 km. Above or under these values, the outputs are clipped to the last results. The temperature follows the trend presented in fig.4.17.

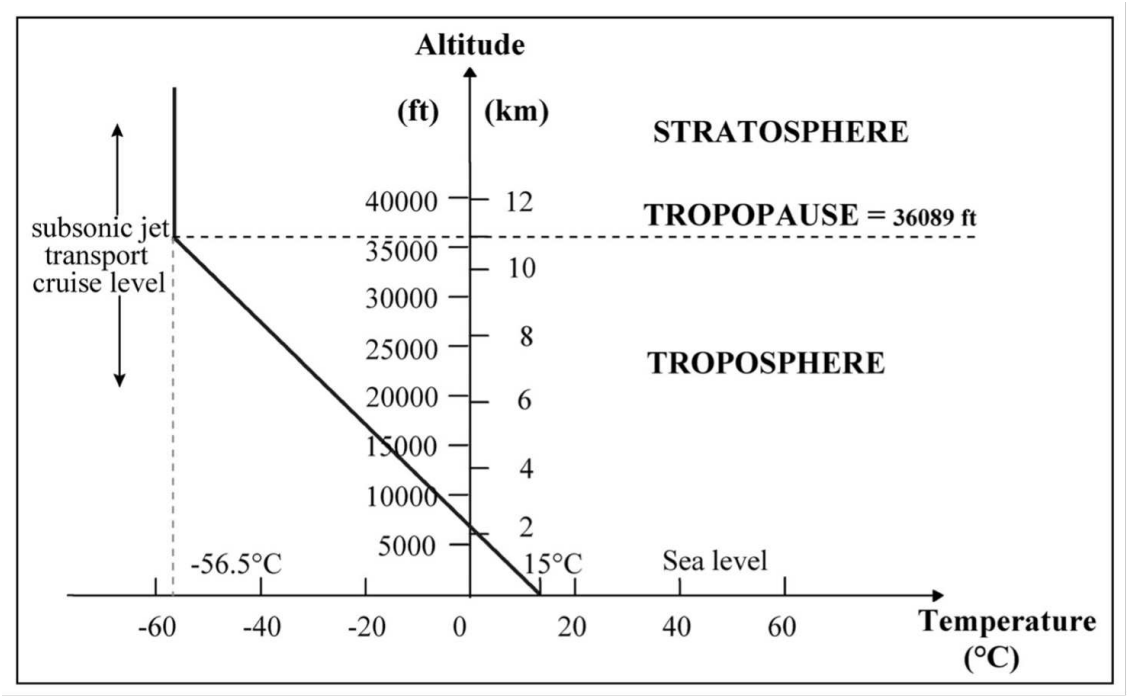

Figure 4.17: Temperature trend of the atmosphere [6]

As it might be noticed from fig. 4.17 the temperature decreases with the increase of altitude

at a constant rate until 11km (36089ft). Above this altitude, the value remains constant at -56.5°C until 20km (65600ft). For the pressure estimation, the air is assumed to be a perfect gas. Calling the altitude PA, from fig. 4.18 the trend of the pressure can be seen.

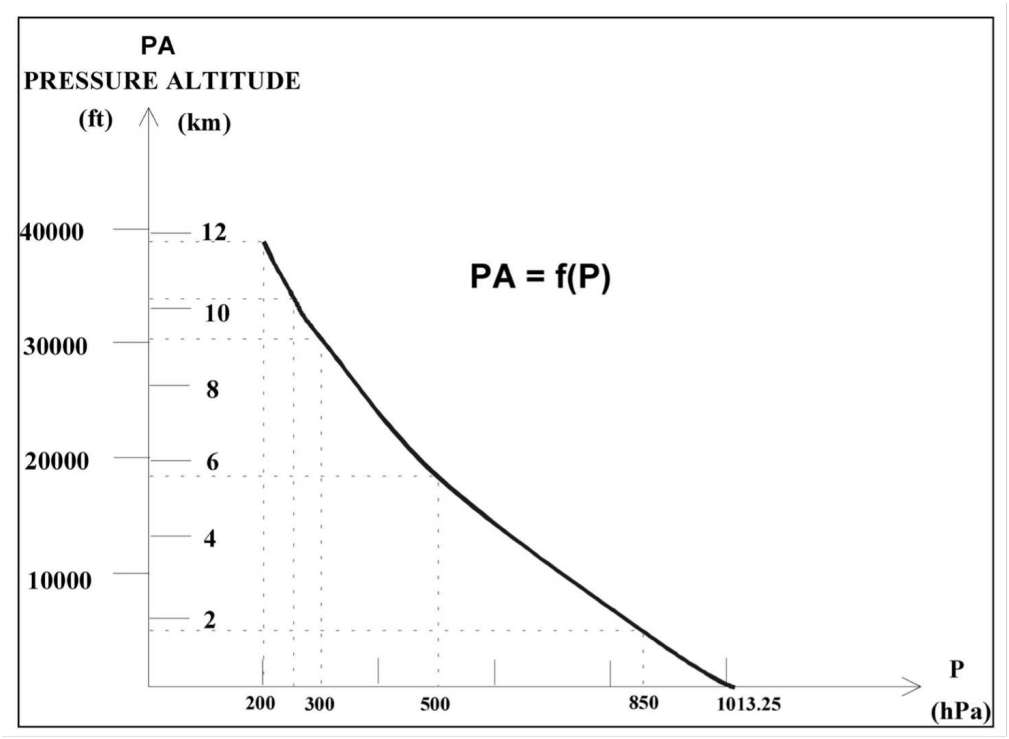

Figure 4.18: Pressure trend of the atmosphere [6]

The pressure variation comes from the hydrostatic equation(fig.4.19), assuming, as already said, the perfect gas law is valid and the temperature follows the previous trend. Then, the density value in every single point of the atmosphere easily comes from the perfect gas equation: $\rho = p/RT$.

4.5.5 Aerodynamic Subsystem

The aerodynamic subsystem, inside the 6DOF model built for this thesis, is probably the most articulated. It is composed of other three subsystems which provide, in order:

- the flight angles, the wind to body direct cosine matrix, and all the aerodynamic coefficients;
- the forces and moments vectors in wind coordinates;
- the transformation from wind to body coordinates.

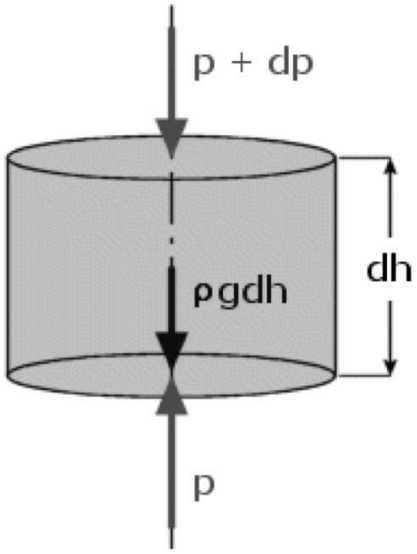

Figure 4.19: Hydrostatic pressure law representation. [6]

In the first subsection of this subsystem, all the flight angles are calculated. For α and β the eq. 2.6 were used, the elevon deflections came from the trimmed motion subsystem and for the heading and flight path angles have been used respectively the equations 4.14:

$$\psi = atan\frac{v_{NED}}{u_{NED}}; \qquad \gamma = atan\frac{-w_{NED}}{\sqrt{u_{NED}^2 + v_{NED}^2}}. \tag{4.14}$$

With heading and flight path angle being the angles presented in fig.4.20.

α and β have also been used to calculate the direct cosine matrix to step from the body coordinate system to the wind one, following the relation 2.5. Then, using the parameters coming from the atmosphere subsystem, the Mach number and the dynamic pressure are evaluated with eq. 4.15:

$$Ma = \frac{V}{a} = \frac{V}{\sqrt{\gamma RT}}; \qquad Q = \frac{1}{2}\rho V^2. \tag{4.15}$$

Finally, the aerodynamic coefficients were evaluated. As said in section 4.4, the aircraft in an object in this thesis is moving with trimmed motion with the addition of a pitch moment to reach a pull-up maneuver. So, the aerodynamic coefficients needed were: the lift, drag, and pitch moment ones, which are C_L, C_D and C_M. These coefficients in the 6DOF model, come from Look-Up Tables extrapolated from the study from where came even the geometry

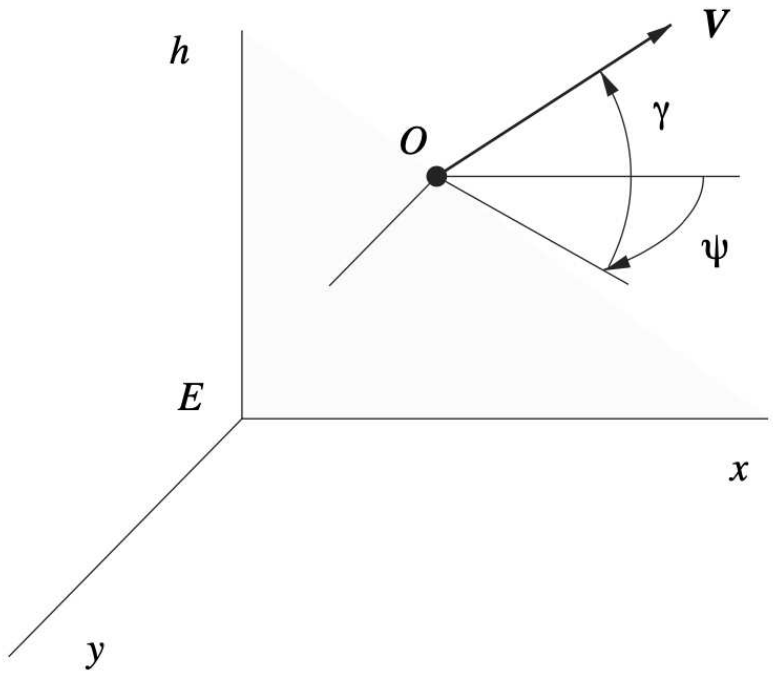

Figure 4.20: Representation of Heading and Flight Path angles. [16]

details, mass, inertia, and propulsion. [12][30] [31] In these studies, were used *Computational Fluid Dynamics (CFD)* and Missile DATCOM to have a preliminary vision of the coefficients. Both were used because of the limitations of the second one, to evaluate the data reliability. In addition to this, the data obtained were compared with one of the X-15 aircraft which flies in mostly the same velocity regime. The X-15 of 1969 was studied to reach Mach 6, with a lot of documented studies conducted in a wind tunnel that was used to test the reliability of Missile DATCOM, and, from fig. 4.21, it can be seen a good resemblance between the actual experiments and the software.

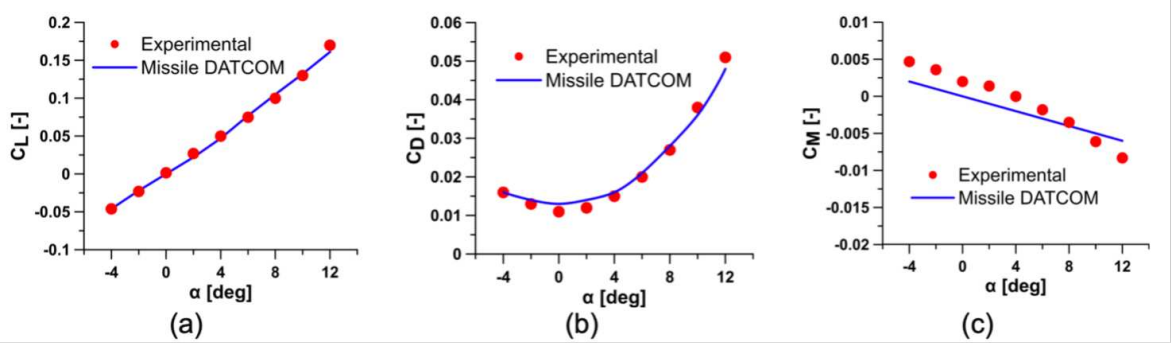

Figure 4.21: Evaluation of aerodynamic coefficients of X-15 vehicle, comparing the wind tunnel tests with Missile DATCOM results at Mach 6 and Reynolds number $2.71 * 10^7$. (a) is the Lift Coefficient, (b) is the Drag Coefficient and (c) is the Pitch Moment Coefficient. [12]

Regimes	Lift Deviation	Drag Deviation	Pitching Moment Deviation	Averaged Deviation
Subsonic	4.6%	15.1%	29.2%	19.0%
Transonic	20.3%	18.2%	39.0%	25.7%
Supersonic	14.4%	6.8%	12.0%	11.1%
Hypersonic	8.3%	12.1%	8.5%	9.6%

Table 4.3: Deviation of CFD analysis results with respect to the ones of Missile DATCOM. [12]

Even the elevon deflections were been evaluated, with their impact on the Drag and Lift coefficients with a deflection of 10°, which results in reliable results once again (fig.4.22).

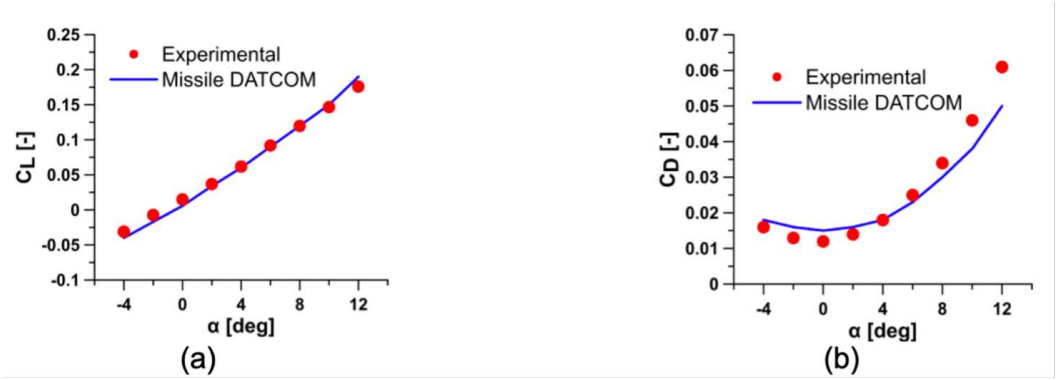

Figure 4.22: Evaluation of aerodynamic coefficients with elevon deflections of 10° of X-15 vehicle, comparing the wind tunnel tests with Missile DATCOM results at Mach 6 and Reynolds number $2.71 * 10^7$. (a) is the Lift Coefficient and (b) is the Drag Coefficient. [12]

So, Missile DATCOM has been considered as an instrument to compare the CFD results. Then, to start the HyPlane aerodynamic study, a lot of simulations were run on Missile DATCOM, at several altitudes as well as Mach Number, to investigate subsonic, transonic, supersonic, and hypersonic motion regimes. Having now a solid reference, the CFD analysis was made, obtaining analog results as it is shown in fig. 4.23.

Confirming once again that Missile DATCOM is reliable to gain preliminary aerodynamic studies, with deviations of coefficients shown in table 4.3.

After this previous step, even the contribution of the elevon deflections was studied, using the convention that a positive elevon deflection produces a negative pitching moment and this deflection is assumed positive when both the surfaces are deflected downward. The results in fig 4.24, 4.25, and 4.26 were found.

After the preliminary study and having an idea of the correct trend of the coefficients, the complete aerodynamic database was built, considering the vehicle configuration and varying flight conditions in a more precise way. The results can be seen in fig. 4.27, 4.28, and 4.29.

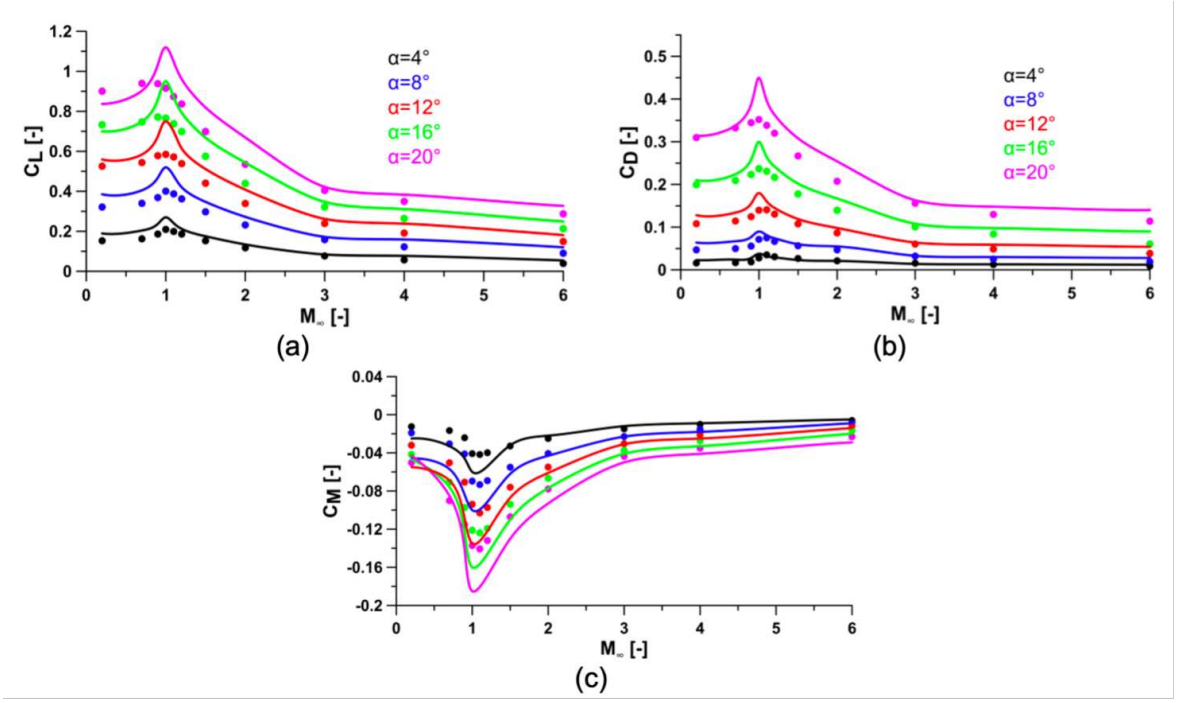

Figure 4.23: Evaluation of aerodynamic coefficients with CFD Software and Missile DATCOM for HyPlane vehicle, varying α and Mach. (a) is the Lift Coefficient, (b) is the Drag Coefficient and (c) is the Pitch Moment Coefficient. [12]

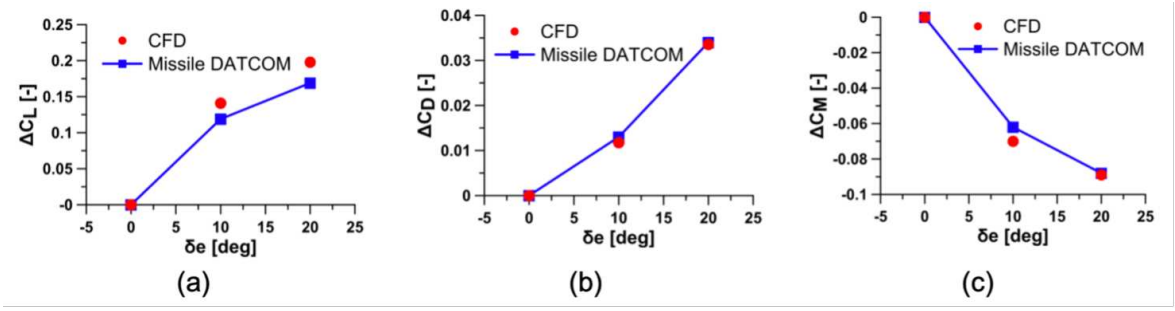

Figure 4.24: Evaluation of aerodynamic coefficients with CFD Software and Missile DATCOM for HyPlane vehicle, varying δ_e for Mach 0.7, altitude of 10km and $\alpha = 0deg$. (a) is the Lift Coefficient, (b) is the Drag Coefficient and (c) is the Pitch Moment Coefficient. [12]

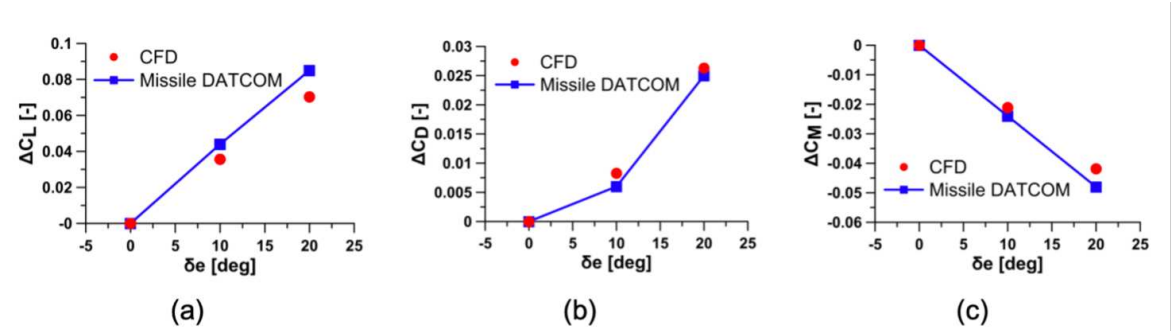

Figure 4.25: Evaluation of aerodynamic coefficients with CFD Software and Missile DATCOM for HyPlane vehicle, varying δ_e for Mach 2, altitude of 20km and $\alpha = 0deg$. (a) is the Lift Coefficient, (b) is the Drag Coefficient and (c) is the Pitch Moment Coefficient. [12]

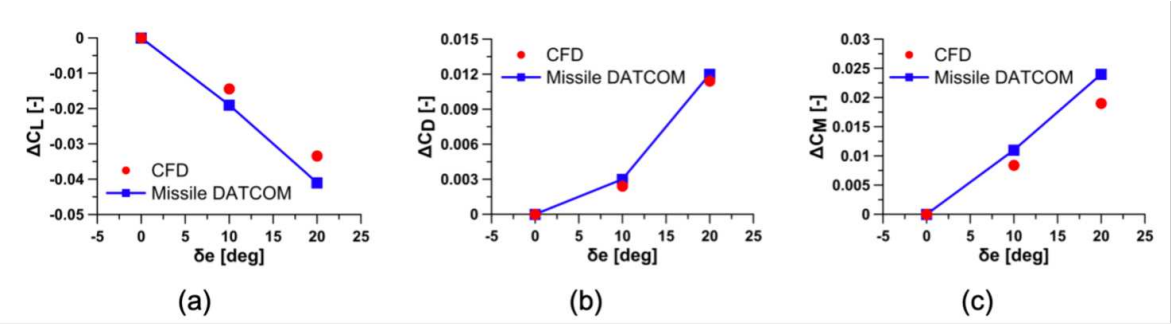

Figure 4.26: Evaluation of aerodynamic coefficients with CFD Software and Missile DATCOM for HyPlane vehicle, varying δ_e for Mach 4, altitude of 30km and $\alpha = 0deg$. (a) is the Lift Coefficient, (b) is the Drag Coefficient and (c) is the Pitch Moment Coefficient. [12]

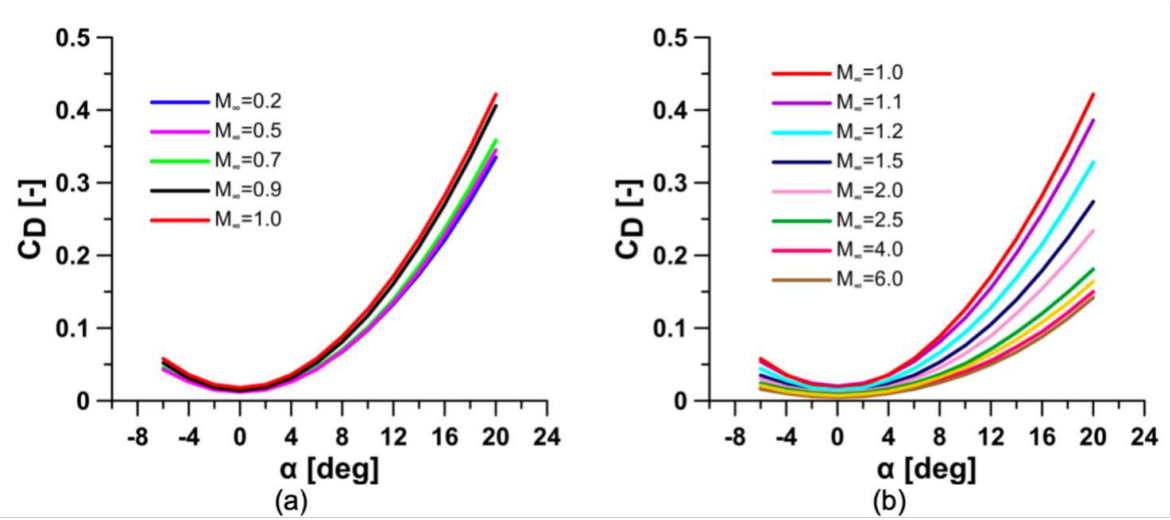

Figure 4.27: Evaluation of Drag coefficient varying α and Mach. (a) is the subsonic case and (b) is the supersonic to hypersonic case. [12]

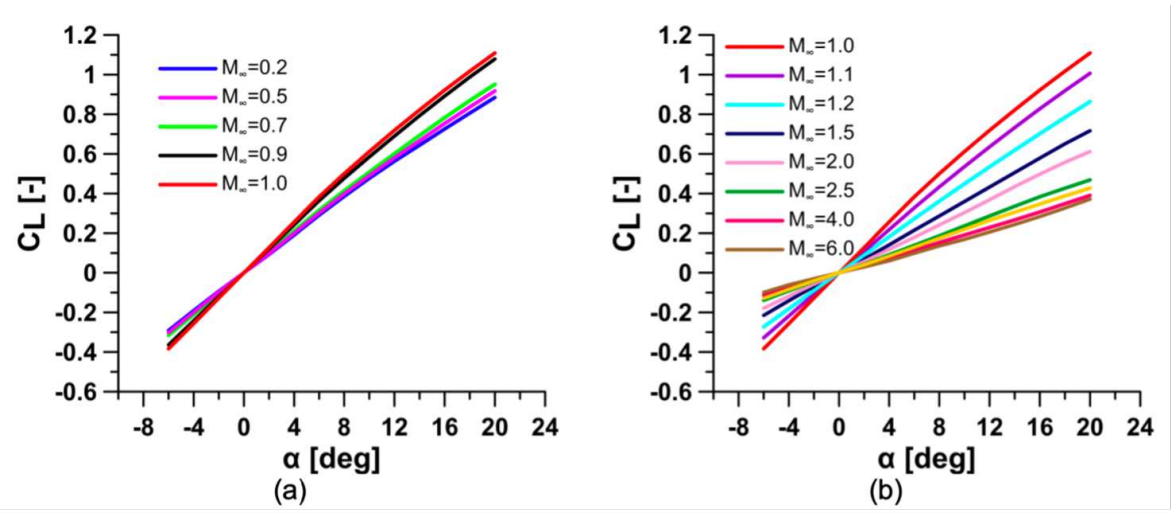

Figure 4.28: Evaluation of Lift coefficient varying α and Mach. (a) is the subsonic case and (b) is the supersonic to hypersonic case. [12]

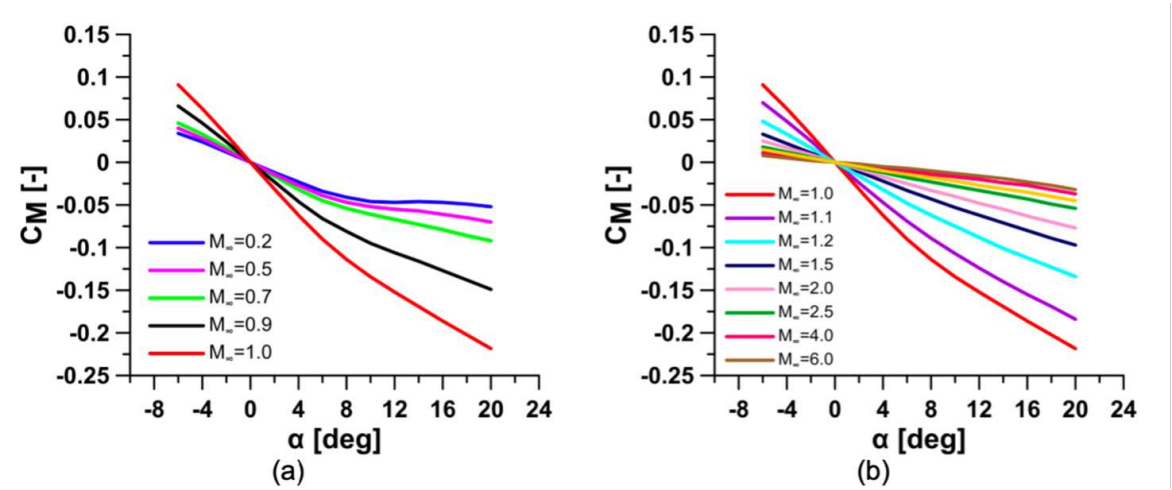

Figure 4.29: Evaluation of Pitching Moment coefficient varying α and Mach. (a) is the subsonic case and (b) is the supersonic to hypersonic case. [12]

Then, again, even the effect of control surface deflection was evaluated, producing the results in fig.4.30 and 4.31 (considering the same assumption that was made for the preliminary study).

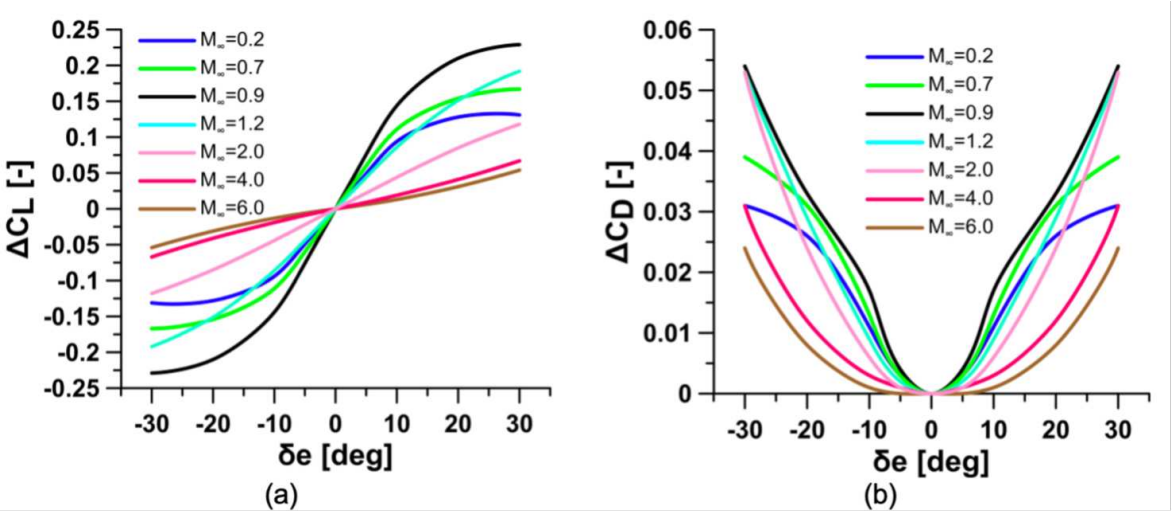

Figure 4.30: Evaluation of coefficients varying δ_e and Mach. (a) is the Lift Coefficient and (b) Drag Coefficient. [12]

Lastly, even the dynamic derivatives were considered as a function of the Mach rate. These results were also included in the 6DOF model, but with the assumption of a negligible alpha rate as well as pitch component of the body rate, these were matched with a zero gain for this previous step. However, in fig. 4.32 and 4.33 their values can be seen.

The coefficients complete calculation derives from eq.4.16:

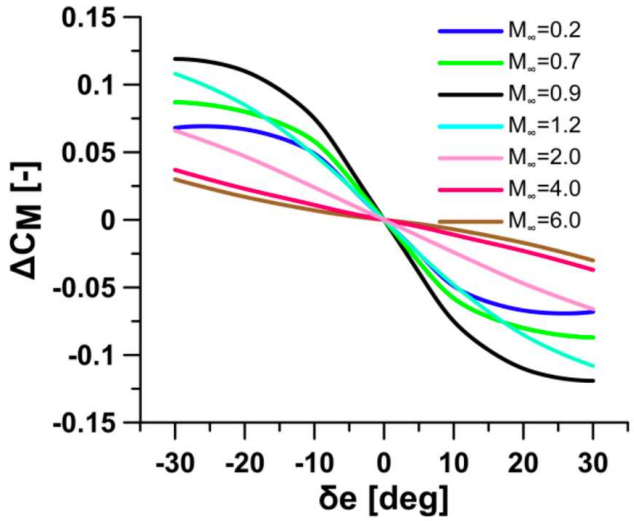

Figure 4.31: Evaluation of Pitching Moment coefficient varying δ_e and Mach. [12]

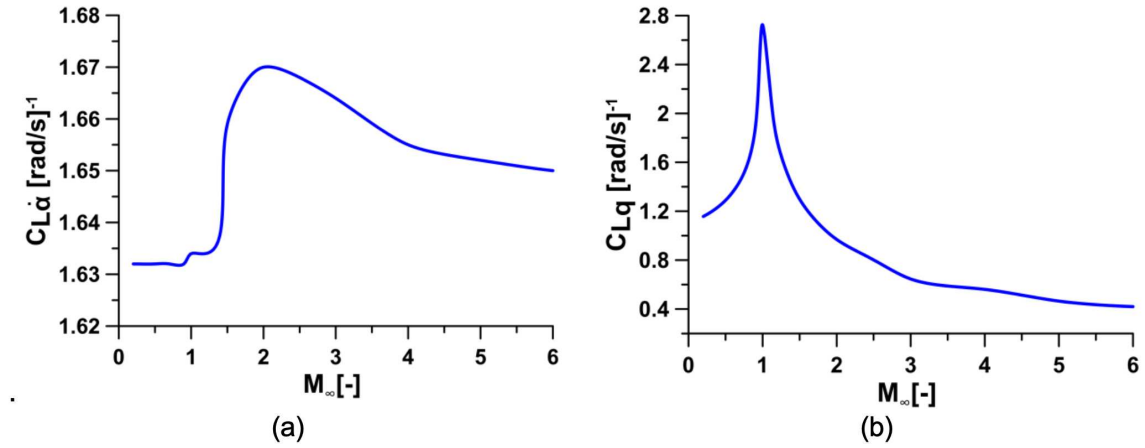

Figure 4.32: Evaluation of Lift coefficient derivative varying Mach number. (a) is the with the α rate and (b) is with pitch rate. [12]

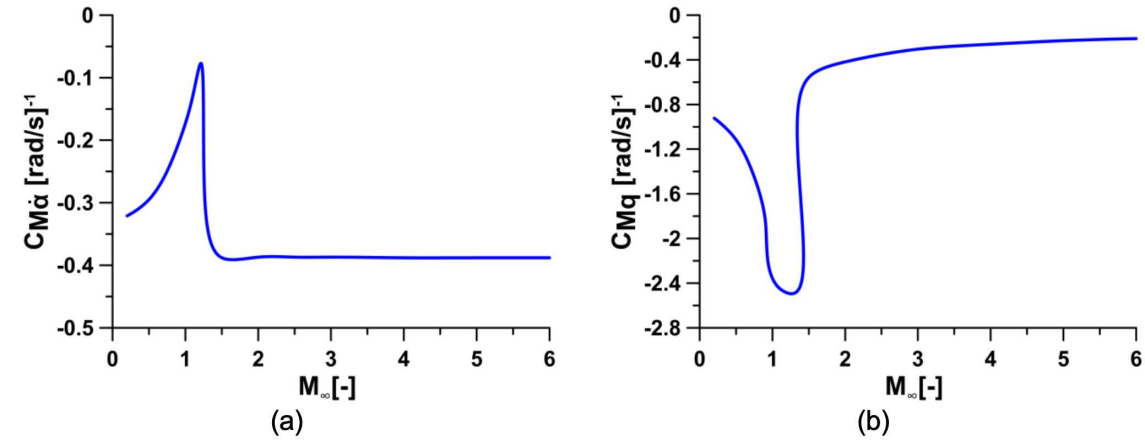

Figure 4.33: Evaluation of Pitching Moment coefficient derivative varying Mach number. (a) is the with the α rate and (b) is with pitch rate. [12]

$$
\begin{aligned}
c_{\mathrm{L}} &= c_{\mathrm{L\ basic}} + \Delta c_{\mathrm{L\ elevons}} + \Delta c_{\mathrm{L\ airelons}} + c_{\mathrm{L}\dot{\alpha}}\frac{\alpha c}{2V} + c_{\mathrm{L}\hat{q}}\frac{qc}{2V} \\
c_{D} &= c_{D\ \mathrm{basic}} + \Delta c_{D\ \mathrm{elevons}} + \Delta c_{L\ \mathrm{airelons}} + \Delta c_{D\ \mathrm{rudder}} + \Delta c_{D\ \mathrm{sideslip}} \\
c_{M} &= c_{M\ \mathrm{basic}} + \Delta c_{M\ \mathrm{elevons}} + \Delta c_{M\ \mathrm{ailerons}} + c_{M\dot{\alpha}}\frac{\dot{\alpha}\bar{c}}{2V} + c_{M\hat{q}}\frac{q\bar{c}}{2V}
\end{aligned}
\tag{4.16}
$$

Where, in the 6DOF model of this thesis, the last three terms of each equation are negligible and the other two depend on Mach number,α angle, and elevons deflection which values were already calculated and are needed to extrapolate all the components of the coefficients from the Look-Up Tables built from the previous plots.

So, all the needed aerodynamic coefficients are evaluated, and the force and moment vectors can be calculated as follows, due to the hypotesis of trimmed motion introduced in sec.4.4:

$$
F_A = SQ\begin{bmatrix} C_D \\ 0 \\ C_L \end{bmatrix}; \quad M_A = SQC\begin{bmatrix} 0 \\ C_M \\ 0 \end{bmatrix} \tag{4.17}
$$

With S as the reference surface which is the wing area and c as the mean aerodynamic chord, both values are written in table 3.1. As it might be noticed, the guidance subsystem (sec. 4.2) can control only the translational acceleration, but here is acting even a pitching moment that, without any control, could lead the vehicle to instability. To avoid this hypothesis, it was introduced a basic saturation of the component of the pitching moment coefficient linked to the attack angle α. This way, only the component of the pitching moment that derives from the deflection of the elevons is involved in the pull-up maneuver and the vehicle can maintain its stability.

The last thing happening in the aerodynamic subsystem is the transformation of both vectors from wind coordinates to body coordinates using the direct cosine matrix calculated with the relation 2.5.

4.5.6 Kinematics Subsystem

This subsystem of the model is the one containing the actual equations of motion presented in sec. 2.4, which are Newton's and Euler's equations visible in fig. 2.10.

To gain a clearer visualization of the Simulink® block, the kinematics subsystem has been

divided in two, following fig. 4.34

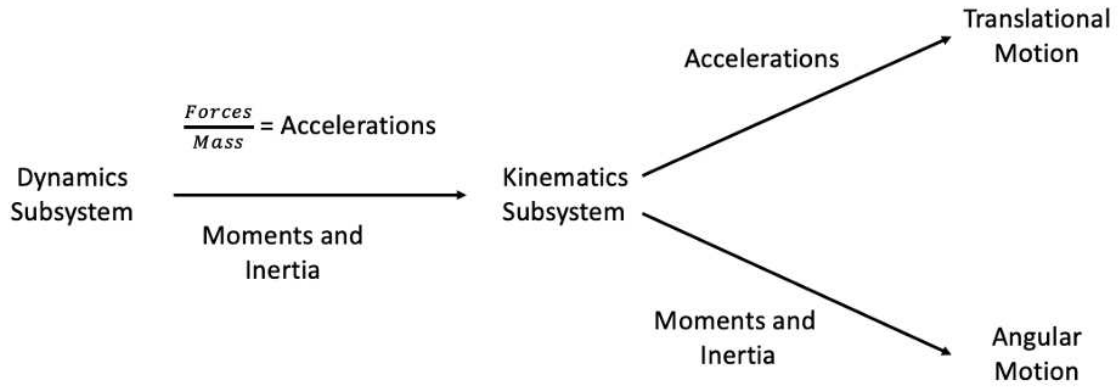

Figure 4.34: Kinematics subsystem scheme.

The angular motion section (fig.4.35) is the one providing the attitude of the aircraft, following the Euler equation.

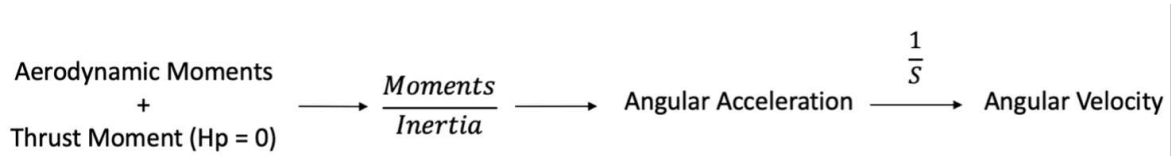

Figure 4.35: Angular motion subsystem scheme.

As it is shown in fig. 4.35, the aerodynamic moments are summed with the thrust ones that, for hypothesis are equal to zero. Dividing the vector obtained for the Inertia matrix which came from the Look-Up Table extrapolated from fig. 3.4, the angular acceleration is calculated. Then, integrating the acceleration follows the angular velocity. Now there is a crucial step to avoid singularities. Following the Simulink® algorithm of eq. 4.18:

$$\begin{bmatrix} \dot{q}_0 \\ \dot{q}_1 \\ \dot{q}_2 \\ \dot{q}_3 \end{bmatrix} = 1/2 \begin{bmatrix} 0 & -p & -q & -r \\ p & 0 & r & -q \\ q & -r & 0 & p \\ r & q & -p & 0 \end{bmatrix} \begin{bmatrix} q_0 \\ q_1 \\ q_2 \\ q_3 \end{bmatrix} + K\varepsilon \begin{bmatrix} q_0 \\ q_1 \\ q_2 \\ q_3 \end{bmatrix} \tag{4.18}$$

$$\varepsilon = 1 - \left(q_0^2 + q_1^2 + q_2^2 + q_3^2\right)$$

The body rates are converted in quaternions derivative, with K which is a gain that drives

the norm of the quaternion state vector to 1.0. The value of K must be chosen carefully because a large value improves the decay rate of the error in the norm, but also slows the simulation because fast dynamics are introduced. An error in the magnitude in one element of the quaternion vector is spread equally among all the elements, potentially increasing the error in the state vector. However, with working with quaternions, the possibility of falling in a singularity case is zero. With another integration step, the quaternion vector is obtained and is converted again in Euler Angles (eq.2.8) for a better data interpretation. It is also obtained the direction cosine matrix(eq.2.3) to step from the NED axis to the Body axis and vice-versa.

Stepping now into the translational motion, Newton's law is applied. Initially, it has been considered to work with the ECEF coordinates system and so it is already implemented in the model, however, for this initial state of the project, it has been chosen to work in the NED axis to appreciate better the results of the model and understanding easily some error which might be possible in this delicate phase. First of all, the thrust force and the aerodynamic one, which are both in the body coordinate system, were summed and divided by the mass becoming accelerations. Then these accelerations were also converted, with the direction cosine matrix coming from the angular motion block, in NED axis to be summed to the other ones, that are gravity, Coriolis, and centrifugal. The results of this sum is the total acceleration acting on the aircraft in NED coordinate system. With a double integration, at the first step, the acceleration becomes the velocity and then the position of the vehicle in the NED axis.

Lastly, all the output obtained from the flight mechanics subsystem are given back as feedback until the vehicle reaches the desired point.

Chapter 5

Model Tests and Performances

The model was settled in its total formation and so it was to time to test it out. This was made in many ways. The first thing to do was to have proof of its working, and to gain a reliable result it was tested out in a random situation with the Simulink® 6DOF model already existing. Then, to investigate the rest of the dynamic model of this thesis, it has been put to the test in different situations:

- it was created a grid with a lot of target positions to see when and how the vehicle reached the desired points;
- the vehicle was put in a linear motion to see if it can handle the position with and without a disturbance effect on the elevons;
- some pull-up maneuvers were imposed to see the aircraft behavior.

5.1 Validation of the Kinematics Subsystem

The only thing that could be tested with the Simulink® model was the motion subsystem (4.5.6) in its translational and rotational parts. To obtain a result that was as truthful as possible, the initial state of the vehicle was chosen randomly, as well as the forces and moments acting on it. The mass was posed as 1 Kg, and so the inertia was considered as an identity matrix. The initial state of the vehicle is expressed in eq. 5.1:

$$\begin{aligned} NEDPosition &= \begin{bmatrix} 0 & 0 & -1 \end{bmatrix} \text{[m]}; \\ BodyVelocity &= \begin{bmatrix} 0 & 0 & -5 \end{bmatrix} \text{[m/s]}; \\ EulerAngles &= \begin{bmatrix} 0 & 0 & 0 \end{bmatrix} \text{[deg]}; \\ AngularAcceleration &= \begin{bmatrix} 0 & 0 & 0 \end{bmatrix} \text{[deg/s}^2\text{]}; \end{aligned} \tag{5.1}$$

And the forces and moments acting in the body system on the vehicle were also chosen randomly as in eq. 5.2 :

$$\begin{aligned} BodyForces &= \begin{bmatrix} 50 & 10 & 50 \end{bmatrix} \text{[N]}; \\ BodyMoments &= \begin{bmatrix} 5 & 1 & 50 \end{bmatrix} \text{[Nm]}; \end{aligned} \tag{5.2}$$

As shown in fig. 5.1 and 5.2, the results produced by both models were barely identical. The position in all three axis is very similar (fig. 5.1) as well as the attitude-behavior with a little difference only on the Yaw axis which might be due to the different integrators used on the models (fig.5.2). In fact, Simulink® used the standard integrator and the 6DOF model built in this thesis uses a discrete-time integrator with a backward Euler method implemented. As solver has been used ode-4 (Runge-Kutta) with a fixed step of 0.05 seconds.

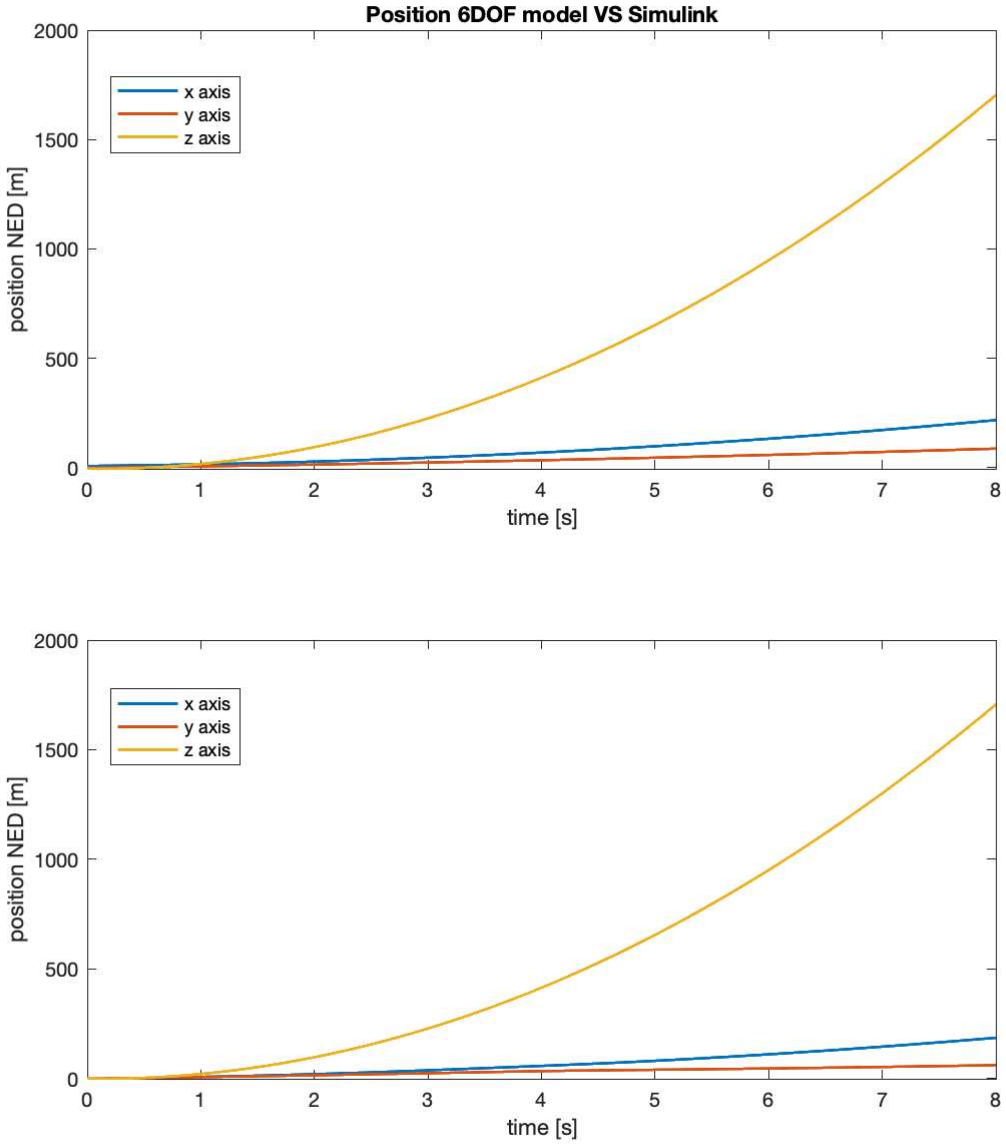

Figure 5.1: Position of the vehicle in NED coordinates system. The first image is referred to the 6DOF model built in this thesis and the second one is referred to the Simulink® one.

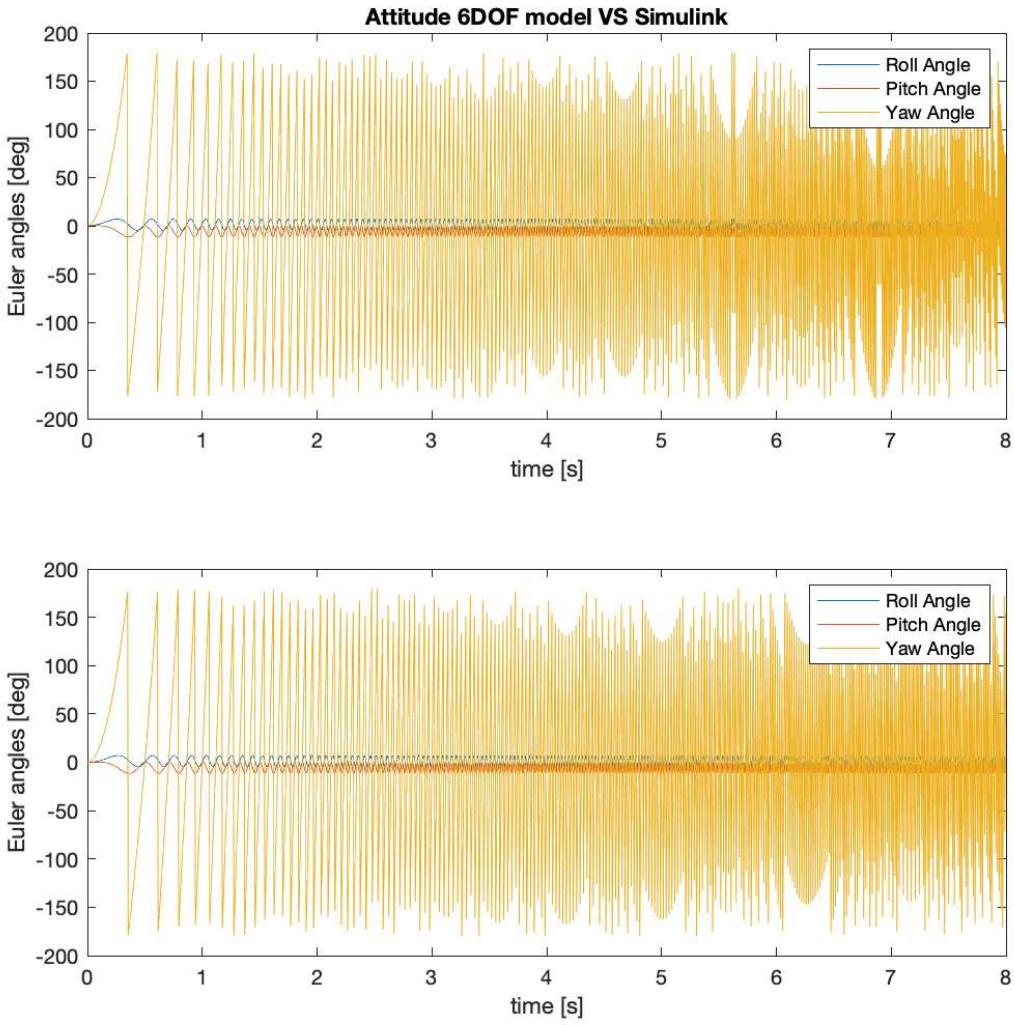

Figure 5.2: Attitude of the vehicle in NED coordinates system. The first image is referred to the 6DOF model built in this thesis and the second one is referred to the Simulink® one.

5.2 Flight Performance Analysis

Once the Kinematics part of the model was verified, it was time to test out the flight performance of the vehicle in its totality.

To do so, it was chosen an area of desired points to be intercepted which was from 0 to -10 km of altitude and from 30 to 60 km of downrange which, in this case of a simple maneuver in the plane, corresponds only to the x position in NED axis.

The initial state of the vehicle was eq. 5.3 :

$$\begin{aligned} NEDPosition &= \begin{bmatrix} 0 & 0 & -5000 \end{bmatrix} [\text{m}]; \\ EulerAngles &= \begin{bmatrix} 0 & 0 & 0 \end{bmatrix} [\text{deg}]; \\ AngularAcceleration &= \begin{bmatrix} 0 & 0 & 0 \end{bmatrix} [\text{deg/s}^2]; \end{aligned} \tag{5.3}$$

Three cases were analyzed: the first one was with an initial Mach of 0.5, the second one with an initial Mach 2, and the third one with an initial Mach of 6.

In fig. 5.3 has been shown the first case, which is the one with a lower initial velocity. To gain a better results view, the z NED axis has been reversed, becoming positive. As it can be noticed, for the desired points to be intercepted down 5km, the vehicle only became supersonic and for this reason, took longer to reach the destination (90 seconds to reach 60km downrange and 0km of altitude). However, with lower velocities, the vehicle is more stable as well as maneuverable and so all the desired points were intercepted. With the increasing of altitude, exceeding the one of departure of the vehicle, the velocity became higher and higher, losing maneuverability and misintercepting points (white zone). However, the time to reach objectives is reduced a lot, reaching 50 seconds when the vehicle has a velocity of Mach 10, even if the distance is the longer one (60km).

As it can be shown in fig. 5.4 for initial Mach 2 and fig. 5.5 for initial Mach 6, increasing the initial velocity, the maneuverability of the aircraft is better with major distances, intercepting way more points at 60km than 30km of downrange. Even if the final Mach is not so different from the first case, stepping from a maximum of 10 to a maximum of 12, increasing the initial velocity, the time of points interception is way lower, reaching 26 seconds to arrive at 60km.

Another thing that is important to notice is that in a full hypersonic flight, the vehicle needs a lot more distance downrange to intercept points above or under its initial altitude.

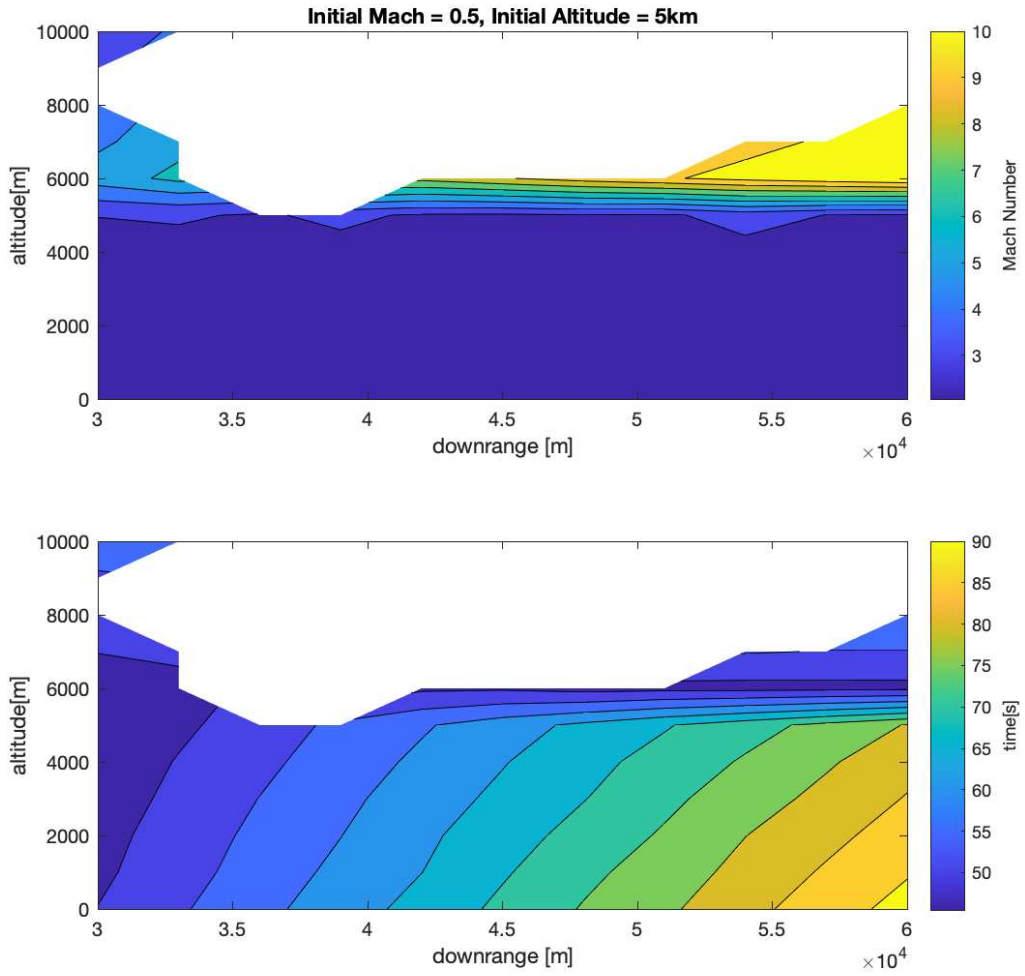

Figure 5.3: Vehicle flight performance analysis at initial 5km of altitude and Mach number of 0.5.

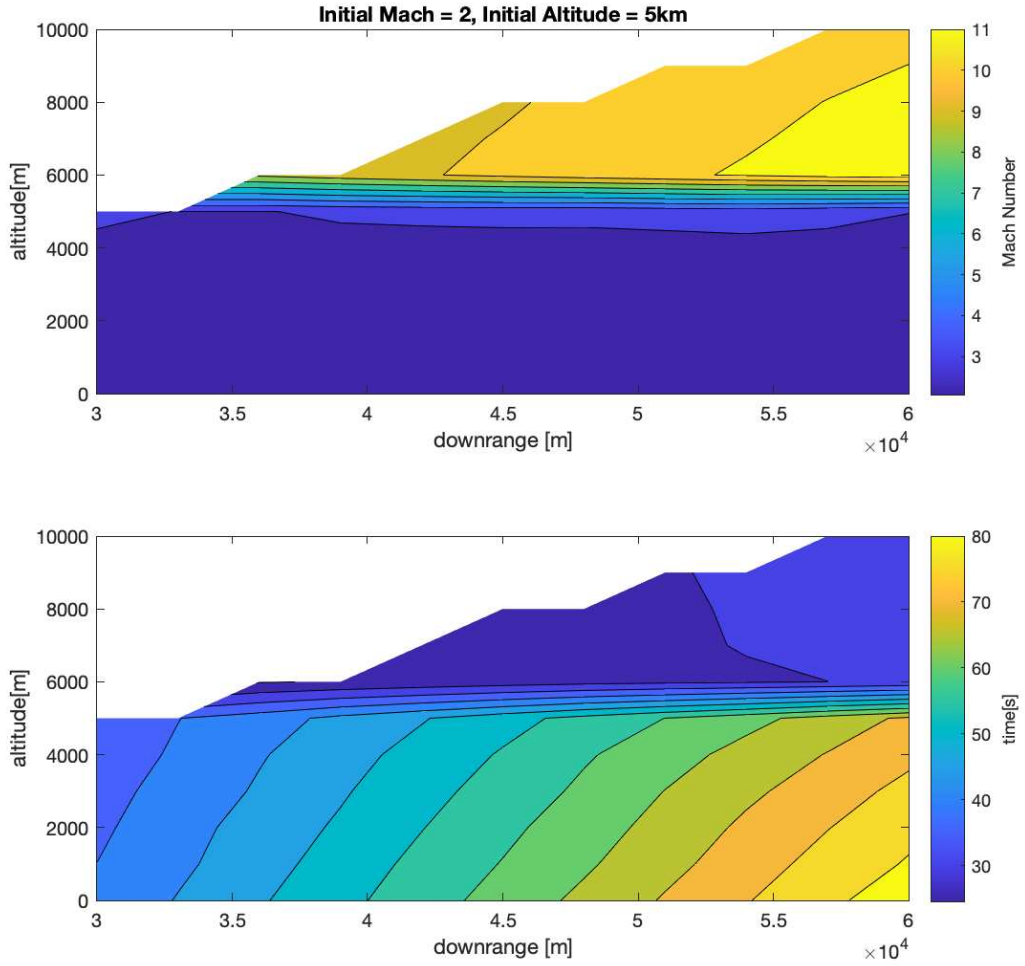

Figure 5.4: Vehicle flight performance analysis at initial 5km of altitude and Mach number of 2.

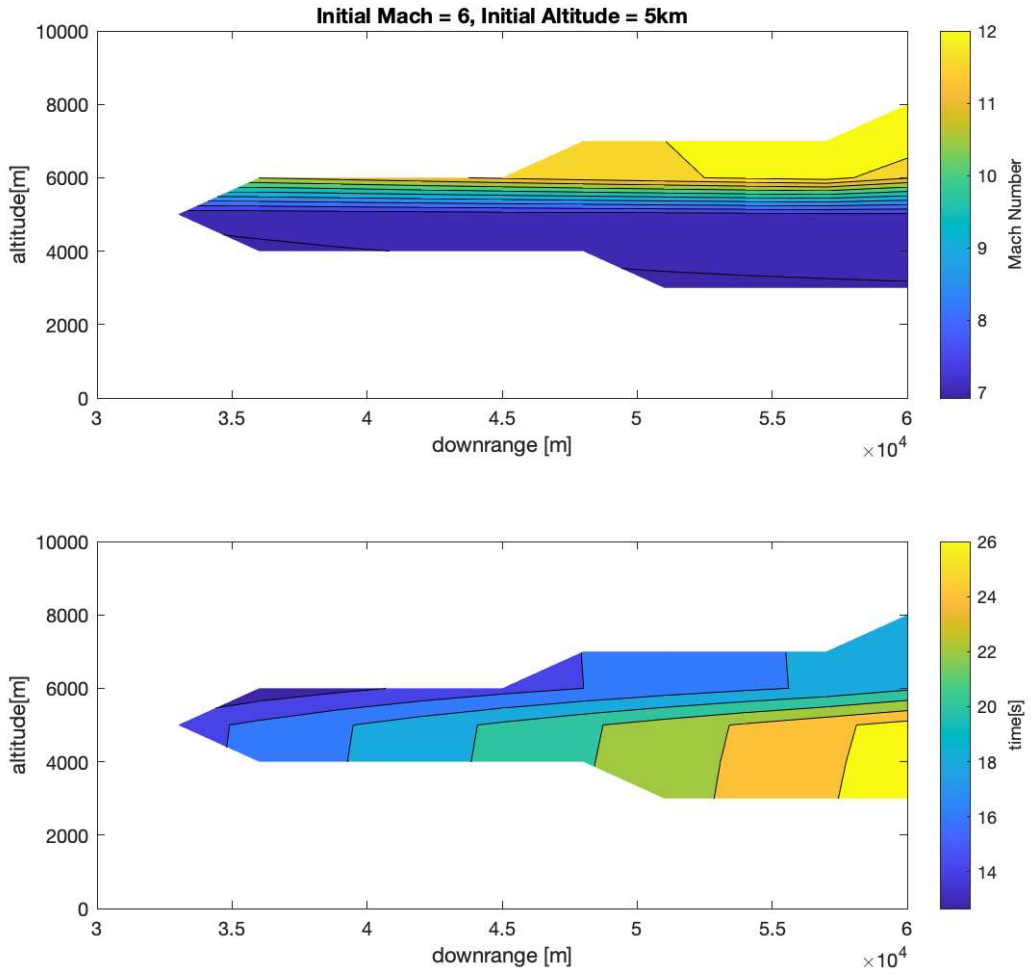

Figure 5.5: Vehicle flight performance analysis at initial 5km of altitude and Mach number of 6.

5.3 Disturbance Effects

After testing the aircraft's flight performance, it was time to see if it was able to maintain a certain stability after a disturbance effect. To do this, but to maintain a linear behavior concerning the model's hypothesis, a disturbance effect of 2 deg after 10 seconds of flight was introduced on the elevons deflection. This situation was analyzed at different initial velocities of the vehicle, in particular at Mach 0.5, 1, and 6. The initial altitude of the aircraft was settled to -10km in NED coordinate system with the target at the same altitude but with a downrange distance of 45 km. Fig. 5.6, 5.7, and 5.8 show the behavior of the aircraft in terms of position (with the z-axis reversed to gain a better data interpretation), angle of attack, elevons deflection, pitch angle, and Mach number through time. As it is shown in fig. 5.6, in the first case, and so with an initial Mach number of 0.5, the aircraft is not able to intercept the target. The initial velocity seems to be not enough to maintain the altitude and so the vehicle starts to drop, once it loose nearly 5km of altitude, the control system failed. So, the aircraft gained velocity and dropped to the ground in a few seconds. However, it is interesting to notice that the disturbance effect on the deflection of the surfaces does not change drastically the behavior of the aircraft. As a matter of fact, it can be seen from the plots in fig. 5.6 that after the disturbance the trajectory of the vehicle is a little lower in terms of altitude, intercepting the ground earlier in terms of time. This can be due to a little loose of velocity, as is shown in the last plot of the Mach number versus time. This, of course, leads to a kind of different behavior even to the angles of attack and pitch, but maintaining nearly the same trend: pretty stable during the subsonic flight, oscillatory in the supersonic regime, and stable again through the hypersonic phase. Increasing the initial velocity a bit, stepping from 0.5 to 1 for the value of the Mach number, the vehicle can intercept the target (fig.5.7). During the 45km long flight, the vehicle loses only 40 meters of altitude, recovering them in less than 40 seconds to intercept the desired point in less than 80 seconds. As can be seen, in this case, the disturbance did not affect any of the parameters analyzed. However, the aircraft did not reach a hypersonic velocity, arriving at a maximum Mach number of 4, remaining supersonic through the flight. For this reason, maintaining the trend explained in fig. 5.6, the angle behavior is oscillatory, but still of small angles, stepping from -4 to 2 deg for the angle of attack and the pitch angle. The last case presented is the one in fig. 5.8 with an initial Mach Number of 6. Here, the flight

is way shorter, intercepting the desired point in only 16 seconds, with a final Mach Number of nearly 10. Here, due to the high speed and the really short flight duration, the disturbance has a significant effect on the flight but without compromising its ability to arrive at a certain desired point. Furthermore, as is shown in the angles part of the image, the angle of attack, the pitch angle, and even the elevons have values close to zero, so a disturbance of 2deg can lead to a significant variation. However, after less than 2 seconds, this disturbance effect has been rebalanced, leading the vehicle to regain the same trend, in terms of angles. Only the altitude has remained a little different, but with a mismatch of some meters.

5.4 Pull-Up Maneuver

The last thing that has been investigated with the model, is a simple pull-up maneuver in different conditions. This time, instead of changing the initial velocity, has been chosen to alter the vehicle's initial altitude and the desired point to intercept. So, the initial velocity has been chosen to be at Mach number equal to 2, and the downrange to travel is 20 in all the cases considered. The positions of the desired points with respect to the vehicle follow table 5.1.

Aircraft Altitude in NED [km]	**Desired Point Altitude in NED [km]**
-1	-5
-5	-10
-10	-15

Table 5.1: Vehicle altitude and desired point altitude for a pull-up maneuver.

Proceeding with the table 5.1 order, the first case taken into consideration was the one with an altitude of the vehicle of -1 km and -5 km for the desired point to intercept which is presented in fig.5.9. As it is shown in the Mach number part of the figure, in this case, the vehicle does not reach hypersonic speed probably due to the atmospheric density producing way more drag to defeat, intercepting the desired point after 30 seconds with a speed of only Mach 2.6. So, the behavior of the aircraft follows the supersonic trend, with the angles swinging from -4 to 4 deg for the angle of attack and from 10 to 15 deg for the pitch angle. This oscillatory behavior is probably due to the saturation of the angle of attack component of the pitching moment, which leads the aircraft to lower the nose when it's induced to raise it. This phenomenon is way more impacting in supersonic speed rather tan subsonic, because when the

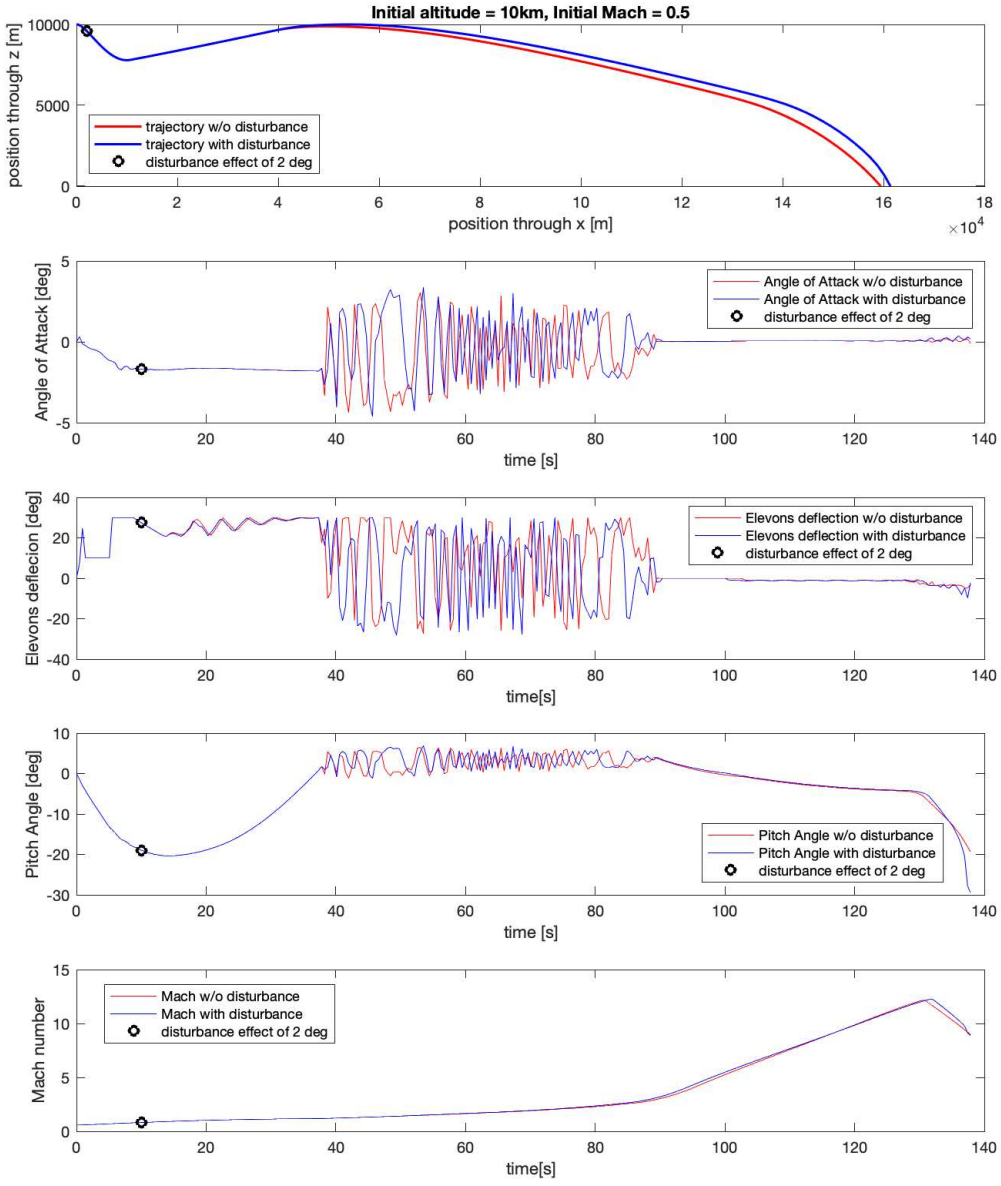

Figure 5.6: Vehicle flight analysis with a surface deflection disturbance of 2 deg after 10 seconds of flight, with 10km of initial altitude and Mach 0.5

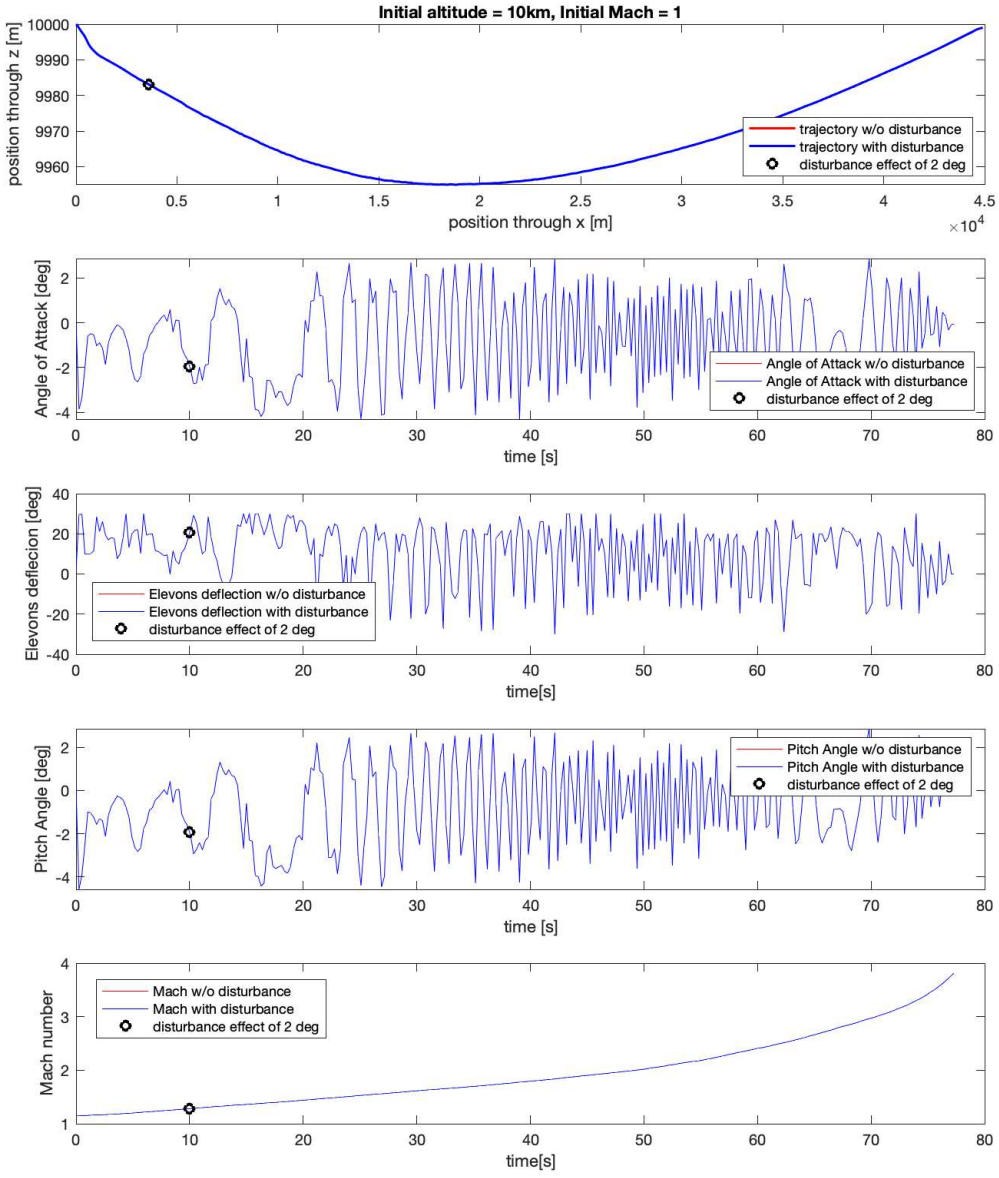

Figure 5.7: Vehicle flight analysis with a surface deflection disturbance of 2 deg after 10 seconds of flight, with 10km of initial altitude and Mach 1.

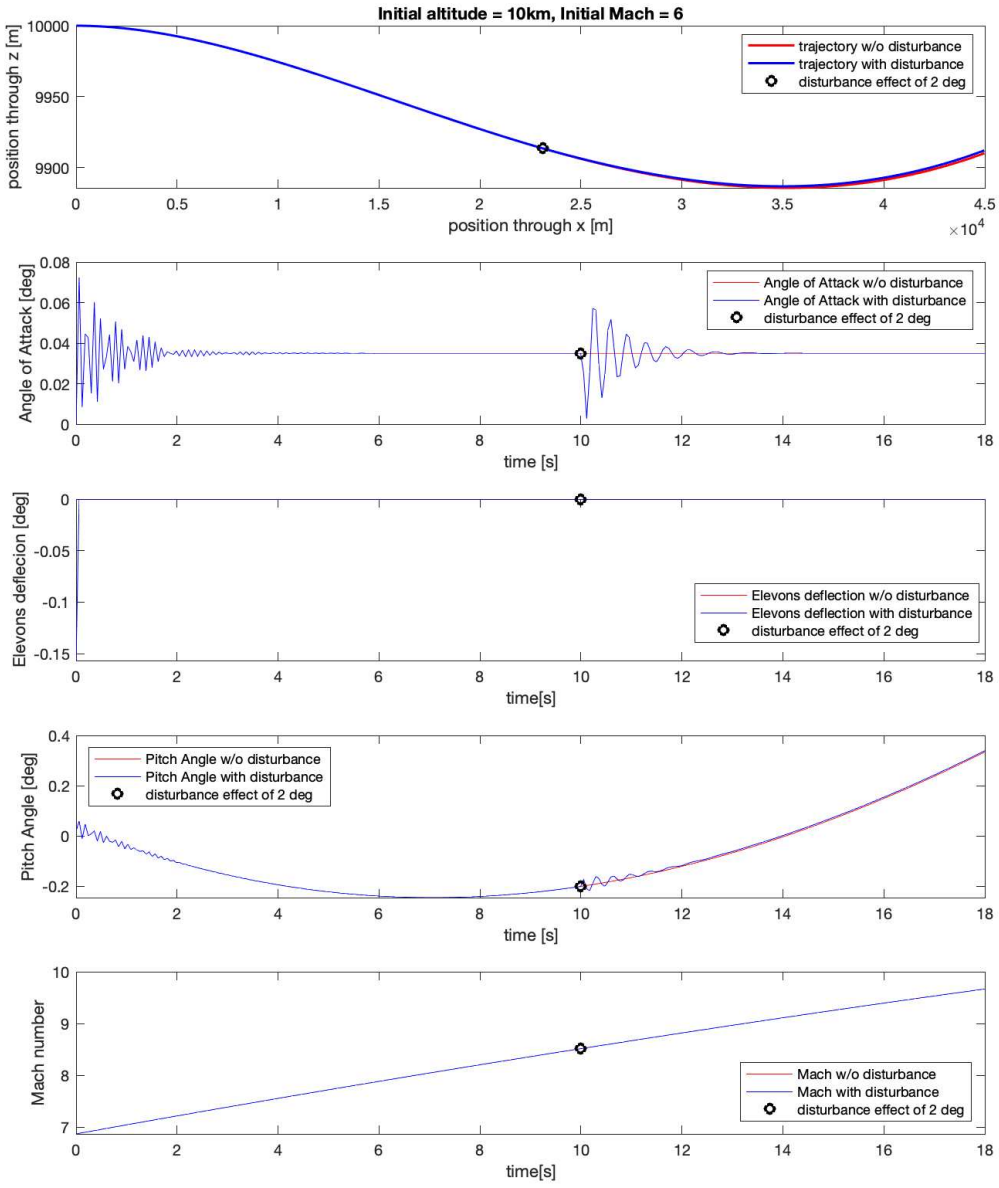

Figure 5.8: Vehicle flight analysis with a surface deflection disturbance of 2 deg after 10 seconds of flight, with 10km of initial altitude and Mach 6.

vehicle moves with a lower velocity the elevons deflection can occur in more time, instead when the vehicle increases its speed, the elevons have to deflect more rapidly. At an initial altitude of 5km (fig.5.10), the vehicle can reach hypersonic speed, arriving at Mach 6 at the moment of interception of the desired point in less than 20 seconds. Here, the elevons deflection have a less oscillatory trend, due to the hypersonic range of velocity, in fact, with the increasing speed, it is needed a much smaller deflection [1]. This is the perfect altitude to have a density that is not enough to raise much drag force and not too small, so it can produce a significant thrust with the airbreathing propulsion system in a small amount of time. In fact, by increasing the initial altitude reaching 10 km (fig.5.11), the air density is halved concerning 5km [15], and the airbreathing thrust system couldn't produce enough thrust to reach hypersonic speed before the target interception, arriving at the desired point at nearly Mach 4 in 25 seconds. This is the proof that, in this specific case, the airbreathing engine performances are not enough to sustain an hypersonic flight.

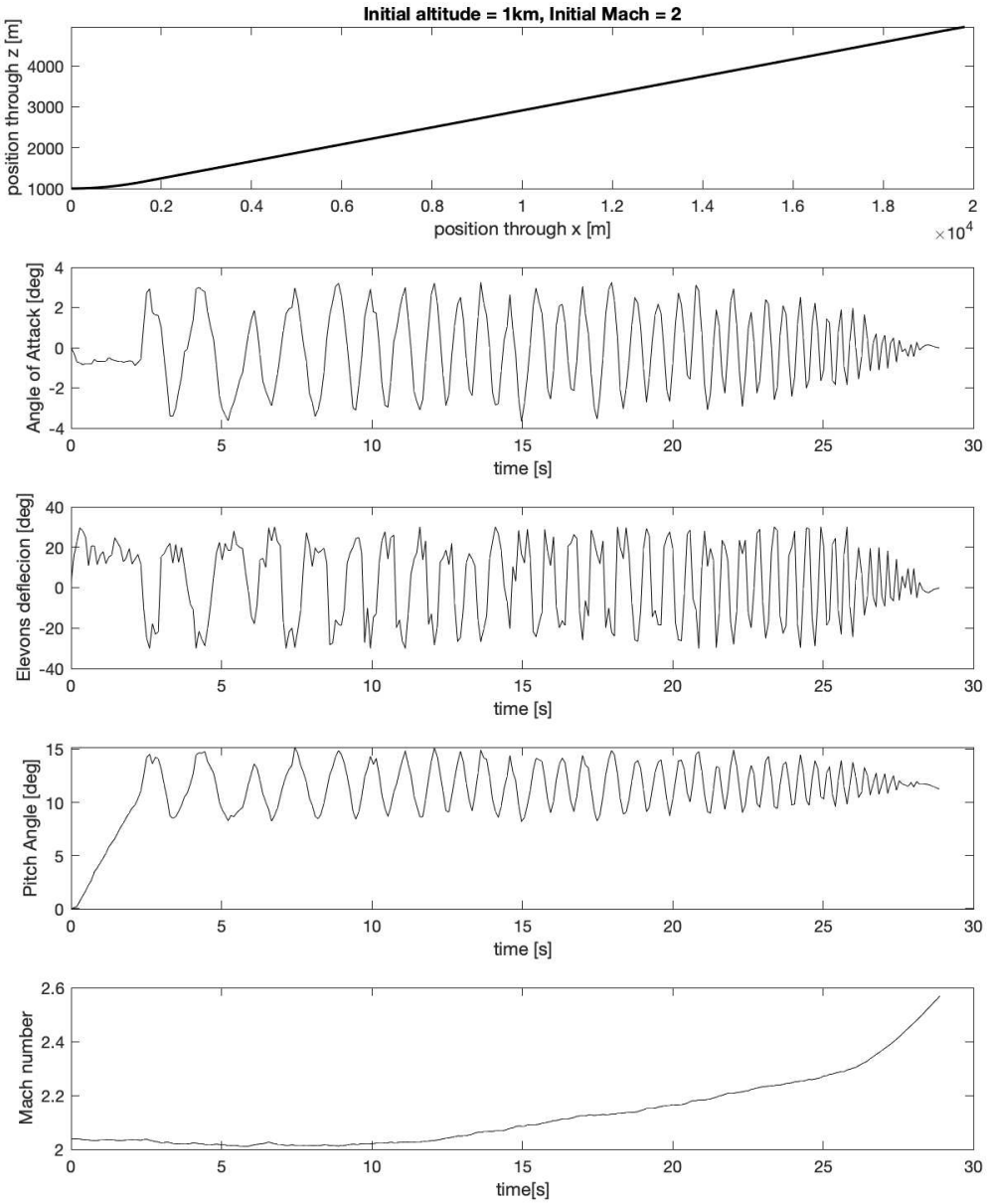

Figure 5.9: Pull-up maneuver with initial altitude of 1km and Mach 2 for a target at 20km of downrange and altitude 5km.

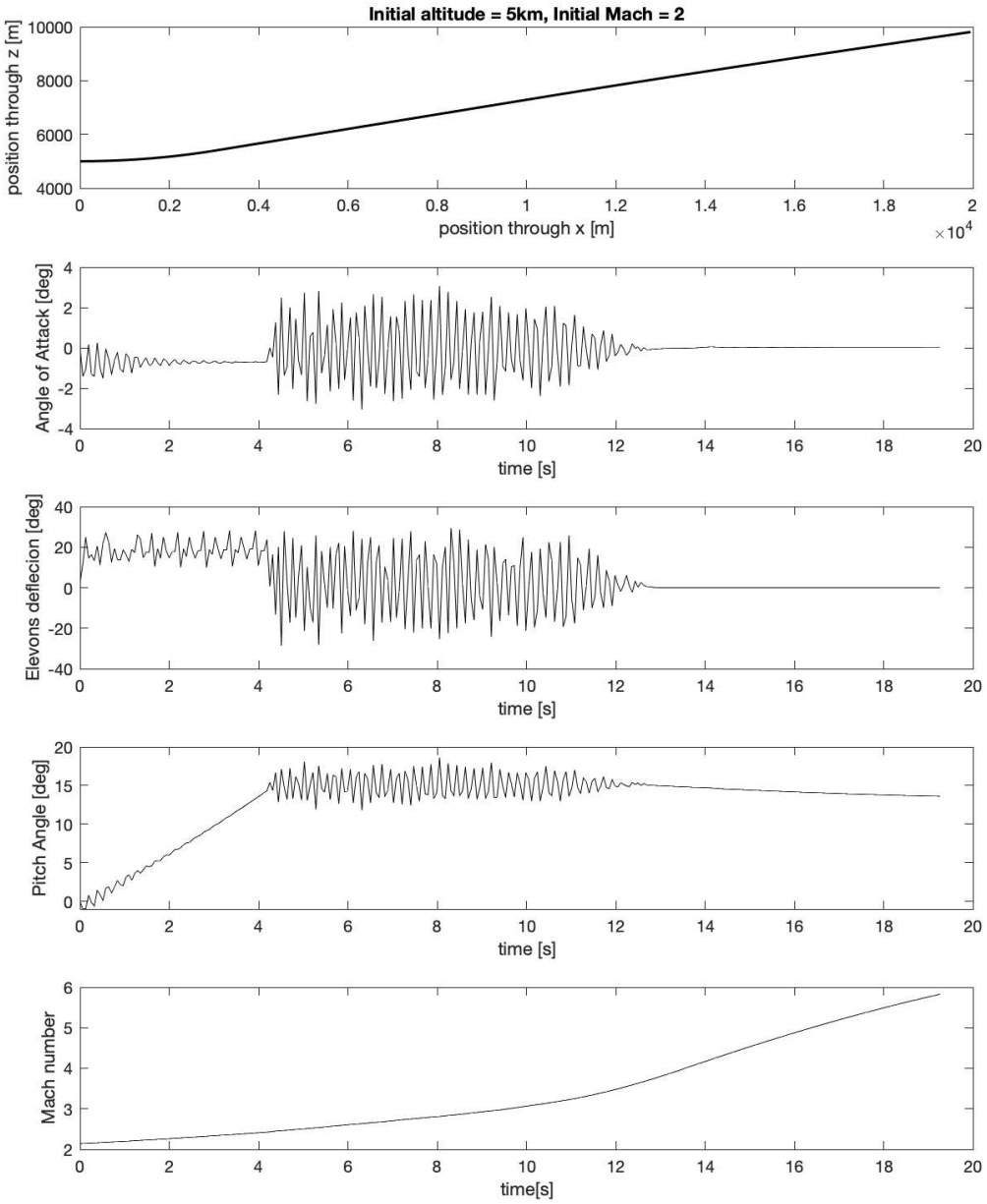

Figure 5.10: Pull-up maneuver with initial altitude of 5km and Mach 2 for a target at 20km of downrange and altitude 10km.

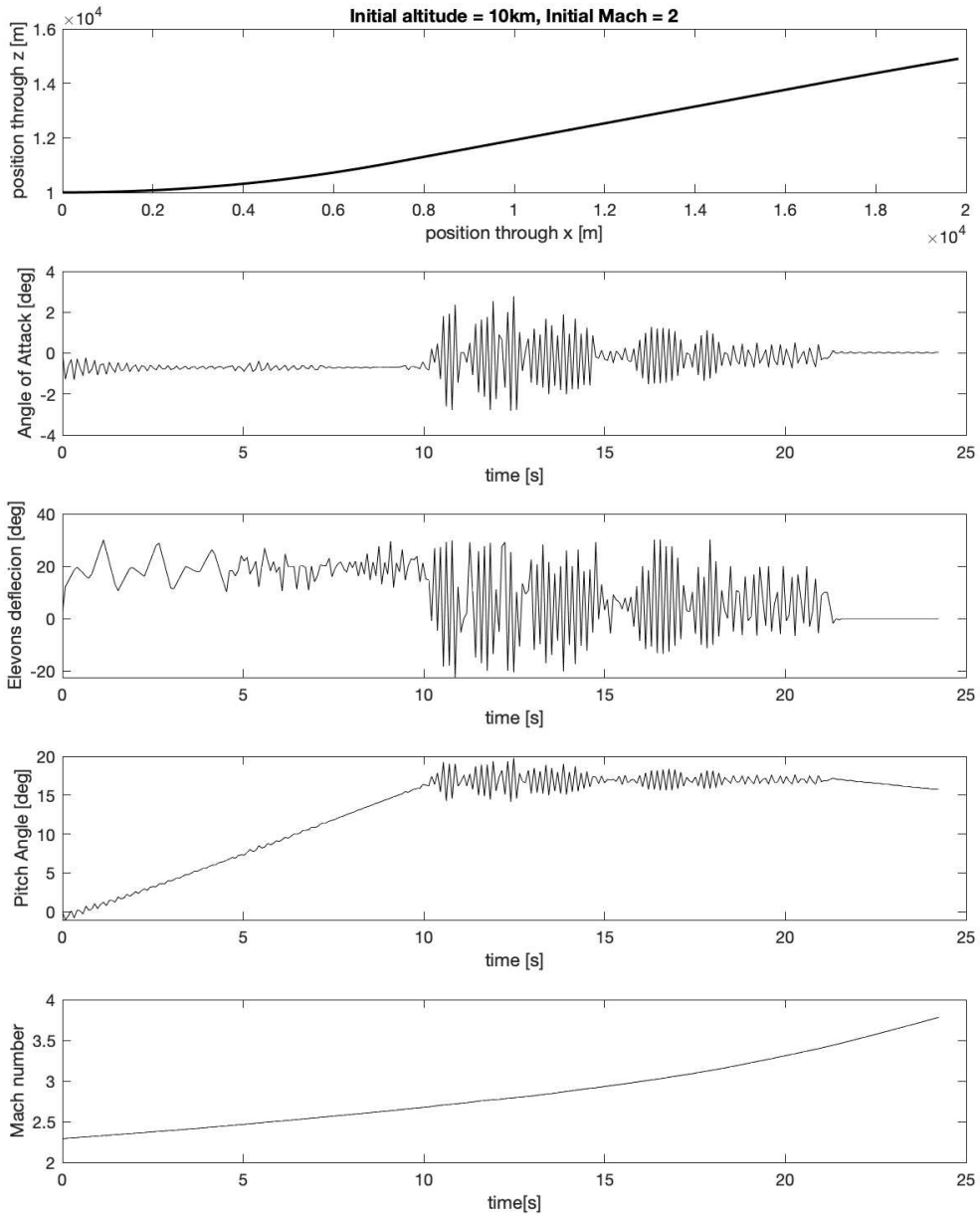

Figure 5.11: Pull-up maneuver with initial altitude of 10km and Mach 2 for a target at 20km of downrange and altitude 15km.

Chapter 6

Hypersonic Effect in the 6DOF Model

For the study of flight mechanics, there is a huge difference in the correspondence of two fields of motion: one for Mach major than 1 and one for Mach minor than 1. The first field of motion is called supersonic, described by an elliptic equation, and the second one is called subsonic described by a hyperbolic equation. So, Mach equal to 1 is a specific value distinguishing two very different motion behavior. Considering the supersonic field and increasing Mach value till, more or less, 5, the phenomenology of motion begins to further differentiate, finding the hypersonic field of motion. However, unlike subsonic motion, the transition between supersonic and hypersonic is not very outlined. The main differences between the hypersonic and supersonic regimes of motion are associated to:

- aerodynamic effects due to body geometry;
- thermochemical effects generated at high temperatures associated with a non-equilibrium condition;
- diffusive effects associated with transport coefficients;
- effects of rarefaction [29].

To gain a reliable model, the implementation of all these effects should be necessary. However, this practice would take a long time and would be very challenging. But, wanting to give to the 6DOF model studied in this thesis a more realistic behavior, one effect has been chosen to be the subject of study.

6.1 Thermoelastic Effect on Elevons Deflection

After literature research, a paper has caught the eye [7] [26]. It was a study based on the deformation of a fuselage due to aircraft and propulsion performance in a high-speed field of motion, especially the hypersonic one which involves an increase in temperature, by its definition, that might deform the vehicle structure. This study is based on the hypothesis that the structural deformation acts on a change of the angle of attack α and a perturbation in the elevons deflection efficiency, interacting this way with aerodynamics and propulsion. To have the esteem of this effect, the fuselage was considered a flexible beam, and its deformation depends on the eq. 6.1:

$$EI\frac{\partial^4 y}{\partial t^4} + \bar{m}\frac{\partial^2 y}{\partial t^2} = p(x,t) \tag{6.1}$$

Where x and y are, respectively, longitudinal and vertical coordinates, t is time, E is the elasticity modulus (Young modulus), I is the beam moment of inertia, $\bar{m}$ mass per unit length, and p is the load per unit length and time.

The integration of this relation and the analysis of its transfer function with the addition of the deflection angle expression (consult the complete study [7] for all the calculation of the parameters), leads to a second order transfer function which combines the elevon normal force with the body deflection angle by the elastic characteristics of the body. The aeroelastic effects considered in this paper came from the change in two angles: the angle of attack and the deflection of the elevons. The change of the angle of attack depends on the body deflection angle of the nose, and the change in the elevons deflection derives from the tail deflection angle. And so, the actual angle of attack α and elevons deflection δe are (eq. 6.2):

$$\begin{aligned} \alpha(s) &= \alpha_r(s) - \Delta\alpha(s) \\ \delta_e(s) &= \delta_{e.r}(s) + \Delta\delta_e(s) \end{aligned} \tag{6.2}$$

Where r denotes the component due to rigid body and Δ the variation due to the aeroelastic effect. Choosing the nose as a critical point of this effect is not casual. This part of the aircraft induces shock waves that affect even the propulsion system and, considering elevons

deflection, the actual influence on vibrations of the deflection surfaces can be investigated. The perturbation δ_e is evaluated considering the transfer function of the significant elastic mode evaluated at the elevon, which, finally, leads to eq. 6.3 for elevons:

$$|\Delta\delta_e| \leq \left\| \frac{T_t}{(1+T_t)} \right\|_\infty \bar{\delta}_{e,r} \tag{6.3}$$

And to eq. 6.4 for alpha:

$$|\Delta\alpha| \leq \left\| T_n \left(1 + \frac{T_t}{(1+T_t)} \right) \right\|_\infty \bar{\delta}_{e,r} \tag{6.4}$$

Where $\bar{\delta}_{e,r}$ is the maximum elevon deflection, and T_t is the total temperature.

6.2 Implementation in the Model

The implementation of this effect in the model has been done with some hypotheses and as a first preview of the high temperature effects on the deflection surfaces considering a non-flexible airframe. The first one is that when the vehicle travels at high speed ($Mach > 1$) the surfaces of deflection might be subjected to the thermoelastic effects described in sec. 6.1. This might be due to the fact that these surfaces are exposed at extremely high temperatures (until $400°C$, sec. 3.2) and this high amount of heat could bend them. The second one is that the total temperature is the temperature of the surfaces in object, which are the elevons. So, as a first approximation of this effect, has been built a Look-Up Table with the maximum temperature as the hypersonic temperature of the surfaces (sec. 3.2) and the minimum one as the air temperature at a certain altitude, building, this way, a matrix of useful in function of Mach number and altitude. Once the Look-Up Table of total temperature has been built, the eq. 6.3 has been added to the 6DOF model. The eq. 6.4 has not been added too, because it would result in a redundant effect. In fact, these two effects are intrinsically connected and the implementation of one results even in the actuation of the other. Last but not least, all the cases investigated to test the 6DOF model in Chapter 5 have been restudied to see the differences with and without the thermoelastic effect on the elevons deflection.

6.3 Flight Perfomance Analysis

To investigate the Flight Performance of the aircraft has been used the same method as the one used in sec. 5.2: a grid of target positions has been built, stepping from 0 to 10 km of altitude and from -30 to -60 km of downrange in the NED coordinate system. The initial state of the vehicle was chosen to be the same as eq. 5.3 and the same cases were considered: with initial Mach numbers of 0.5, 2, and 6. What is immediately evident when comparing figs. 5.3, 5.4, and 5.5 with the 6.1, 6.2, and 6.3 is that way more desired points have been intercepted, with the same initial and final conditions, especially with lower initial Mach. Taking a closer look at the plots, what can be noticed is that this is due to a drastic decrease in velocity, which makes the aircraft much more controllable with respect to the cases analyzed in sec.5.2 . In fact, confronting fig. 5.3 with fig. 6.1, in the first one there is a big blank zone of points where the vehicle is not well maneuverable due to high speed, that touch even Mach 10. Instead, in the second one all the points have been intercepted, but with a maximum Mach of 2.1 in correspondence to the initial altitude of the aircraft which probably means that the vehicle needs more downrange distance to reach a higher Mach number and increase its velocity. Of course,if the velocity has decreased, and the time of interception has increased, stepping from a maximum of 90 seconds to 140 seconds. The same reasoning can be done even for fig. 6.2 and 6.3, in fact, increasing the initial velocity, the desired point misinterception increase as well, but still intercepting way more objectives than previously.

6.4 Disturbance Effects

Again, even to test the stability after a disturbance effect has been used the same method as the one in sec. 5.3. And so, a disturbance effect of 2 deg was inserted after 10 seconds of flight, considering three different initial velocities. Initial and final altitudes were settled again at 10km with a downrange distance of 45km to study the behavior of the angle of attack, pitch angle, elevons deflection, and Mach through time as well as the aircraft trajectory. Already in sec. 5.3 there were a bunch of problems: in fig. 5.6 the velocity increased rapidly causing the misinterception of the desired point and in fig. 5.7 the vehicle was able to reach only Mach 4, instead of a proper hypersonic velocity. With the implementation of the thermoelastic effect

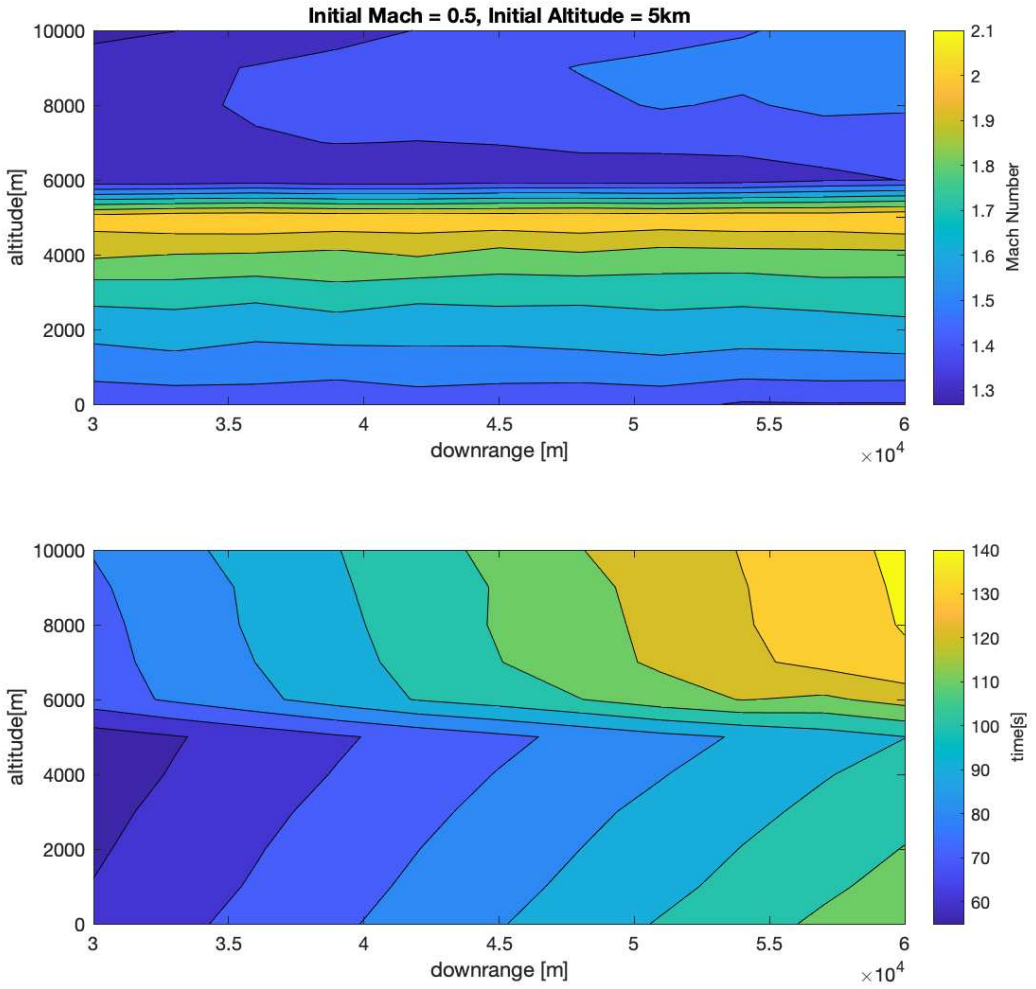

Figure 6.1: Vehicle flight performance analysis at initial 5km of altitude and Mach number of 0.5 with elevons thermoelastic effect.

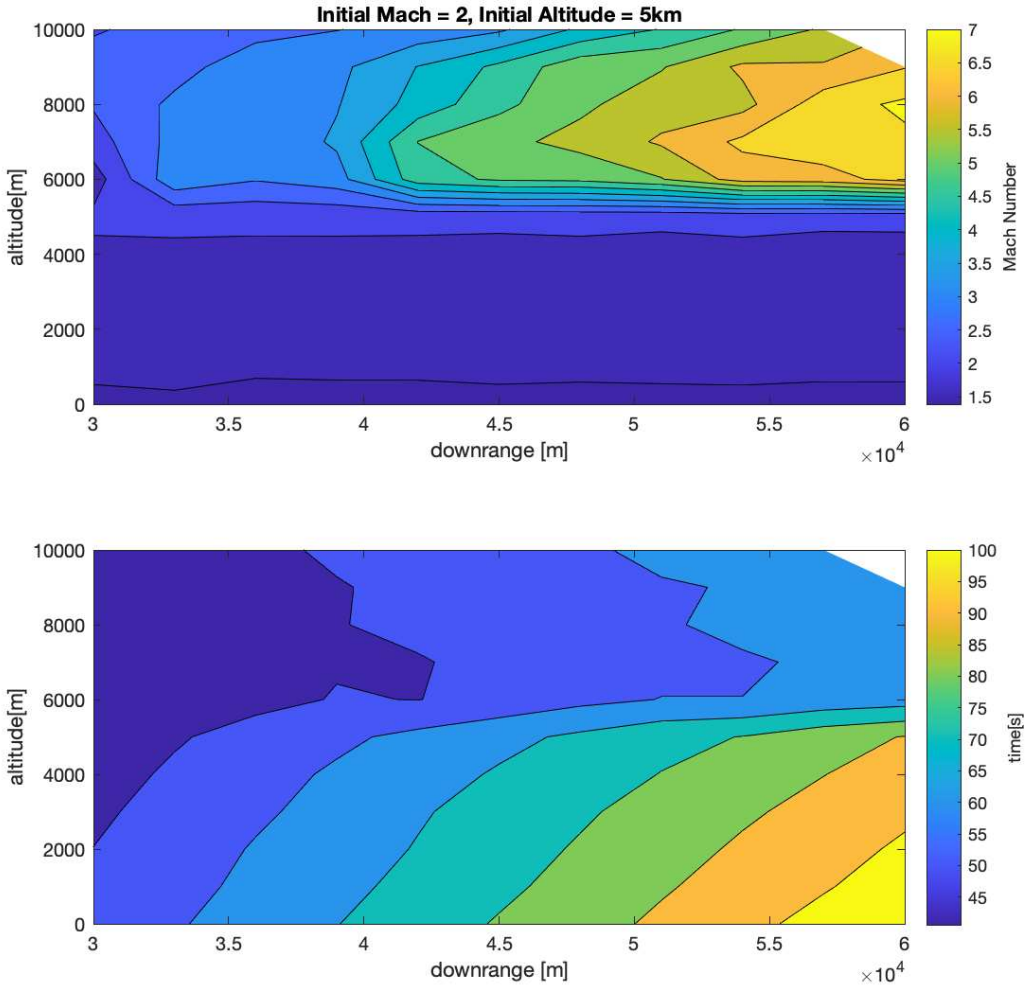

Figure 6.2: Vehicle flight performance analysis at initial 5km of altitude and Mach number of 2 with elevons thermoelastic effect.

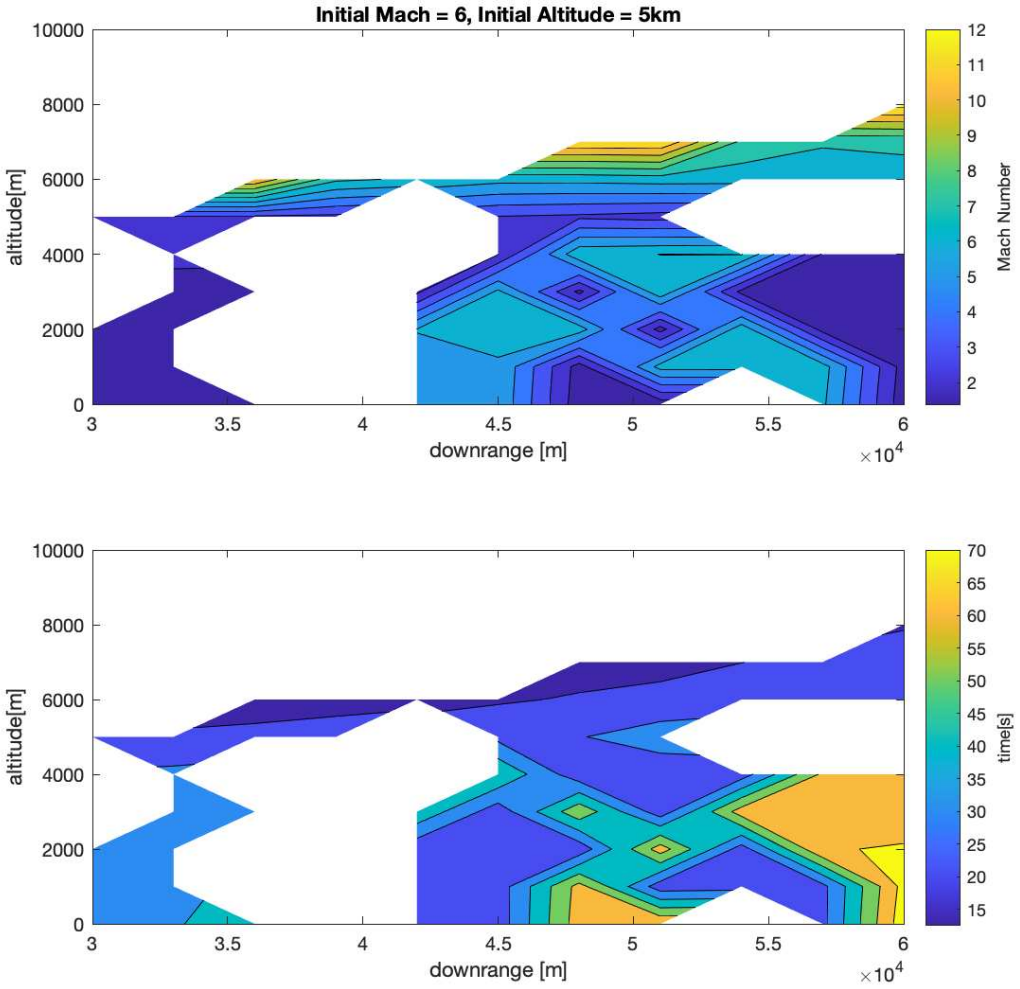

Figure 6.3: Vehicle flight performance analysis at initial 5km of altitude and Mach number of 6 with elevons thermoelastic effect.

on the elevons deflection, as said in sec. 6.3, the velocity is way less than without the effect and so the desired point was always reached, however only in the third case, with Mach number equl to 6, the aircraft became hypersonic. Observing fig. 5.8, without the implementation of the effect and considering the not disturbed case in fig. 6.4, there are no main differences between the behavior of the vehicle, however, as soon as a little angle was imposed on the deflection surfaces, the velocity decreased a lot, returning to Mach 6, and the vehicle employs way more time to settle its angle of attack and pitch angle with respect to fig. 5.8. This is due to the $\Delta\delta_e$ component of eq. 6.2 which provides a massive increase of the drag, decreasing of velocity and unstabilizing the vehicle. These effects are traduced in an increase of time to intercept the target.

6.5 Pull-Up Maneuver

The last thing to test with the 6DOF model with the thermoelastic effect on elevons deflection was the Pull-Up Maneuver. Initially, has been chosen to test again the same conditions as in sec. 5.4, however, the results were not so relevant: even if the desired point was always intercepted, the velocity was very low, increasing a bit and not arriving even at Mach 3. As said in sec. 5.2 this was due to the brief downrange distance that wasn't enough to reach hypersonic velocity. Because of this, it was decided to investigate another case, which was way more exemplary of the effect. The initial and final altitude has remained the same as in sec. 5.4, starting from 5km and arriving at 10km, with an initial Mach number of 2. The only difference was in the downrange, which was chosen to be 55km. This situation, presented in fig. 6.5 for the case without the elevons effect and in fig. 6.6 for the case with the effect, has finished being the one most representative of the thermoelasticity on the deflection surfaces. What can be seen in fig. 6.5 is that the elevons deflection step from -20 to 20 deg only in the first part of the flight, providing a little change in the angle of attack and pitch angle. Once the hypersonic velocity was reached the surfaces deflection step to 0 deg, providing a strong increase of velocity, reaching Mach 10. This led to intercepting the desired point in nearly 30 seconds. Introducing the thermoelastic effect on the elevons the aircraft behavior drastically changed. Here, the elevons deflection is way more impacting, stepping from -50 to 50 deg during all the vehicle flight and, for this reason, producing a stronger drag force which

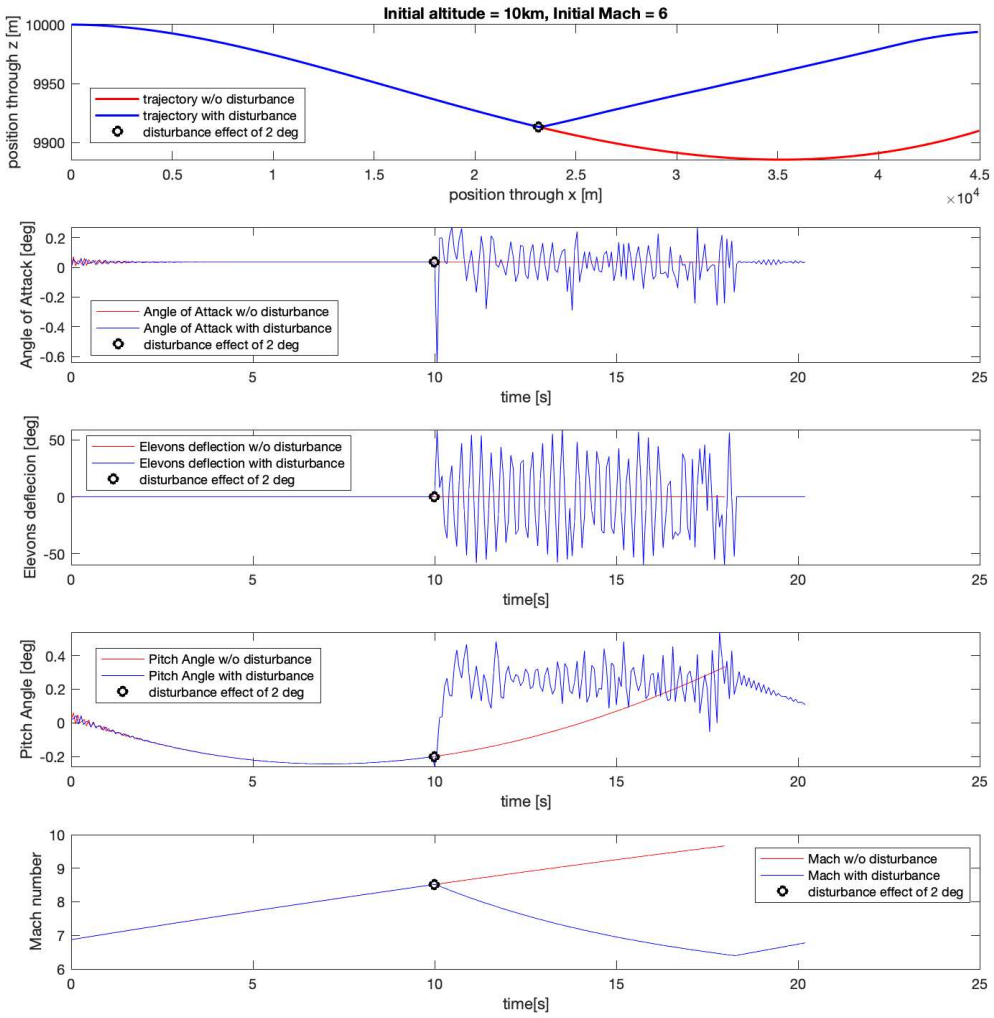

Figure 6.4: Vehicle flight analysis with a surface deflection disturbance of 2 deg after 10 seconds of flight, with 10km of initial altitude and Mach 6, with elevons thermoelastic effect.

prevents the vehicle to increase a lot its velocity. This effect affects even the angle of attack and the pitch angle, which suffer from a larger variation. In these conditions, the aircraft is able to intercept the desired point at a Mach number of only nearly 6, in more than 60 seconds.

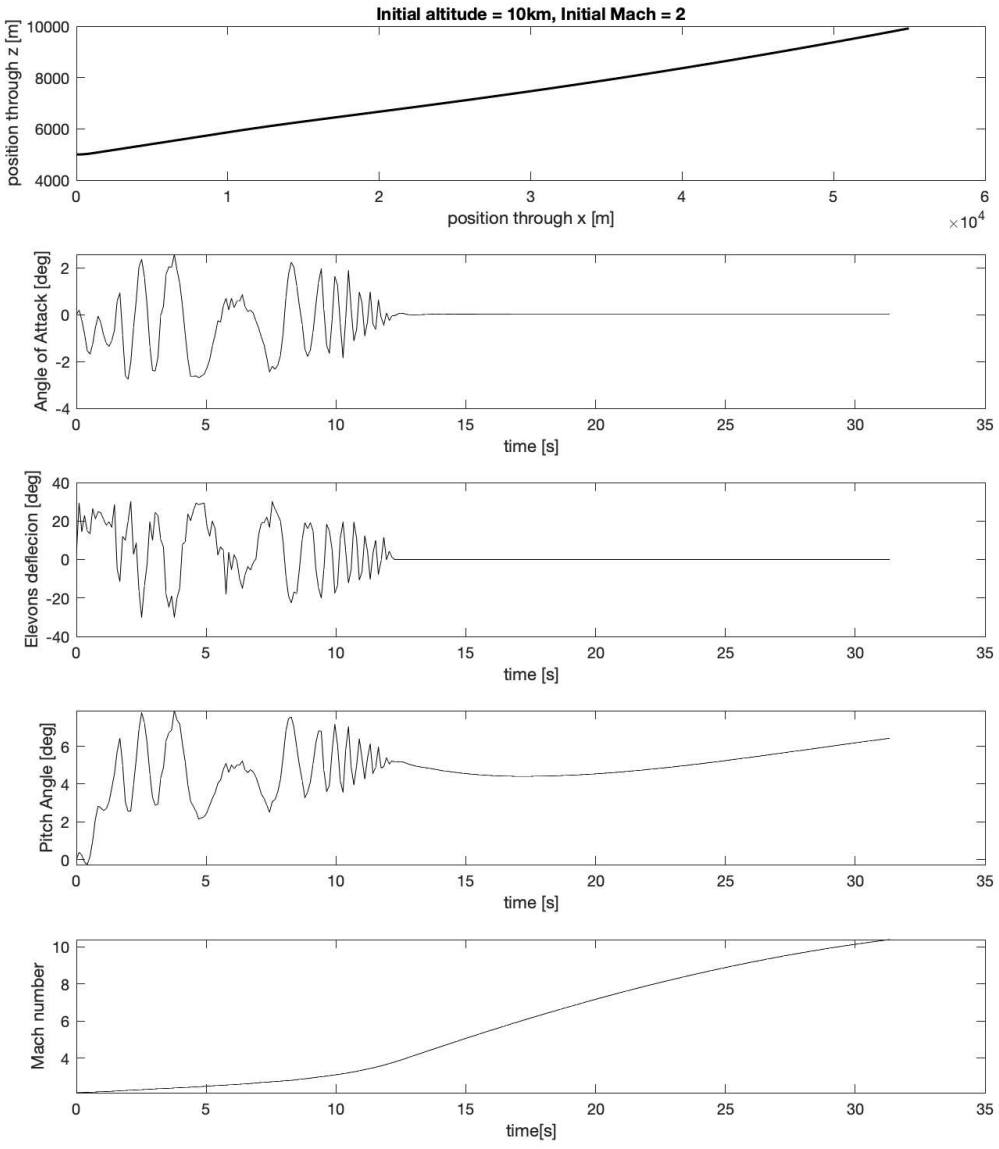

Figure 6.5: Pull-up maneuver with initial altitude of 5km and Mach 2 for a target at 55km of downrange and altitude 10km, without elevons thermoelastic effect.

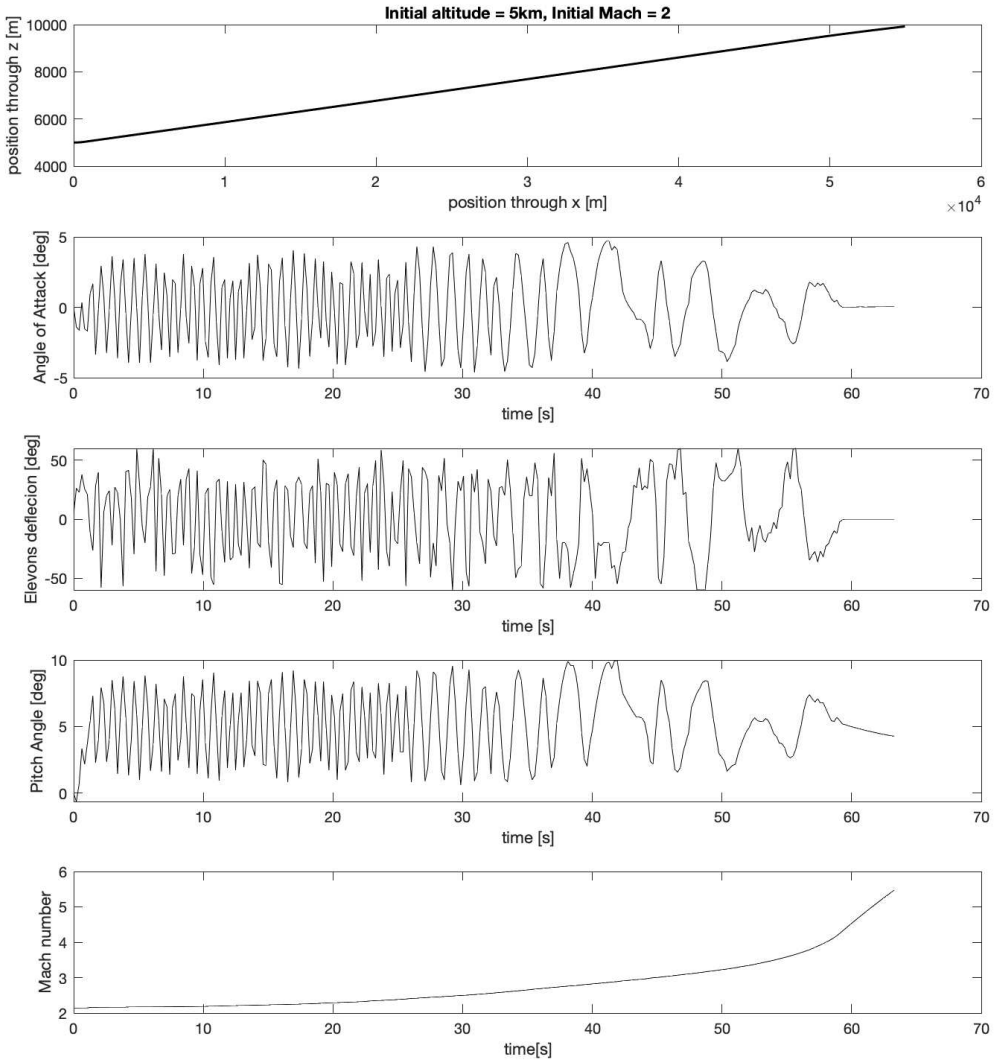

Figure 6.6: Pull-up maneuver with initial altitude of 5km and Mach 2 for a target at 55km of downrange and altitude 10km, with elevons thermoelastic effect.

Chapter 7

Conclusion

Summarizing what has been done in this thesis, six degrees of freedom model has been built to gain a projection of the behavior of a hypersonic vehicle during, especially, a pull-up maneuver. It was employed a top-down approach, from simple to more complicated details implemented in the model. It was chosen an already studied aircraft in order to have a reliable aerodynamic and propulsive database, as well as an actual geometry, mass, and inertia matrix. Then, the model has been built. Respecting the logic of the 6DOF model, the first thing that can be seen is an initialization block that implements the initial state conditions of the aircraft which are written in a MATLAB® script. This initialization block leads directly to the guidance subsystem, which is also related to the initial state of the desired point to intercept. For this thesis, it was chosen the Proportional Navigation law as the foundation for the guidance subsystem block. It is the oldest method known to intercept desired points and it is based on a simple rule: the line of sight vector is the displacement vector between the vehicle and the desired point, to gain the interception of the objective, the LOS vector orientation has to be fixed in inertial space. This simple rule leads to the command of acceleration which is given to the autopilot subsystem. Here, this command of acceleration is compared to the aerodynamic accelerations, in particular, the aerodynamic acceleration acting on the x-axis is compensated by thrust, and the ones acting on the y and z-axis need extra compensation which derives from a surface deflection. So, the accelerations imposed by the guidance subsystem are compared to the aerodynamic ones and the minimum of the two is the actual active acceleration. To intercept the desired point, this active acceleration needs to be traduced in

an angular command. This is done by the Trimmed Motion Subsystem of the model. Here a particular condition of trimming is imposed on the vehicle, in fact, the aircraft needs to be able to do a pull-up maneuver. To do so, some hypothesis needs to be done:

- β is equal to zero
- q and $\dot{\alpha}$ are neglectable;
- L is nearly W and D is nearly Thrust (α is little);
- $L - W = 0$;
- p and r are zero, as well as the rudder and the aileron deflections;
- the elevons move symmetrically, so the right and left elevon deflections are the same.

Once all the hypotheses were made, the actual angular deflection was easy to determine. The active accelerations commanded by autopilot were transformed into wind axes, where the third component of the vector divided by the aircraft mass is the lift force. From the lift force, the lift coefficient is easily determinable and, from a Look-Up Table built from the database of the vehicle, the angular deflection of the elevons surfaces to reach the desired point is found. At this point, the angular command needs to be passed to the vehicle environment in which is studied its flight mechanics. This subsystem is divided into other two: the kinematics one in which the equations of motion are investigated, and the dynamics one in which all the forces acting on the flight body are studied. Beginning with the second one, the first force that was written in the model was the thrust one. It came from a Look-Up Table built from the database vehicle and is given by two Turbine-Based Combine Cycle engines performing very well at high Mach number velocities. The force was supposed to act only on the x-axis of the body coordinate system and generate zero momentum. Then the gravity force as an acceleration in NED coordinate system, was implemented in the model as a vector in which the first two components are equal to zero and the third one is $9.81[m/s^2]$. After this, it was time to study the apparent acceleration acting on the system which are Coriolis and centrifugal, following the simple equations presented in sec. 2.4. At this moment it was time to add the Aerodynamic subsystem which was maybe the most articulated one. To do this, it was necessary to implement even an Atmosphere environment inside the model which was provided

by Simulink® as an algorithm of the ISA Atmosphere giving, in the function of altitude, the temperature, pressure, density, and speed of sound. The Aerodynamic subsystem is composed of three subsystems as well, which provide:

- the flight angles, the wind coordinate system kinematics, and all the aerodynamic coefficients;
- the forces and moments vectors in wind coordinates;
- the transformation from wind to body coordinates.

All the aerodynamic coefficients are evaluated using Look-Up Tables built with the vehicle database, remembering that only drag, lift, and pitching moment coefficients are used, due to the hypothesis made for the 6DOF model construction. With this subsystem, the dynamic part of the model was complete, and all the forces and moments coming from there were passed to the kinematics block. Here the equations of motion were studied: Newton's one for the translational motion and Euler's one for the angular motion, providing acceleration, velocity, position, and attitude which can be reiterated to gain the next aircraft state of motion. Once the model was finished, it was time to test its functioning. To verify the equations of motion part it was compared to the Simulink® 6DOF model already existing in the software, gaining the same solution. Then, the vehicle flight performances were evaluated, building a grid of desired points to intercept. This practice made it noticeable that the control provided by the trimmed motion hypothesis is weak: the aircraft tend to reach too high velocities which are no longer controllable by this strategy. After this, it was introduced a disturbance effect to test the aircraft's stability. It was chosen an interference of 2 deg after 10 seconds of flight in the elevons deflection, thus making it known that if the vehicle is going to intercept the desired point without the disturbance effect, is going to do as well with the disturbance effect. However, the disturbance is more appreciable in the hypersonic regime where the time of flight is much shorter and the elevons deflection tends to be nearly zero. Finally, it was investigated a pull-up maneuver at three different initial and final altitudes, with the same initial speed and downrange. This has made it simple to see that, in 20km of downrange, only at an altitude of 5km is possible to reach hypersonic velocities, because under this value the drag is much stronger due to the air density and above it, the air density is too rarefied, this way the

airbreathing propulsion system needs much more time to reach higher Mach number. The last thing done was introducing in the 6DOF model a hypersonic effect on the elevons deflection which, due to the high speed tends to increase their temperature, leading to the bending of the surfaces themselves. This effect came from a thermoelastic study of vehicle bending and it leads to a massive decrease in terms of velocity of the aircraft. In fact, the elevons bending implies the need for deflects even more those surfaces, increasing the drag force which provides a decrease velocity. For future development of this 6DOF, a sure thing to do is to build a stronger control system to control better the increasing of velocity and reach more desired points. Also, doing this is possible to implement much more interesting hypersonic effects as uncertainties in the control of surface deflections [5]. Not to mention that this practice would lead the model to be able to use all six degrees of freedom, making it possible to complicate some of its subsystems, such as the aerodynamic one, to which the deviance coefficient, as well as the roll and yaw moment ones would be added.

Bibliography

[1] W. H. Andrews. *Summary of Preliminary Data Derived From the XB-70 Airplanes*. National Aeronautics and Space Administration, 1966.

[2] E. Baumann, C. Bahm, B. Strovers, R. Beck, and M. Richard. The x-43a six degree of freedom monte carlo analysis. In *46th AIAA Aerospace Sciences Meeting and Exhibit*, page 203, 2008.

[3] L. D. R. Bernard Etkin. *Dynamics of Flight. Stability and Control*, volume 3nd ed. 1996.

[4] M. A. Brock. Performance study of two-stage-to-orbit reusable launch vehicle propulsion alternatives. 2004.

[5] H. Buschek and A. J. Calise. Uncertainty modeling and fixed-order controller design for a hypersonic vehicle model. *Journal of Guidance, Control, and Dynamics*, 20(1):42–48, 1997.

[6] M. Cavcar. The international standard atmosphere (isa). *Anadolu University, Turkey*, 30(9):1–6, 2000.

[7] A. Clark, M. Mirmirani, S. Choi, and C. Wu. An aero-propulsion integrated elastic model of a generic airbreathing hypersonic vehicle. In *AIAA guidance, navigation, and control conference and exhibit*, page 6560, 2006.

[8] C. Clark, K. Kloesel, and N. Ratnayake. A technology pathway for airbreathing, combined-cycle, horizontal space launch through sr-71 based trajectory modeling. In *17th AIAA International Space Planes and Hypersonic Systems and Technologies Conference*, page 2229, 2011.

[9] D. M. A. W. DC. *Department of Defense World Geodetic System 1984: Its Definition and Relationships with Local Geodetic Systems. Second Edition.* 1991.

[10] J. V. R. de Sousa and P. V. Gamboa. Aerial forest fire detection and monitoring using a small uav. *KnE Engineering*, pages 242–256, 2020.

[11] N. D. Diviitis. *Elementi di Meccanica del Volo (Parte 1).*

[12] P. L. D. L. D'oriano Vera. Aerodynamic study of a small hypersonic plane. *PHD Thesis, Università degli Studi di Napoli, Federico II.*

[13] V. D'Oriano, R. Savino, and M. Visone. Aerothermodynamic study of a small hypersonic plane. *Aircraft Engineering and Aerospace Technology*, 2018.

[14] G. J. Harloff and B. M. Berkowitz. Hasa: Hypersonic aerospace sizing analysis for the preliminary design of aerospace vehicles. Technical report, 1988.

[15] R. Havens, R. Koll, and H. LaGow. The pressure, density, and temperature of the earth's atmosphere to 160 kilometers. *Journal of Geophysical Research*, 57(1):59–72, 1952.

[16] D. G. Hull. *Fundamentals of Airplane Flight Mechanics.* 2007.

[17] J. P. Jones, L. Kuffel, E. Sorto-Ramos, K. Seyed Alavi, T. Mccall, and B. Chudoba. Investigating the legacy of air-breathing and rocket propulsion systems. In *AIAA Propulsion and Energy 2020 Forum*, page 3916, 2020.

[18] S. Keshmiri, R. Colgren, S. Farokhi, and M. Mirmirani. Ramjet and scramjet engine cycle analysis for a generic hypersonic vehicle. In *14th AIAA/AHI Space Planes and Hypersonic Systems and Technologies Conference*, page 8158, 2006.

[19] S. Keshmiri, R. Colgren, and M. Mirmirani. Development of an aerodynamic database for a generic hypersonic air vehicle. In *AIAA Guidance, Navigation, and Control Conference and Exhibit*, page 6257, 2005.

[20] S. Keshmiri, R. Colgren, and M. Mirmirani. Modeling and simulation of a generic hypersonic vehicle using merged aerodynamic models. In *14th AIAA/AHI Space Planes and Hypersonic Systems and Technologies Conference*, page 8087, 2006.

[21] S. Keshmiri, R. Colgren, and M. Mirmirani. Six-dof modeling and simulation of a generic hypersonic vehicle, for control and navigation purposes. In *AIAA guidance, navigation, and control conference and exhibit*, page 6694, 2006.

[22] S. Keshmiri, R. Colgren, and M. Mirmirani. Trajectory optimization for a generic hypersonic vehicle. In *14th AIAA/AHI Space Planes and Hypersonic Systems and Technologies Conference*, page 8157, 2006.

[23] S. Keshmiri, R. Colgren, and M. Mirmirani. Six dof nonlinear equations of motion for a generic hypersonic vehicle. In *AIAA atmospheric flight mechanics conference and exhibit*, page 6626, 2007.

[24] A. S. Korad. Modeling, analysis, and control of a hypersonic vehicle with significant aero-thermo-elastic-propulsion interactions, and propulsive uncertainty. Technical report, Arizona State University, 2010.

[25] J. Longo, K. Hannemann, and V. Hannemann. The challenge of modeling high speed flows. 2007.

[26] M. Mirmirani, M. Kuipers, J. Levin, and A. D. Clark. Flight dynamic characteristics of a scramjet-powered generic hypersonic vehicle. In *2009 American Control Conference*, pages 2525–2532. IEEE, 2009.

[27] D. D. Mueller. The coriolis effect in zero-gravity research aircraft. Technical report, AIR FORCE AEROSPACE MEDICAL RESEARCH LAB WRIGHT-PATTERSON AFB OH, 1962.

[28] U. S. N. Oceanic, A. Administration, and U. S. A. Force. *US standard atmosphere, 1976*, volume 76. National Oceanic and Atmospheric Administration, 1976.

[29] G. Z. Rodolfo Monti. *Elementi di aerodinamica ipersonica*. Liguori Editore, 2012.

[30] R. Savino, G. Russo, V. Carandente, and V. D'oriano. Hyplane: challenges for space tourism and business transportation. *J Aeronaut Aerospace Eng*, 2(123):2, 2013.

[31] R. Savino, G. Russo, V. D'Oriano, M. Visone, M. Battipede, and P. Gili. Performances of a small hypersonic airplane (hyplane). *Acta Astronautica*, 115:338–348, 2015.

[32] J. D. Shaughnessy, S. Z. Pinckney, J. D. McMinn, C. I. Cruz, and M.-L. Kelley. Hypersonic vehicle simulation model: winged-cone configuration. Technical report, 1990.

[33] C. L. Tracy and D. Wright. Modeling the performance of hypersonic boost-glide missiles. *Science & Global Security*, 28(3):135–170, 2020.

[34] P. H. Zipfel. *Modeling and Simulation of Aerospace Vehicle Dynamics*, volume 2nd ed. 2007.

[35] P. H. Zipfel. *Missile and Rocket Simulation Workshop in Four Days*. 2020.

Acknowledgements

Grazie a tutte le persone che hanno fatto parte di questo mio percorso.

Grazie al mio relatore, il professor Carlo Bettanini, che ha accolto la proposta di tesi in modo propositivo e grazie al mio tutor aziendale, ingegner Federico Fune, per avermi accompagna durante il percorso in MBDA.

Ringrazio molto Eleonora, per avermi sostenuta da che io abbia memoria con la sua amicizia e la sua delicatezza.

Alla mia famiglia va un altro ringraziamento speciale: ai miei genitori, Damiano e Mariastella, oltre che a mio fratello Manuel, che hanno sempre supportato le mie scelte senza mai ostacolarmi, dandomi la forza quando, a volte, l'ho sentita mancare.

Grazie infinite anche a Mattia per essere sempre stato in grado di vedere in me ciò che io non riuscivo, spronandomi e facendomi rendere conto di quello che fosse in realtà il mio valore.

Infine, grazie anche a tutti quelli che hanno fatto parte della mia vita, per tanto o per poco tempo, perché se oggi sono qui è anche per ognuno di voi, che avete segnato il mio percorso.